

NANOCOMPOSITES BASED ON
RECYCLED POLY(ETHYLENE TEREPHTHALATE)

A THESIS SUBMITTED TO
THE GRADUATE SCHOOL OF NATURAL AND APPLIED SCIENCES
OF
MIDDLE EAST TECHNICAL UNIVERSITY

BY

ASLI TOLGA

IN PARTIAL FULLFILMENT OF THE REQUIREMENTS
FOR
THE DEGREE OF MASTER OF SCIENCE
IN
CHEMICAL ENGINEERING

JULY 2005

Approval of the Graduate School of Natural and Applied Sciences

Prof. Dr. Canan Özgen
Director

I certify that this thesis satisfies all the requirements as a thesis for the degree of Master of Science.

Prof. Dr. Nurcan Baç
Head of Department

This is to certify that we have read this thesis and that in our opinion it is fully adequate, in scope and quality, as a thesis and for the degree of Master of Science.

Prof. Dr. Ülkü Yilmazer
Supervisor

Examining Committee Members

Prof. Dr. Güngör Gündüz	(METU,CHE)	_____
Prof. Dr. Ülkü Yilmazer	(METU,CHE)	_____
Prof. Dr. Teoman Tinçer	(METU,CHEM)	_____
Prof. Dr. Erdal Bayramlı	(METU,CHE)	_____
Assoc. Prof. Dr. Göknur Bayram	(METU,CHE)	_____

I hereby declare that all information in this document has been obtained and presented in accordance with academic rules and ethical conduct. I also declare that, as required by these rules and conduct, I have fully cited and referenced all material and results that are not original to this work.

Name, Last name: Asli Tolga

Signature :

ABSTRACT

NANOCOMPOSITES BASED ON RECYCLED POLY(ETHYLENE TEREPHTHALATE)

Tolga, Asli

M.S., Department of Chemical Engineering

Supervisor: Prof. Dr. Ülkü Yilmazer

July 2005, 120 pages

In this study, the effects of glycol type, organoclay type and concentration on the final properties of nanocomposites based on recycled poly(ethylene terephthalate) was investigated. For this purpose, first recycled PET was glycolysed and after that unsaturated polyester-montmorillonite nanocomposites were synthesized by using three different types of glycols (i.e. ethylene glycol (EG), propylene glycol (PG) and diethylene glycol (DEG)). As the first step, all the compositions were prepared by Cloisite 30B type of clay, and then for comparison of clay type, nanocomposites containing 1 wt. % of Cloisite 15A and Cloisite 25A type of clay were also synthesized. Morphological and mechanical analyses were performed for the characterization of the nanocomposites.

According to the results of XRD analysis, for all glycol types maximum intercalation was observed in Cloisite 30B containing samples. Exfoliated structures were obtained in the samples containing EG at 1 wt. % Cloisite 30B content and DEG at 3 wt. % Cloisite 30B content.

Mechanical tests showed that, for all properties, glycol type is the most effective experimental parameter. DEG based samples are the most flexible whereas PG

based samples are the least flexible. EG and DEG based samples give maximum tensile strength and tensile modulus values at 1 wt. % clay loading. Samples prepared by DEG exhibited maxima in both flexural strength and modulus at 1 wt. % clay content. With respect to the organoclay type, Cloisite 30B containing samples gave the highest compatibility with the unsaturated polyester matrix as indicated by the tensile test results.

Organoclay type and content had no positive effect on the impact strength. Clay particles acted as stress concentrators and lowered the impact strength.

Keywords: PET glycolysis, unsaturated polyester, nanocomposites, organoclay, mechanical properties

ÖZ

GERİKAZANILMIŞ POLİ(ETİLEN TEREFTALAT) BAZLI NANOKOMPOZİTLER

Tolga, Aslı

Yüksek Lisans, Kimya Mühendisliği Bölümü

Tez Yöneticisi: Prof. Dr. Ülkü Yılmaz

Temmuz 2005, 120 sayfa

Bu çalışmada, gerikazanılmış poli(etilen tereftalat) bazlı nanokompozitlerin özelliklerine glikol tipinin, organokil tipinin ve konsantrasyonunun etkileri araştırılmıştır. Bu amaçla öncelikle atık PET etilen glikol (EG), propilen glikol (PG) ve dietilen glikol (DEG) kullanılarak glikoliz edilmiş ve bundan sonra doymamış poliester-montmorillonit nanokompozitleri sentezlenmiştir. İlk basamak olarak, bütün kompozisyonlar Cloisite 30B kil tipi ile hazırlanmıştır; daha sonra, kil tiplerini karşılaştırmak için ağırlıkça %1 Cloisite 15A ve Cloisite 25A kili içeren nanokompozitler ayrıca sentezlenmiştir. Nanokompozitlerin karakterizasyonu için morfolojik ve mekanik analizler yapılmıştır.

XRD analizi sonuçlarına göre, bütün glikol tiplerinde en fazla açılma Cloisite 30B içeren numunelerde gözlenmiştir. EG içeren numunelerde ağırlıkça %1 Cloisite 30B eklendiğinde ve DEG içeren numunelerde ağırlıkça %3 Cloisite 30B eklendiğinde tamamen dağılmış bir yapı elde edilmiştir.

Mekanik testler, bütün özellikler için glikol tipinin en etkili deneysel parametre olduğunu göstermiştir. DEG içeren numuneler en tok, PG içeren numuneler ise en kırılabilir yapıya sahiptir. EG ve DEG içeren numuneler en yüksek gerilme

direnci ve gerilme modülü deęerlerini aęırlıkça %1 kil eklendięinde vermiřtir. DEG ile hazırlanan numunelerde en yksek eęilme dayanımı ve modl %1 kil eklendięinde grlmřtr. Organokil tipleri gz nne alındıęında, gerilme testlerine gre, Cloisite 30B ięeren numuneler doymamıř poliester matriksi ile en yksek uyumu gstermiřtir.

Organokil tipi ve konsantrasyonunun darbe dayanımı testi sonuęlarına olumlu bir etkisi olmamıřtır. Kil tanecikleri gerilimi arttıran noktalar olarak hareket etmiř ve darbe dayanımını dřrmřtr.

Anahtar Kelimeler: PET`in glikolizi, doymamıř poliester, nanokompozit, organokil, mekanik zellikler

To Mom and my grandma...

ACKNOWLEDGEMENTS

I would like to express my deepest gratitude to my supervisor Prof. Dr. Ülkü Yilmazer, for his guidance, continuous support, encouragement and valuable advices throughout this study. It was a pleasing honor for me to work with him.

I am very grateful to Assoc. Prof. Dr. Göknur Bayram from Department of Chemical Engineering for giving me every opportunity to use the instruments in her laboratory. I also would like to thank Prof. Dr. Teoman Tinçer from Department of Chemistry for providing me the impact test instrument in his laboratory.

I also wish to extend my acknowledgements and sincere thanks to Çiğdem Zeytin and Pelin Toprak for their help and support.

Special thanks go to Cengiz Tan from Department of Metallurgical and Materials Engineering for SEM Analysis and Necmi Avcı from Department of Metallurgical and Materials Engineering for XRD Analysis.

I would sincerely thank to Buket Işık and Nursel Göçmen for their endless friendship, support and encouragement in all parts of my life. I also would like to thank all my friends in Polymer Research Group including Güralp Özkoç, Mert Kılınc, Işıl Işık, Fatma Işık, İlknur Çakar, Sertan Yeşil, Özcan Köysüren and Elif Alyamaç for their friendship, and for helping me in all the possible ways.

This thesis could not be written without the encouragement, patience and understanding of Mert Baysal. I express my sincerest thanks to him for always being right beside me. Finally, I want to thank my family for supporting, encouraging, and loving me all through my life. It would not have been possible to complete this study without their love.

TABLE OF CONTENTS

PLAGIARISM	iii
ABSTRACT	iv
ÖZ.....	vi
DEDICATION.....	viii
ACKNOWLEDGEMENTS	ix
TABLE OF CONTENTS	x
LIST OF TABLES	xiii
LIST OF FIGURES	xv
CHAPTER	
1. INTRODUCTION.....	1
2. BACKGROUND	3
2.1 Poly(ethylene terephthalate), PET	3
2.1.1 Formation Mechanism	3
2.1.2 Product Description and Uses	5
2.2 Recycling of Plastics	5
2.2.1 Introduction	5
2.2.2 PET Recycling	6
2.2.2.1 Chemical Recycling Methods.....	7
2.2.2.1.1 Methanolysis	7
2.2.2.1.2 Hydrolysis	8
2.2.2.1.3 Glycolysis.....	10
2.3 Unsaturated Polyesters	11
2.3.1 Synthesis of Unsaturated Polyester Resins	11
2.3.2 Classification of Unsaturated Polyester Resins.....	12
2.3.3 Curing of Unsaturated Polyester Resins.....	13
2.3.4 Application Areas of Unsaturated Polyesters	17
2.4 Composites	18
2.4.1 Matrix.....	18
2.4.1.1 Polymer Matrix Composites	18
2.4.2 Reinforcement	19
2.5 Nanocomposites	20
2.6 Polymer Layered Silicate Nanocomposites.....	20
2.6.1 Layered Silicates.....	21

2.6.1.1 Cation-Exchange Process	22
2.6.2 Synthesis of Nanocomposites	23
2.6.2.1 In-Situ Polymerization Method	23
2.6.2.2 Solution Intercalation Method	24
2.6.2.3 Melt Intercalation Method.....	25
2.6.3 Nanocomposite Structures	26
2.7 Characterization	27
2.7.1 Mechanical Properties	27
2.7.1.1 Tensile Tests	27
2.7.1.2 Flexural Tests.....	29
2.7.1.3 Impact Tests.....	30
2.7.2 Scanning Electron Microscopy (SEM)	30
2.7.3 X-Ray Diffraction (XRD).....	31
2.8 Previous Studies	32
2.8.1 Unsaturated Polyester Resins from PET Waste	33
2.8.2 Unsaturated Polyester-Clay Nanocomposites	34
3. EXPERIMENTAL.....	37
3.1 Materials	37
3.1.1 Recycled PET	37
3.1.2 Glycols.....	37
3.1.2.1 Ethylene Glycol (EG)	37
3.1.2.2 Propylene Glycol (PG).....	38
3.1.2.3 Diethylene Glycol (DEG).....	38
3.1.3 Zinc Acetate	39
3.1.4 Maleic Anhydride (MA)	39
3.1.5 Organoclays	40
3.1.5.1 Cloisite 30B.....	41
3.1.5.2 Cloisite 25A.....	41
3.1.5.3 Cloisite 15A.....	42
3.1.6 Styrene.....	43
3.1.7 Hydroquinone	44
3.1.8 Cobalt Naphthenate	44
3.1.9 Methyl Ethyl Ketone Peroxide (MEKP)	44
3.1.10 Release Agent	44
3.2 Experimental Procedure	44
3.2.1 Glycolysis Reaction	44

3.2.2 Preparation of UP-MMT Nanocomposites	46
3.2.3 Acid Number Determination	47
3.2.4 Determination of Styrene Percentage in the Resin	48
3.3 Characterization	50
3.3.1 Mechanical Testing Procedure and Equipment	50
3.3.1.1 Tensile Tests	50
3.3.1.2 Flexural Tests	51
3.3.1.3 Impact Tests	51
3.3.2 Morphological Analysis	52
3.3.2.1 Scanning Electron Microscopy (SEM) Analysis	52
3.3.2.2 X-Ray Diffraction (XRD) Analysis	52
4. RESULTS AND DISCUSSION	53
4.1 Morphological Analysis	53
4.1.1 X-Ray Diffraction (XRD) Analysis	53
4.1.2 Scanning Electron Microscopy (SEM) Analysis	63
4.2 Mechanical Analysis	71
4.2.1 Tensile Test Analysis	71
4.2.2 Flexural Test Analysis	84
4.2.3 Impact Test Analysis	95
5. CONCLUSIONS	99
REFERENCES	101
APPENDIX A	106
APPENDIX B	116

LIST OF TABLES

Table 3.1 Properties of recycled PET	37
Table 3.2 Physical properties of Ethylene Glycol	38
Table 3.3 Physical properties of Propylene Glycol.....	38
Table 3.4 Physical properties of Diethylene Glycol	39
Table 3.5 Physical properties of Maleic Anhydride	39
Table 3.6 Physical data of Cloisite 30B.....	41
Table 3.7 Physical data of Cloisite 25A.....	42
Table 3.8 Physical data of Cloisite 15A.....	43
Table 3.9 Physical properties of Styrene.....	43
Table 3.10 Theoretical and experimental molecular weights (g/mol) of different glycol based oligomers	46
Table 3.11 Formulations and acid numbers of the resins.....	49
Table 3.12 Tensile test specimen dimensions.....	50
Table 4.1 X-ray diffraction results of all compositions prepared by Cloisite 30B.....	54
Table 4.2 X-ray diffraction results of compositions prepared by different types of organoclays (1 wt. % organoclay).....	61
Table 4.3 % increase in the d-spacings of organoclays with respect to organoclay types (1 wt. % organoclay).....	62
Table B.1 Arithmetic means and standard deviations of tensile strength values of samples with respect to glycol type and organoclay (Cloisite 30B) content	116
Table B.2 Arithmetic means and standard deviations of tensile strength values of samples with respect to glycol type and organoclay type	116
Table B.3 Arithmetic means and standard deviations of tensile modulus values of samples with respect to glycol type and organoclay (Cloisite 30B) content	116
Table B.4 Arithmetic means and standard deviations of tensile modulus values of samples with respect to glycol type and organoclay type	117

Table B.5 Arithmetic means and standard deviations of tensile strain at break (%) values of samples with respect to glycol type and organoclay (Cloisite 30B) content	117
Table B.6 Arithmetic means and standard deviations of tensile strain at break (%) values of samples with respect to glycol type and organoclay type	117
Table B.7 Arithmetic means and standard deviations of flexural strength values of samples with respect to glycol type and organoclay (Cloisite 30B) content	118
Table B.8 Arithmetic means and standard deviations of flexural strength values of samples with respect to glycol type and organoclay type	118
Table B.9 Arithmetic means and standard deviations of flexural modulus values of samples with respect to glycol type and organoclay (Cloisite 30B) content	118
Table B.10 Arithmetic means and standard deviations of flexural modulus values of samples with respect to glycol type and organoclay type	119
Table B.11 Arithmetic means and standard deviations of flexural strain at maximum stress values of samples with respect to glycol type and organoclay (Cloisite 30B) content	119
Table B.12 Arithmetic means and standard deviations of flexural strain at maximum stress values of samples with respect to glycol type and organoclay type	119
Table B.13 Arithmetic means and standard deviations of impact strength values of samples with respect to glycol type and organoclay (Cloisite 30B) content	120
Table B.14 Arithmetic means and standard deviations of impact strength values of samples with respect to glycol type and organoclay type	120

LIST OF FIGURES

Figure 2.1 Chemical structure of PET	3
Figure 2.2 PET formation via acid route.....	4
Figure 2.3 PET formation via ester interchange	4
Figure 2.4 High temperature esterification.....	5
Figure 2.5 Methanolysis of PET	8
Figure 2.6 Glycolysis of PET with EG	10
Figure 2.7 Schematic view of cross-linking reaction of unsaturated polyester...	15
Figure 2.8 Structure of 2:1 phyllosilicates	21
Figure 2.9 The cation-exchange process between alkylammonium ions and cations initially intercalated between the clay layers	23
Figure 2.10 The in-situ polymerization	24
Figure 2.11 The solution intercalation method.....	25
Figure 2.12 The melt intercalation method	25
Figure 2.13 Schematic illustrations of a phase-separated, an intercalated and an exfoliated polymer-layered silicate nanocomposites.....	26
Figure 2.14 Stress-strain behavior over the entire strain range for a typical polymeric material.....	28
Figure 2.15 The stresses on the sample during flexural testing	29
Figure 2.16 Principle of X-Ray diffraction.....	32
Figure 3.1 Chemical structure of Ethylene Glycol	37
Figure 3.2 Chemical structure of Propylene Glycol	38
Figure 3.3 Chemical structure of Diethylene Glycol	38
Figure 3.4 Chemical structure of Maleic Anhydride.....	39
Figure 3.5 Cloisite® selection chart from Southern Clay Products	40
Figure 3.6 Chemical structures of the quaternary ammonium and the anion, chloride used in the manufacture of Cloisite 30B	41
Figure 3.7 Chemical structures of the quaternary ammonium and the anion, methyl sulfate used in the manufacture of Cloisite 25A	42
Figure 3.8 Chemical structures of the quaternary ammonium and the anion, chloride used in the manufacture of Cloisite 15A	42
Figure 3.9 Chemical structure of Styrene	43
Figure 3.10 Flowchart of the glycolysis of PET	45
Figure 3.11 Flowchart of UP-MMT nanocomposites preparation	47

Figure 3.12 Tensile test specimen	50
Figure 3.13 Three-point loading diagram.....	51
Figure 3.14 Charpy-type impact instrument.....	52
Figure 4.1 X-ray diffraction patterns of nanocomposites synthesized by ethylene glycol containing 1 and 3 wt. % organoclay (Cloisite 30B).....	55
Figure 4.2 X-ray diffraction patterns of nanocomposites synthesized by propylene glycol containing 1, 3 and 5 wt. % organoclay (Cloisite 30B).....	55
Figure 4.3 X-ray diffraction patterns of nanocomposites synthesized by diethylene glycol containing 1, 3 and 5 wt. % organoclay (Cloisite 30B).....	56
Figure 4.4 X-ray diffraction patterns of nanocomposites prepared by different types of glycols containing 1 wt. % organoclay (Cloisite 30B).....	57
Figure 4.5 X-ray diffraction patterns of nanocomposites prepared by different types of glycols containing 3 wt. % organoclay (Cloisite 30B).....	58
Figure 4.6 X-ray diffraction patterns of nanocomposites prepared by different types of glycols containing 5 wt. % organoclay (Cloisite 30B).....	58
Figure 4.7 X-ray diffraction patterns of nanocomposites prepared by ethylene glycol and different types of organoclays (1 wt. % organoclay)	59
Figure 4.8 X-ray diffraction patterns of nanocomposites prepared by propylene glycol and different types of organoclays (1 wt. % organoclay)	60
Figure 4.9 X-ray diffraction patterns of nanocomposites prepared by diethylene glycol and different types of organoclays (1 wt. % organoclay)	60
Figure 4.10 SEM micrographs of pure unsaturated polyesters synthesized by (a) EG ×250, (b) EG ×3000, (c) PG ×250, (d) PG ×3000, (e) DEG ×250, (f) DEG ×3000.....	64

Figure 4.11 SEM micrographs of unsaturated polyester nanocomposites containing 1 wt. % Cloisite 30B synthesized by (a) EG ×250, (b) EG ×3000, (c) PG ×250, (d) PG ×3000, (e) DEG ×250, (f) DEG ×3000.	65
Figure 4.12 SEM micrographs of unsaturated polyester nanocomposites containing 3 wt. % Cloisite 30B synthesized by (a) EG ×250, (b) EG ×3000, (c) PG ×250, (d) PG ×3000, (e) DEG ×250, (f) DEG ×3000.	66
Figure 4.13 SEM micrographs of unsaturated polyester nanocomposites containing 5 wt. % Cloisite 30B synthesized by (a) PG ×250, (b) PG ×3000, (c) DEG ×250, (d) DEG ×3000.....	67
Figure 4.14 SEM micrographs of unsaturated polyester nanocomposites synthesized by EG containing 1 wt. % organoclay; (a) Cloisite 30B ×250, (b) Cloisite 30B ×3000, (c) Cloisite 25A ×250, (d) Cloisite 25A ×3000, (e) Cloisite 15A ×250, (f) Cloisite 15A ×3000.	68
Figure 4.15 SEM micrographs of unsaturated polyester nanocomposites synthesized by PG containing 1 wt. % organoclay; (a) Cloisite 30B ×250, (b) Cloisite 30B ×3000, (c) Cloisite 25A ×250, (d) Cloisite 25A ×3000, (e) Cloisite 15A ×250, (f) Cloisite 15A ×3000.	69
Figure 4.16 SEM micrographs of unsaturated polyester nanocomposites synthesized by DEG containing 1 wt. % organoclay; (a) Cloisite 30B ×250, (b) Cloisite 30B ×3000, (c) Cloisite 25A ×250, (d) Cloisite 25A ×3000, (e) Cloisite 15A ×250, (f) Cloisite 15A ×3000.	70
Figure 4.17 Isomerization of maleate to fumarate	71
Figure 4.18 Effect of glycol type on the stress-strain curves of pure unsaturated polyesters.....	72
Figure 4.19 Effect of glycol type on the stress-strain curves of nanocomposites containing 1 wt. % organoclay (Cloisite 30B).....	73
Figure 4.20 Effect of glycol type on the stress-strain curves of nanocomposites containing 3 wt. % organoclay (Cloisite 30B).....	73
Figure 4.21 Effect of glycol type on the stress-strain curves of nanocomposites containing 5 wt. % organoclay (Cloisite 30B).....	74

Figure 4.22 Effect of organoclay (Cloisite 30B) content on the stress-strain curves of nanocomposites prepared by EG	75
Figure 4.23 Effect of organoclay (Cloisite 30B) content on the stress-strain curves of nanocomposites prepared by PG	75
Figure 4.24 Effect of organoclay (Cloisite 30B) content on the stress-strain curves of nanocomposites prepared by DEG	76
Figure 4.25 Effect of organoclay (Cloisite 30B) content on the tensile strength values of nanocomposites prepared by different glycol types.....	77
Figure 4.26 Effect of organoclay (Cloisite 30B) content on the tensile modulus values of nanocomposites prepared by different glycol types.....	78
Figure 4.27 Effect of organoclay (Cloisite 30B) content on the tensile strain at break values of nanocomposites prepared by different glycol types.....	78
Figure 4.28 Effect of organoclay type (1 wt. %) on the stress-strain curves of nanocomposites prepared by EG	79
Figure 4.29 Effect of organoclay type (1 wt. %) on the stress-strain curves of nanocomposites prepared by PG	80
Figure 4.30 Effect of organoclay type (1 wt. %) on the stress-strain curves of nanocomposites prepared by DEG	80
Figure 4.31 Effect of organoclay type (1 wt. %) on the tensile strength values of nanocomposites prepared by different glycol types	81
Figure 4.32 Effect of organoclay type (1 wt. %) on the tensile modulus values of nanocomposites prepared by different glycol types	82
Figure 4.33 Effect of organoclay type (1 wt. %) on the tensile strain at break values of nanocomposites prepared by different glycol types.....	83
Figure 4.34 Effect of glycol type on the flexural stress-strain behavior of pure unsaturated polyesters.....	85
Figure 4.35 Effect of glycol type on the flexural stress-strain behavior of nanocomposites containing 1 wt. % organoclay (Cloisite 30B).....	85
Figure 4.36 Effect of glycol type on the flexural stress-strain behavior of nanocomposites containing 3 wt. % organoclay (Cloisite 30B).....	86
Figure 4.37 Effect of glycol type on the flexural stress-strain behavior of nanocomposites containing 5 wt. % organoclay (Cloisite 30B).....	86

Figure 4.38 Effect of organoclay (Cloisite 30B) content on the flexural stress-strain behavior of nanocomposites prepared by EG	87
Figure 4.39 Effect of organoclay (Cloisite 30B) content on the flexural stress-strain behavior of nanocomposites prepared by PG	88
Figure 4.40 Effect of organoclay (Cloisite 30B) content on the flexural stress-strain behavior of nanocomposites prepared by DEG	88
Figure 4.41 Effect of organoclay (Cloisite 30B) content on the flexural strength values of nanocomposites prepared by different glycol types.....	90
Figure 4.42 Effect of organoclay (Cloisite 30B) content on the flexural modulus values of nanocomposites prepared by different glycol types.....	90
Figure 4.43 Effect of organoclay (Cloisite 30B) content on the flexural strain at maximum stress values of nanocomposites prepared by different glycol types	91
Figure 4.44 Effect of organoclay type (1 wt. %) on the flexural stress-strain behavior of nanocomposites prepared by EG	92
Figure 4.45 Effect of organoclay type (1 wt. %) on the flexural stress-strain behavior of nanocomposites prepared by PG	92
Figure 4.46 Effect of organoclay type (1 wt. %) on the flexural stress-strain behavior of nanocomposites prepared by DEG	93
Figure 4.47 Effect of organoclay type (1 wt. %) on the flexural strength values of nanocomposites prepared by different glycol types	93
Figure 4.48 Effect of organoclay type (1 wt. %) on the flexural modulus values of nanocomposites prepared by different glycol types	94
Figure 4.49 Effect of organoclay type (1 wt. %) on the flexural strain at maximum stress values of nanocomposites prepared by different glycol types	95
Figure 4.50 Effect of organoclay (Cloisite 30B) content on the impact strength values of nanocomposites prepared by different glycol types.....	96
Figure 4.51 Effect of organoclay type (1 wt. %) on the impact strength values of nanocomposites prepared by different glycol types	97
Figure A.1 X-ray diffraction pattern of Cloisite 30B	106
Figure A.2 X-ray diffraction pattern of Cloisite 25A	106
Figure A.3 X-ray diffraction pattern of Cloisite 15A	107

Figure A.4	X-ray diffraction pattern of pure unsaturated polyester synthesized by ethylene glycol	107
Figure A.5	X-ray diffraction pattern of nanocomposite synthesized by ethylene glycol containing 1 wt. % Cloisite 30B	108
Figure A.6	X-ray diffraction pattern of nanocomposite synthesized by ethylene glycol containing 3 wt. % Cloisite 30B	108
Figure A.7	X-ray diffraction pattern of nanocomposite synthesized by ethylene glycol containing 1 wt. % Cloisite 25A	109
Figure A.8	X-ray diffraction pattern of nanocomposite synthesized by ethylene glycol containing 1 wt. % Cloisite 15A	109
Figure A.9	X-ray diffraction pattern of pure unsaturated polyester synthesized by propylene glycol	110
Figure A.10	X-ray diffraction pattern of nanocomposite synthesized by propylene glycol containing 1 wt. % Cloisite 30B.....	110
Figure A.11	X-ray diffraction pattern of nanocomposite synthesized by propylene glycol containing 3 wt. % Cloisite 30B.....	111
Figure A.12	X-ray diffraction pattern of nanocomposite synthesized by propylene glycol containing 5 wt. % Cloisite 30B.....	111
Figure A.13	X-ray diffraction pattern of nanocomposite synthesized by propylene glycol containing 1 wt. % Cloisite 25A.....	112
Figure A.14	X-ray diffraction pattern of nanocomposite synthesized by propylene glycol containing 1 wt. % Cloisite 15A.....	112
Figure A.15	X-ray diffraction pattern of pure unsaturated polyester synthesized by diethylene glycol.....	113
Figure A.16	X-ray diffraction pattern of nanocomposite synthesized by diethylene glycol containing 1 wt. % Cloisite 30B.....	113
Figure A.17	X-ray diffraction pattern of nanocomposite synthesized by diethylene glycol containing 3 wt. % Cloisite 30B.....	114
Figure A.18	X-ray diffraction pattern of nanocomposite synthesized by diethylene glycol containing 5 wt. % Cloisite 30B.....	114
Figure A.19	X-ray diffraction pattern of nanocomposite synthesized by diethylene glycol containing 1 wt. % Cloisite 25A.....	115
Figure A.20	X-ray diffraction pattern of nanocomposite synthesized by diethylene glycol containing 1 wt. % Cloisite 15A.....	115

CHAPTER 1

INTRODUCTION

In materials science, a composite implies that the material has a structure comprising two or more different phases. They offer unusual combinations of stiffness, strength and weight that is difficult to attain separately from the individual components. Nanocomposites, on the other hand, are a relatively new class of materials with ultrafine phase dimensions, typically of the order of a few nanometers [1]. Polymer nanocomposites, especially polymer-layered silicate nanocomposites, represent a radical alternative to conventionally (macroscopically) filled polymers. Because of their nanometer-size dispersion, the nanocomposites exhibit markedly improved properties when compared with the pure polymers or conventional composites. These include increased modulus and strength, decreased gas permeability, increased solvent and heat resistance and decreased flammability [2].

Poly(ethylene terephthalate) is one of the versatile engineering plastics which is used to manufacture films and bottles for packaging. PET does not create a direct hazard to the environment, but due to its substantial volumes in the waste stream it is seen as a noxious material [3]. The literature is full of with studies on both synthesis of unsaturated polyesters based on glycolysis of PET and UP-clay nanocomposites. However, there is only one study that reports the properties and formation mechanism of UP nanocomposite based on recycled PET [4].

Unsaturated polyesters are the most versatile class of thermosetting polymers which are macromolecules consisting of unsaturated prepolymers dissolved in unsaturated vinyl monomers. Polyesters, if used as matrix for composite production, have improved tensile and flexural values; their sensitivity to brittle fracture is usually improved [5].

In this study, the effects of glycol type, organoclay type and concentration, on the final properties of nanocomposites composed of organically modified clay and

unsaturated polyester produced from glycolysis of poly(ethylene terephthalate) were investigated.

In this context, first recycled PET was glycolysed and after that the nanocomposites were prepared by "in-situ polymerization" method. In the "in-situ method", the organoclay is added to the reaction medium simultaneously with the monomers. The penetration of the monomers into the clay layers is followed by polymerization. Then, prepolymers were dissolved in a reactive vinyl monomer, styrene and the resin was cured to obtain a 3D network structure.

Mechanical tests were performed for characterizing the nanocomposites. These included the investigation of tensile strength, tensile modulus, tensile strain at break, flexural strength, flexural modulus, flexural strain at maximum stress and impact strength. The morphology was analyzed by X-Ray Diffraction and Scanning Electron Microscopy in order to investigate the extent of dispersion of the filler in the matrix.

CHAPTER 2

BACKGROUND

2.1 Poly(ethylene terephthalate), PET

Poly(ethylene terephthalate) is one of the most versatile engineering plastics. The extensive range of products is used in applications starting from textile and industrial fibers sector, through films and container packaging up to technical thermoplastics [6]. The chemical structure of PET is given in Figure 2.1.

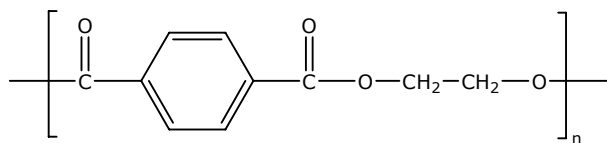


Figure 2.1 Chemical structure of PET

2.1.1 Formation Mechanism

PET is usually prepared by polymerization of ethylene glycol (EG) with terephthalic acid (TA) or its dimethyl ester, dimethyl terephthalate (DMT). The reaction is carried out in two stages. The first stage involves the reaction of terephthalic acid or dimethyl terephthalate with ethylene glycol to produce dimers and trimers with two hydroxyl end groups.

Figure 2.2 shows the preparation of PET via acid route and Figure 2.3 shows the preparation of PET via ester interchange.

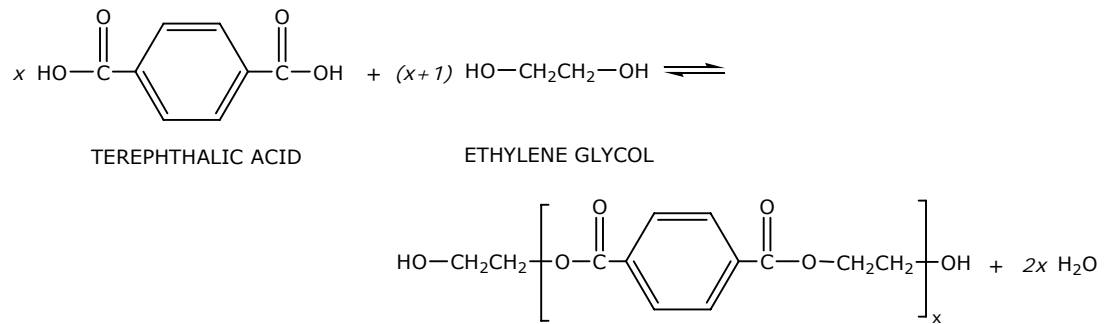


Figure 2.2 PET formation via acid route

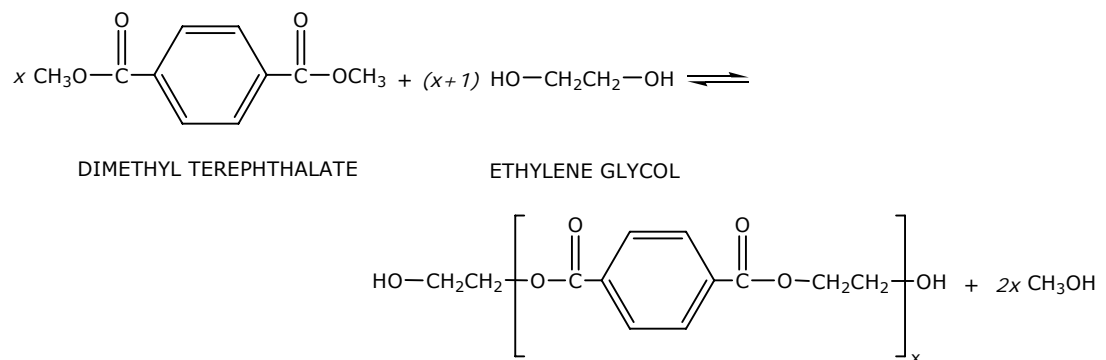


Figure 2.3 PET formation via ester interchange

Both reactions are equilibrium reactions with low equilibrium constants (<1), and therefore water and methanol have to be continuously removed in order to shift the equilibrium towards the products. The products resulting from the first stage are similar for both polymerization routes.

The second stage (Figure 2.4) involves adding an antimony catalyst to the system and increasing the temperature. The equilibrium constant is also low in this case and EG has to be removed efficiently in order to obtain high molecular weight PET. Generally lower molecular weight material ($M_n \sim 20000$) is used for fiber applications, with other applications using higher molecular weights.

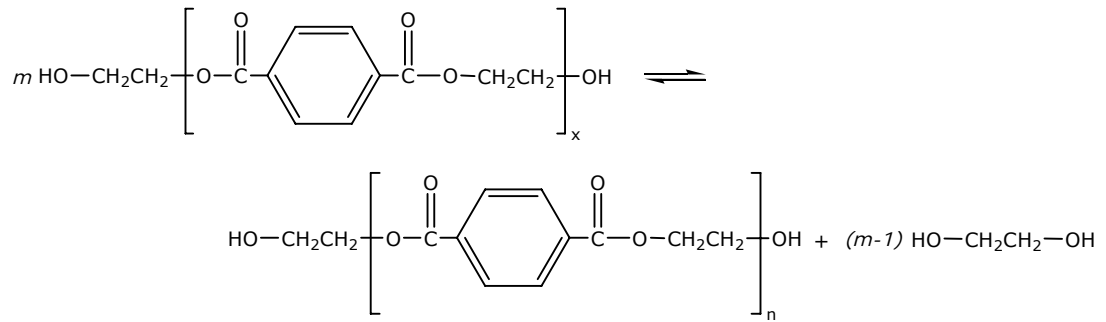


Figure 2.4 High temperature esterification [7]

2.1.2 Product Description and Uses

PET is a linear molecule that exists either in an amorphous or a crystalline state. The great variety of uses for PET, both unblended (blow moldings) and in a large number of blends (especially in the case of textiles), is achieved by selective adjustment of these two phases, to yield considerable variability in properties. For example, good mechanical properties, such as high strength and stiffness, are achieved by orientation of the linear molecular chains and simultaneous crystallization [6].

PET is used in a variety of products, such as textile fibers, tire cord, bottles and containers, audio and video films, medical x-ray films, film for blister packaging, transparent sheets for signage, thermoformed articles and injection molded engineering components [8].

2.2 Recycling of Plastics

2.2.1 Introduction

Plastics recycling has focused mainly on plastics packaging and primarily on plastic bottles and containers. Plastics packaging is considered a significant component of the solid-waste stream. Packaging has an estimated life cycle of less than one year. As a consequence, plastics packaging continuously enters the solid-waste stream on a short turnaround time [9].

There are four types of recycling processes: primary, secondary, tertiary and quaternary. Each depends on the level of contamination of the plastic, its composition and, ultimately, the type of product it will become [10].

- *Primary Recycling* is the conversion of scrap plastics by standard processing methods into products having performance characteristics equivalent to the original products made of virgin plastics. The technology is practiced mainly in the manufacturing sector for recycling in-plant scrap. Historically, the recycling of in-plant scrap has not been considered part of plastics recycling since such a scrap does not normally enter the solid-waste stream.
- *Secondary Recycling* is the conversion of scrap or waste plastics by one or a combination of process operations into products having less demanding performance requirements than the original material [9].
- *Tertiary Recycling* involves converting plastic waste into a chemical feedstock, which can be reprocessed into new plastics [10].
- *Quaternary Recycling* produces energy by burning plastic waste. This process is the most common and widely used in recycling. The reason this process is widely used is because of the high heat content of most plastics [11].

2.2.2 PET Recycling

Poly(ethylene terephthalate) (PET) is the most frequently recycled plastic material. The growing interest in PET recycling is due to the wide-spread use of packaging made of this polymer, mainly as bottles. Since the middle of the 1970s, first in the USA and Canada and subsequently in Western Europe, increased quantities of PET are used for the production of soft drink bottles, and a further increase in its application in this area is predicted.

PET does not create a direct hazard to the environment, but due to its substantial fraction by volume in the waste stream and its high resistance to the atmospheric and biological agents, it is seen as a noxious material. Ecological as well as economic considerations advocate the introduction of wide-scale PET recycling, similar to the recycling of traditional materials such as glass, paper or metals [12].

2.2.2.1 Chemical Recycling Methods

Mechanical recycling (primary or secondary recycling) is the preferred route for plastics recycling because it preserves the maximum value contained in the plastic waste. However, it is often severely limited by factors such as contamination, progressive degradation of properties, marketing of the resulting products, etc.

On the other hand, combustion is a very efficient method for the disposal of large volumes of plastic wastes, but it only allows a small part of the overall value of the waste to be reclaimed.

Between these two extremes, chemical recycling (tertiary recycling) is another option, which allows the recovery of more value from the plastic wastes than incineration, and overcomes some of the problems that limit mechanical recycling.

Different technological approaches are used to the chemical recycling of PET. Methanolysis, hydrolysis and glycolysis are mainly applied on a commercial scale [7].

2.2.2.1.1 Methanolysis

This process consists of the degradation of PET by methanol at high temperatures and under high pressure conditions (Figure 2.5). The main products of PET methanolysis are dimethyl terephthalate (DMT) and ethylene glycol (EG). The reaction is catalyzed by typical transesterification catalysts such as zinc acetate, magnesium acetate, cobalt acetate and lead dioxide; however, the most commonly used catalyst is zinc acetate.

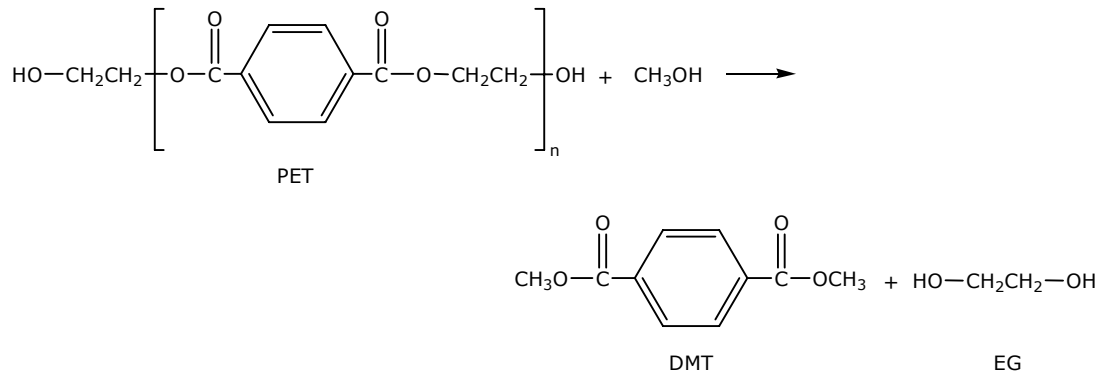


Figure 2.5 Methanolysis of PET [12]

Methanolysis is cumbersome, involving a large number of unit operations, such as crystallization, filtration distillation, besides being hazardous due to the use of an explosive chemical like methanol [8]. On the other hand, this process has the advantage of being relatively insensitive to all kind of contaminants, additives, modifying components, colorants, etc., and in combining the recrystallization and distillation stages used in the purification of the DMT [6]. The possibility of locating an installation for methanolysis, in the polymer production line, is another advantage of this method. In this way, waste PET arising in the production cycle is utilized and the monomers recovered are used in the manufacture of full value polymer [12].

2.2.2.1.2 Hydrolysis

Various hydrolysis processes have been proposed to recover TA and EG from PET.

a. Acid Hydrolysis

Although the application of other concentrated mineral acids is permissible, acid hydrolysis is performed most frequently using concentrated sulfuric acid. In the first stage, the ground PET waste is mixed with sulfuric acid of a concentration not less than 87 wt%. As a result of dissolution and PET degradation to TA and EG, an oily, viscous liquid is obtained. It is introduced into an aqueous solution of sodium hydroxide, in order to neutralize TA and raise the system's pH. The solution obtained has a dark coloration and contains TA in the form of sodium

salt soluble in water, sodium sulfate, EG and sodium hydroxide as well as a small amount of insoluble impurities, which are filtered off using traditional methods. If there is such a need, it is possible to remove the coloration of the filtrate using ion-exchange columns. The next stage of the process is the acidification of the solution, in order to reprecipitate TA. After filtering, washing off with water and drying TA a purity of >99% is obtained.

A substantial drawback of PET hydrolysis by concentrated sulfuric acid is the high corrosivity of the reaction system and the generation of large quantities of waste inorganic salts and aqueous wastes [12].

b. Alkaline Hydrolysis

Alkaline hydrolysis is usually carried out with the use of an aqueous solution of NaOH. The reaction proceeds slowly; therefore, amines with dissociation constant $K > 10^{-5}$ can be used to accelerate the process [12]. The sodium terephthalate obtained is diluted with water, stored and purified, and then TA is precipitated by acidification with sulfuric acid, filtered, washed and dried. TA is recovered in a yield close to 100% at the end of the process.

It is claimed that this process allows treatment of recycled PET whatever the color of the feedstock and even in the presence of other polymers (up to 10% of, for example, polyvinyl chloride (PVC)) and of contaminants such as oil, paper, glue [7].

c. Neutral Hydrolysis

Neutral hydrolysis is carried out with the use of water or steam. The process usually runs at a pressure of 1-4 MPa at temperatures of 200-300°C. The ratio by weight of PET to water is from 1:2 to 1:12.

Its drawback is that all mechanical impurities present in the polymer are left in the TA; thus, the product has a considerably worse purity than the product of acid or alkaline hydrolysis. Consequently, a much more sophisticated purification process is necessary. During the hydrolysis of PET, a substantial volume of diluted EG is generated, which can be recovered through extraction or by distillation [12].

2.2.2.1.3 Glycolysis

This is the most cost effective and commercially viable process for chemical recycling of PET waste. The process can be operated in a batch or continuous mode [8]. PET degradation is carried out most frequently using ethylene glycol, diethylene glycol, propylene glycol and dipropylene glycol. The process is conducted in a wide range of temperatures 180-250°C, during a time period of 0.5-8 h. Usually, 0.5% by weight of catalyst (acetates of zinc, manganese, cobalt, sodium or calcium) in relation to the PET content is added [12].

When EG is used in large excess, the process converts the waste into monomer, bis(hydroxyethyl) terephthalate (BHET) and oligomers (Figure 2.6). The glycolysis reaction conditions are required to be optimized to control the amount of BHET vs. higher oligomers and the formation of DEG as a byproduct [8].

BHET can be obtained in high yield (>90%) and with a high degree of purity. Pure BHET can be added into the reactor of the second polymerization stage to produce new PET or it could be used in different chemical processes [7].

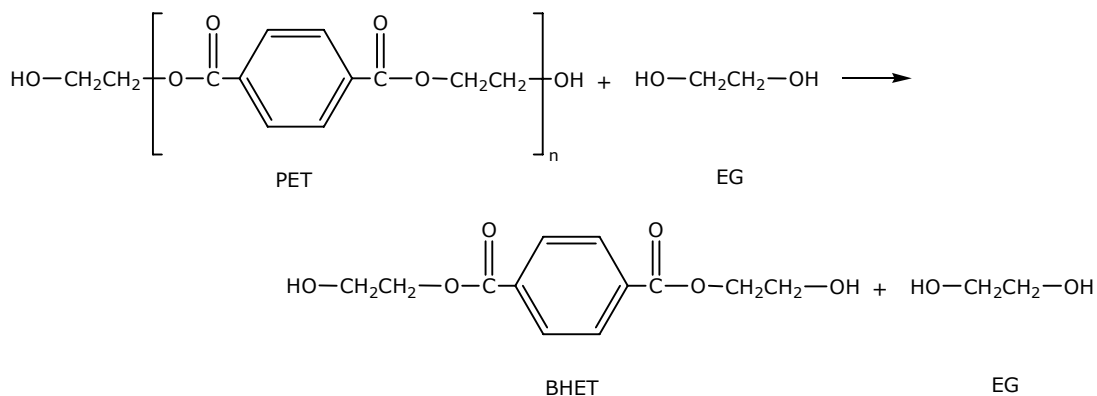


Figure 2.6 Glycolysis of PET with EG [12]

If the glycolysis of the waste is carried out with propylene glycol, then a mixture of monomers is formed, containing molecules with hydroxyethylene and hydroxypropylene end groups. Such a glycolysed product can then be converted into an unsaturated polyester (UP) resin via reaction with maleic anhydride. The resulting polyester, when mixed with a cross-linking agent like styrene, gives UP resins with high chemical and thermal resistance.

The hydroxyl terminated glycolysed waste products also can be converted into polyester polyols via reaction with dicarboxylic acids or anhydrides. The resulting polyols are then used for formulating polyurethane resins for making foam or elastomeric products by reaction with a range of diisocyanates [8].

Glycolysis is mainly suitable for clean scrap and scrap that may possibly have been pre-treated to remove adhering contaminants. Such scrap would stem from integrated polyesters, fiber or film production and its composition and origin would be known. Post consumer PET bottles may also be used, provided it has been cleaned and carefully checked to reduce the risk of introducing unwanted contaminants into production [6].

2.3 Unsaturated Polyesters

Unsaturated polyesters (UP) are linear polycondensation products based on unsaturated and saturated acids/anhydrides and diols or oxides. These resins are generally pale yellow oligomers with a low degree of polymerization. Depending on the chemical composition and the molecular weight (1200-3000 g/mol), these oligomers may be viscous liquids or brittle solids. The unsaturation in the backbone provides sites for reaction with vinyl monomers using free-radical initiators, leading to the formation of a three-dimensional network. The solutions of unsaturated polyesters and vinyl monomers which are reactive diluents are known as UP resins [13].

2.3.1 Synthesis of Unsaturated Polyester Resins

Unsaturated polyester resins are synthesized by the polycondensation reaction of unsaturated and saturated dicarboxylic acids or anhydrides with glycols [14]. In the case of the general-purpose polyester, these components usually consist of phthalic acid, maleic acid and propylene glycol [15]. On the other hand, recycled poly(ethylene terephthalate), which offers excellent properties at potentially lower cost, is finding wider use as a raw material component [16].

The unsaturated acid provides the sites for cross-linking, the saturated acid determines the degree of spacing or concentration of the unsaturated acid

molecules along the polyester chains and the glycol, of course, provides the means for esterification and for bridging the acids to form a polymer [15].

The obtained unsaturated polyester prepolymer is then mixed with a polymerizable unsaturated monomer such as styrene. Styrene not only can act as solvent but also copolymerize with the unsaturated groups along the polyester chains. Curing reaction occurs in the presence of a polymerization catalyst such as an organic peroxide [14, 15].

2.3.2 Classification of Unsaturated Polyester Resins

Polyester resins may be classified on the basis of their structure as *ortho*-resins, *iso*-resins, bisphenol-A fumarates, chlorendics and vinyl ester resins.

a. *Ortho*-Resins

They comprise the largest group of polyester resins which are known as the general-purpose resins. They are synthesized with *ortho*-phthalic anhydride (PA), maleic anhydride (MA) and glycols. PA is relatively low in price and provides an inflexible link in the backbone. However, it reduces the thermal resistance of laminates. Limited chemical resistance and processability are other problems associated with these resins [13]. The glycol generally controls required performance; the phthalic-maleic anhydride ratio is adjusted to modify the reactivity according to fabrication needs [16].

b. *Iso*-Resins

They are prepared using *iso*-phthalic acid (IPA), MA/fumaric acid and glycol. These resins are higher in cost than *ortho*-resins and also have considerably higher viscosities; hence a higher proportion of reactive diluent (styrene) is needed. The presence of higher quantities of styrene imparts improved water and alkali resistance to the cured resins. *Iso*-phthalic resins are thus of higher quality since they have better thermal and chemical resistance and mechanical properties.

c. Bisphenol-A Fumarates

Derivatives of bisphenol-A form the basis for two distinct resin groups that demonstrate superior thermal and corrosion resistance. The addition product of propylene oxide and bisphenol-A, reacted with fumaric acid and dissolved in styrene monomer, has established commercial significance in applications involving extreme corrosive environments [16]. The introduction of bisphenol-A in the backbone imparts a higher degree of hardness and rigidity and improvement in thermal performance.

d. Chlorendics

For chlorendics, to enhance flame retardancy, chlorine/bromine-containing anhydrides or phenols are used in the preparation of UP resins. For example, reaction of chlorendic anhydride/chlorendic acid with MA/fumaric acid and glycol yields the resin with better flame retardancy than general-purpose UP resin. Other monomers used include tetrachloro or tetrabromophthalic anhydride.

e. Vinyl Ester (VE) Resins

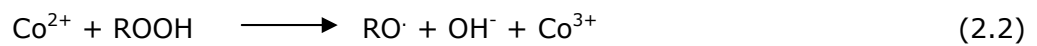
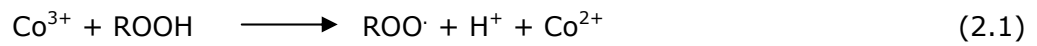
Bisacryloxy or bismethacryloxy derivatives of epoxy resins contain unsaturated sites only in the terminal position and the prepared by reaction of acrylic acid or methacrylic acid with epoxy resin. The viscosity of neat resins is high; hence, reactive diluent (e.g., styrene) is added to obtain a lower viscosity solution. Notable advances in VE resin formulations are low-styrene-emission resins, automotive grades with high tensile strength and heat deflection temperature and materials for corrosion resistance [13].

2.3.3 Curing of Unsaturated Polyester Resins

The curing reaction of unsaturated polyester resins is a free-radical chain growth cross-linking polymerization between the reactive diluent (e.g., styrene monomer) and UP resin. Polyester molecules are the cross-linkers, while styrene serves as an agent to link the adjacent polyester molecules [13].

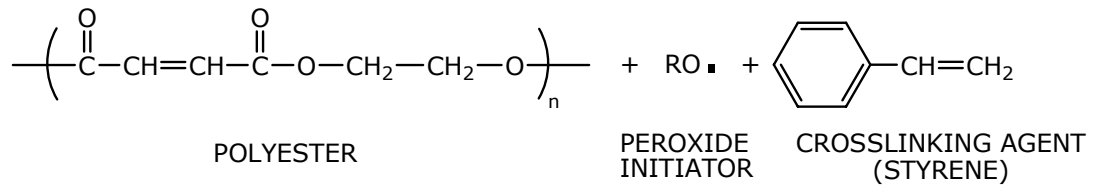
Hydroquinone is widely used in commercial resins to provide stability during the dissolution of the hot prepolymer in styrene. The addition polymerization

reaction between the unsaturated prepolymer and the styrene monomer is initiated by free-radical catalysts usually benzoyl peroxide (BPO) or methyl ethyl ketone peroxide (MEKP), which can be dissociated by heat or redox metal activators like cobalt naphthenate into peroxy and hydroperoxy free radicals. The reaction takes the following course (Equations 2.1 and 2.2):

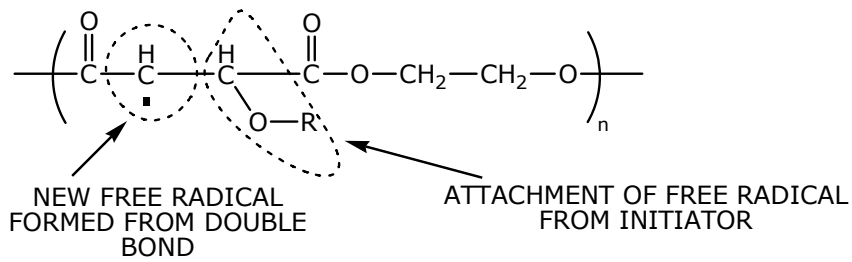


This catalyst system is temperature sensitive and does not function effectively at temperatures below 10°C, but at temperatures over 35°C the generation of free radicals can be too prolific, giving rise to incomplete cross-linking formation [16]. Figure 2.7 shows a schematic view of cross-linking reaction of unsaturated polyester.

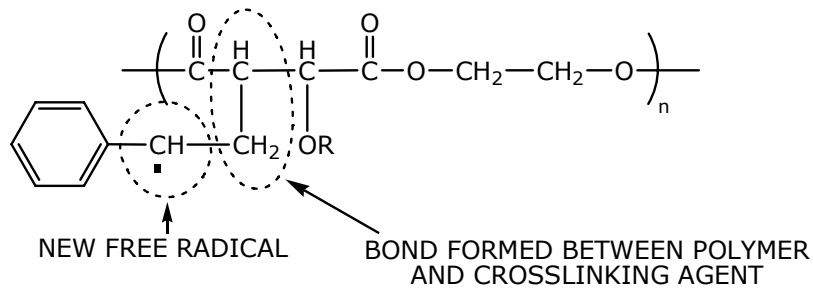
REACTANTS



INITIATION STEP



BRIDGING STEP



CROSSLINKED POLYMERS

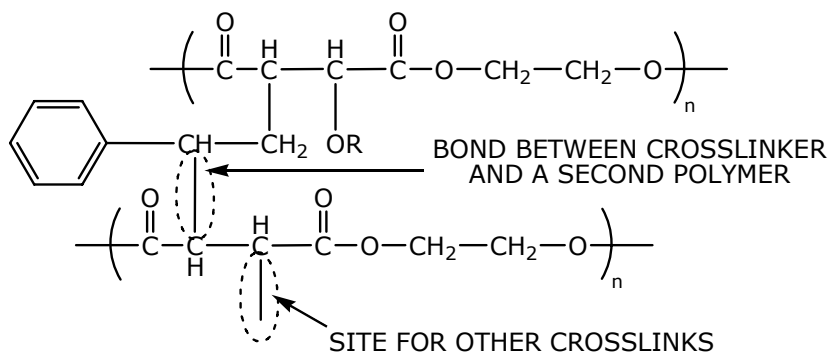


Figure 2.7 Schematic view of cross-linking reaction of unsaturated polyester [17]

The curing process of unsaturated polyester resins can be divided into five stages;

a. Induction Stage

This stage is caused by the presence of inhibitor which consumes the radicals generated by initiators. Because of the high reaction rate constant between the radical and the inhibitor, propagation of radicals is suppressed by the inhibition effect. Radical concentration remains at a constant value because of the balance between radical generation and inhibition effect [18]. This temporary induction period between catalysis and the change to a semisolid gelatinous mass is referred to as "gelation time" and can be controlled between 1-60 min by varying stabilizer and catalyst levels [16].

b. Primary Polymer (Microgel) Formation Stage

As the amount of inhibitor is reduced to a very low level at the end of the induction period, monomeric radicals gain the chance to link with adjacent monomers and form primary polymers. The microgels can be described as weakly cross-linked networks. The radical concentration starts to increase gradually and reaches a constant rate because of the formation of stable radicals during the microgel formation stage.

c. Transition Stage

In this stage, intermolecular reaction occurs among microgels to form larger clusters. The number of microgels reaches a high level and the amount of unreacted UP monomers decreases to such a level that the ratio between the pendant vinylene and the unreacted UP monomers is very high. Consequently, pendant vinylene groups of microgels start to react with other microgels. Phase separation can occur in this stage due to the changes of resin composition and phase boundary. If there is no phase separation, both microgels and clusters can be found in this stage.

d. Macrogelation Stage

As the polymerization progresses, more and more microgels form and the resin system reaches the gel point. At the gel point, a cross-linking network is formed through either the intermolecular reaction among microgels, microgel clusters or dispersed UP-rich domains. For systems with very strong phase separation, macrogelation can occur through the phase inversion process.

e. Post-gelation Stage

The radical concentration increases at a constant rate at the beginning of the post-gelation stage then gradually levels off at the end of reaction. The final radical concentration depends on the cross-linking density of the resin system. The styrene-end stable radicals appear in this stage and dominate the radical population at the end of the reaction [18].

2.3.4 Application Areas of Unsaturated Polyesters

Unsaturated polyesters constitute a wide variety of materials with different chemical structures and mechanical properties, since a large amount of different glycols and unsaturated as well as saturated acids can be used to design different polymers. The composition of the prepolymer and the curing process can also be tailored for a specific purpose [14]. Some special chemicals such as plasticizers, antioxidants, heat and ultraviolet stabilizers and flame retarders can be added to the resin depending on the area of application.

One of the early uses of unsaturated polyesters was to produce cast items such as knife and umbrella handles, encapsulation of electronic assemblies and embedding decorative specimens. The most important casting application is the manufacture of pearl buttons. Another important application is to manufacture floor-tiles by mixing UP resin with fillers such as limestone, baryte, silica and china clay and pigments. Polyester compounds can be formulated for the manufacture of bathroom fixtures such as tubs and lavatories and also vanity tops, bar tops, kitchen tops and panels. Coating of concrete, pipe or cast-iron for corrosion control can be successfully accomplished by using UP resins.

UP-based composites have extensive applications in manufacture of tanks, containers, automobile bumpers, aircraft components, office, household and outdoor furniture, caskets and sporting equipment. UPs find also large applications in the optical and electrical industries [19].

2.4 Composites

Since the early 1960's, there has been an increasing demand for materials that are stiffer and stronger, yet lighter in aeronautic, energy, civil engineering and in various structural applications. Unfortunately, no monolithic material is available to satisfy them. This need and demand certainly led to the concept of combining different materials in an integral composite structure [5]. The goal in creating a composite is to combine similar or dissimilar materials in order to develop specific properties that are related to desired characteristics.

A composite is a combined material created by the synthetic assembly of two or more components, a selected filler or reinforcing agent and a compatible matrix binder, in order to obtain specific characteristics and properties. Many of the properties of the resulting composites are superior to those of their components. Although it is composed of several different materials, the composite itself behaves as a single product [20].

2.4.1 Matrix

The matrix in a composite can be thought of as performing two major roles. First, it transfers loads to the reinforcement. Secondly, it protects the reinforcement from adverse environmental effects. Matrix materials are generally polymers, ceramics or metals [17].

2.4.1.1 Polymer Matrix Composites

Polymers are the most developed matrix materials, and they find widespread applications owing to the ease of fabrication into any large complex shape [5]. The polymer matrices, also called resins, are usually divided into two general classifications, thermosets and thermoplastics. Thermosets have historically been

the principal matrix material for composites although thermoplastics use is now increasing in many applications [17].

Thermoplastics soften when heated and harden when cooled. These processes are totally reversible and may be repeated. These materials are normally fabricated by the simultaneous application of heat and pressure. Most linear polymers and those having some branched structures with flexible chains are thermoplastics [21].

Conversely, thermosets are crosslinked and shaped during the final fabrication step, after which they do not soften by heating. They have a covalently-bonded, insoluble and infusible three dimensional network structure [5]. Once formed, these crosslinked networks resist heat softening, creep, and solvent attack. Such properties make thermosets suitable materials for composites, coating and adhesive applications [22].

2.4.2 Reinforcement

The reinforcing component in a composite structure can be either fibrous, powdered, spherical, crystalline or whiskered and either an organic, inorganic, metallic or ceramic material. The choice of reinforcing agent varies depending to a great extent on the requirements of the end item and method of fabrication.

Reinforcing agents offer a variety of benefits; increased strength and stiffness, heat resistance, heat conductivity, stability, wet strength, fabrication mobility, viscosity, abrasion resistance and impact strength; reduced cost, shrinkage, exothermic heat, thermal expansion coefficient, porosity and crazing; and improved surface appearance. However, reinforcing agents also possess disadvantages. They may limit the method of fabrication, inhibit curing of certain resins and shorten the pot life of the resin [20].

2.5 Nanocomposites

Nanocomposites are a new class of composites in which the filler dimensions are in the nanometer (10^{-9}) range [23]. International interest and research in nanocomposites has grown dramatically due to unique property enhancements demonstrated in the late 1980s. Significant effects on mechanical, thermal and physical properties have been observed. A key attribute of nanocomposites is the fact that such enhancements are achievable at very low volume fractions (as low as 3-5%) [24].

Three types of nanocomposites can be distinguished, depending on how many dimensions of the dispersed particles are in the nanometer range:

- When the three dimensions are in the order of nanometers, they are called isodimensional nanoparticles, such as spherical silica nanoparticles.
- When two dimensions are in the nanometer scale and the third is larger, they form elongated structures like nanotubes or whiskers.
- When only one dimension is in nanometer range, the filler is present in the form of sheets of one to a few nanometer thick to hundreds to thousands nanometers long.

The third type constitutes the family of composites, which can be gathered under the name of polymer-layered silicate nanocomposites [25].

2.6 Polymer Layered Silicate Nanocomposites

Layered silicates dispersed as a reinforcing phase in an engineering polymer matrix are one of the most important forms of nanocomposites [26]. Owing to the high aspect ratio of the layered silicates, mechanical, thermal, flame retardant and barrier properties are enhanced without significant loss of clarity, toughness or impact strength [27].

Polymer nanocomposites, especially polymer-layered silicate nanocomposites, represent a radical alternative to conventionally (macroscopically) filled

polymers. Because of their nanometer-size dispersion, the nanocomposites exhibit markedly improved properties when compared with the pure polymers or conventional composites [2]. Uses for this new class of materials can be found in aerospace, automotive, electronics and biotechnology applications, to list only a few [28].

2.6.1 Layered Silicates

There is a wide variety of both synthetic and natural crystalline fillers that are able, under specific conditions, to intercalate a polymer. Amongst all the potential nanocomposite precursors, those based on clays and layered silicates have been more widely investigated probably because the starting clay minerals are easily available and because their intercalation chemistry has been studied for a long time [25].

The commonly used layered silicates for the preparation of polymer layered silicate nanocomposites belong to the same general family of 2:1 phyllosilicates. Their crystal structure consists of layers made up of two tetrahedrally coordinated silicon atoms fused to an edge-shared octahedral sheet of either aluminum or magnesium hydroxide [29]. Their structure is shown in Figure 2.8.

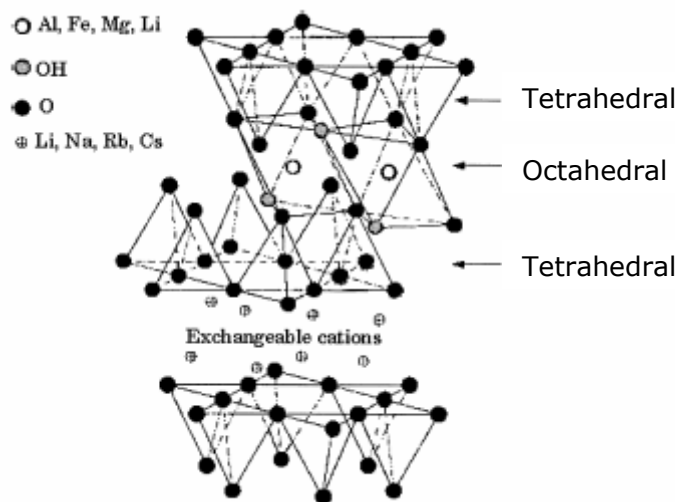


Figure 2.8 Structure of 2:1 phyllosilicates [25]

The layer thickness is around 1nm, and the lateral dimensions of these layers may vary from 30nm to several microns or larger, depending on the particular layered silicate. Stacking of the layers leads to a regular van der Waals gap between the layers called the interlayer or gallery [29]. Isomorphic substitutions within the layers (for example, Al^{3+} replaced by Mg^{2+} or by Fe^{2+} , or Mg^{2+} replaced by Li^+) generate negative charges that are counterbalanced by alkali or alkaline earth cations situated in the interlayer [25].

For a given clay, the maximum amount of cations that can be taken up is constant and is known as the cation-exchange capacity (CEC). It is measured in milliequivalents per gram (meq/g) and more frequently per 100g (meq/100g). The CEC of montmorillonite varies from 80 to 150 meq/100g. Because of its suitable layer charge density, montmorillonite is nowadays the most widely used clay as nanofiller [30].

2.6.1.1 Cation-Exchange Process

Pristine layered silicates usually contain hydrated Na^+ or K^+ ions. Obviously, in the pristine state, layered silicates are only miscible with hydrophilic polymers. To render layered silicates miscible with other polymer matrices, one must convert the normally hydrophilic silicate surface to an organophilic one, making the intercalation of many engineering polymers possible. Generally, this can be done by ion-exchange reactions with cationic surfactants including primary, secondary, tertiary and quaternary alkylammonium or alkylphosphonium cations [29].

The cation-exchange process between the alkylammonium ions and the cations initially intercalated between the clay layers is shown in Figure 2.9.

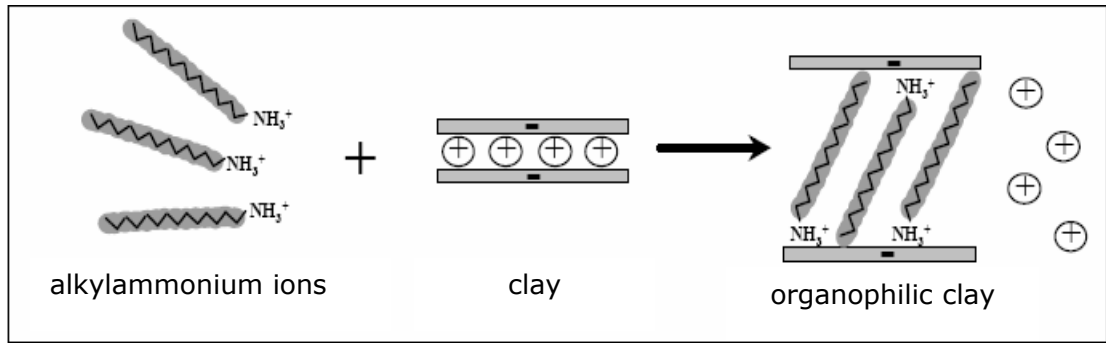


Figure 2.9 The cation-exchange process between alkylammonium ions and cations initially intercalated between the clay layers [30]

The role of the alkylammonium cations in the organosilicates is to lower the surface energy of the inorganic component and improve the wetting characteristics with the polymer. Additionally, the alkylammonium cations can provide functional groups that can react with the polymer or initiate polymerization of monomers to improve the strength of the interface between the inorganic component and the polymer [2].

2.6.2 Synthesis of Nanocomposites

2.6.2.1 In-Situ Polymerization Method

It is the conventional process used to synthesize thermoset-clay nanocomposites (Figure 2.10). First, the organoclay is swollen in the monomer. This step requires a certain amount of time, which depends on the polarity of the monomer molecules, the surface treatment of the organoclay, and the swelling temperature. Then, the reaction is initiated. For thermosets such as epoxies or unsaturated polyesters, a curing agent or a peroxide, respectively, is added to initiate the polymerization. For thermoplastics, the polymerization can be initiated either by the addition of a curing agent or by an increase of temperature.

During the swelling phase, the high surface energy of the clay attracts polar monomer molecules so that they diffuse between the clay layers. When a certain equilibrium is reached the diffusion stops and the clay is swollen in the monomer to a certain extent. When the polymerization is initiated, the monomer starts to

react with the curing agent. This reaction lowers the overall polarity of the intercalated molecules and displaces the thermodynamic equilibrium so that more polar molecules are driven between the clay layers. As this mechanism occurs, the organic molecules can eventually delaminate the clay.

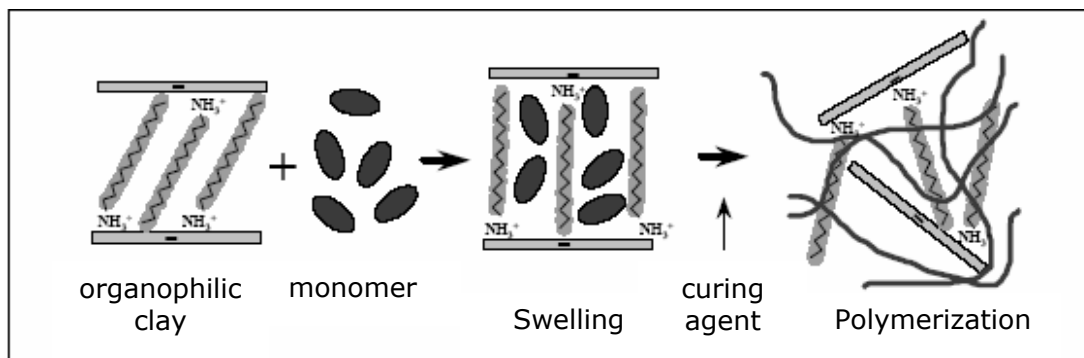


Figure 2.10 The in-situ polymerization [30]

Polymer-clay nanocomposites based on epoxy, unsaturated polyester, polyurethanes and polyethylene terephthalate have been synthesized by this method [30].

2.6.2.2 Solution Intercalation Method

This is based on a solvent system in which the polymer is soluble and the silicate layers are swellable. The layered silicate is first swollen in a solvent, such as water, chloroform or toluene. When the polymer and layered silicate solutions are mixed, the polymer chains intercalate and displace the solvent within the interlayer of the silicate. Upon solvent removal, the intercalated structure remains resulting in polymer layered silicate nanocomposite [29]. Solution intercalation method is shown in Figure 2.11.

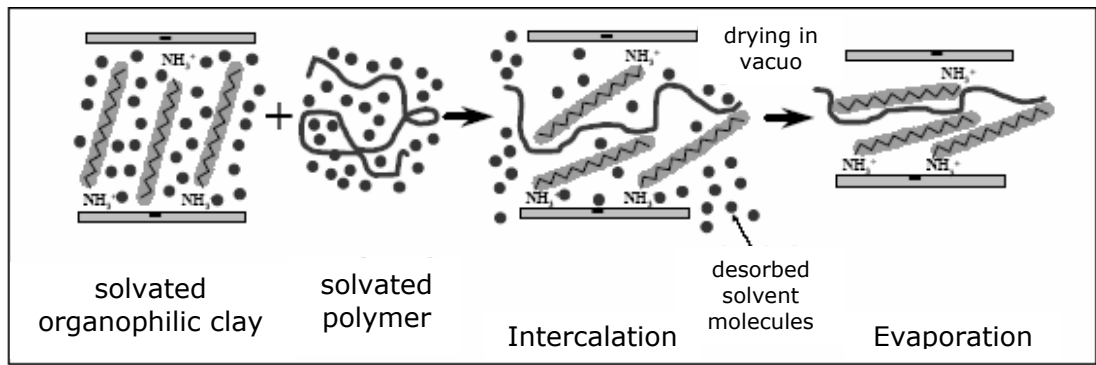


Figure 2.11 The solution intercalation method [30]

Nanocomposites based on high-density polyethylene, polyimide and nematic liquid crystal polymers have been synthesized by this method [30].

2.6.2.3 Melt Intercalation Method

The layered silicate is mixed with the polymer matrix in the molten state. Under these conditions and if the layer surfaces are sufficiently compatible with the chosen polymer, the polymer can crawl into the interlayer space and form either an intercalated or an exfoliated nanocomposite [25]. Melt intercalation method is shown in Figure 2.12.

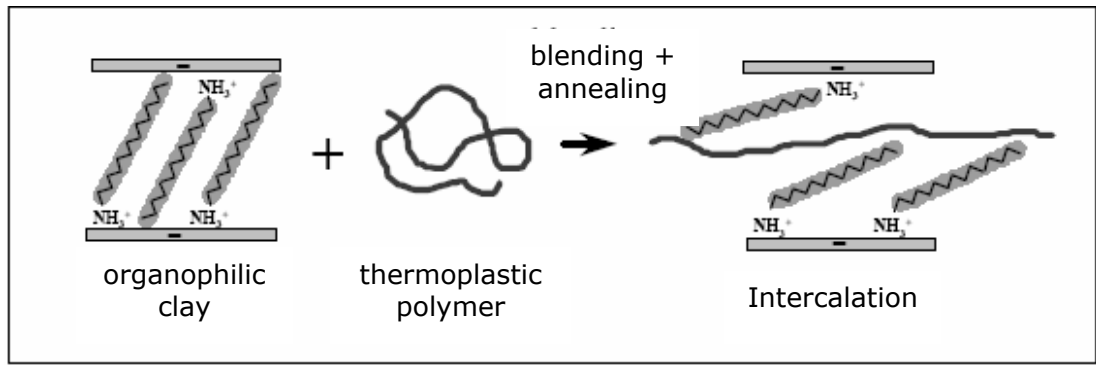


Figure 2.12 The melt intercalation method [30]

A wide range of thermoplastics, from strongly polar polyamide 6 to styrene have been intercalated between clay layers by this method [30].

2.6.3 Nanocomposite Structures

Depending on the nature of the components used (layered silicate, organic cation and polymer matrix) and the method of preparation, three main types of composites may be obtained when a layered clay is associated with a polymer. Figure 2.13 shows the types of nanocomposite structures.

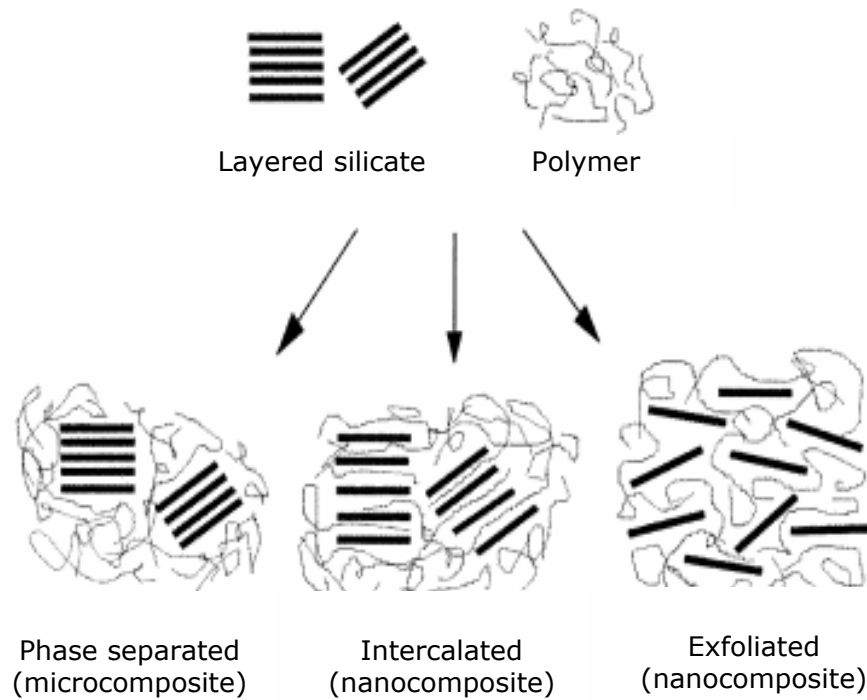


Figure 2.13 Schematic illustrations of a phase-separated, an intercalated and an exfoliated polymer-layered silicate nanocomposites [25]

- When the polymer is unable to intercalate between silicate sheets, a *phase separated composite* is obtained whose properties stay in the same range as traditional microcomposites [25].
- *Intercalated nanocomposites* contain self-assembled, well-ordered multilayer structures where the extended polymer chains are inserted into the gallery space between parallel individual silicate layers.

- *Exfoliated nanocomposites* consists of individual nanometer-thick silicate layers suspended in a polymer matrix, and result from extensive penetration of the polymer within and delamination of the crystallites [31].

The key to the performance of nano-clays is how well they can be dispersed into a polymer matrix. The fully dispersed form is most useful for the majority of commercial applications and is the one that is normally aimed for, although conventional processing methods often give mixed structures [32].

2.7 Characterization

2.7.1 Mechanical Properties

2.7.1.1 Tensile Tests

Standard test method for tensile properties (ASTM D638M-91a) employs samples of a specified shape, typically a dogbone, as depicted in Figure 3.12. The sample is clamped at one end and pulled at a constant rate of elongation until the center of the specimen fails [33].

The initial length of a central section contained within the narrow region of the tensile specimen is called the initial gauge length, L_0 . During deformation, force F , is measured as a function of elongation at the fixed end by means of a transducer. Usually, the tensile response is plotted as nominal stress σ , versus nominal strain ϵ ,

$$\sigma = F/A_0 \quad (2.3)$$

$$\epsilon = \Delta L/L_0 \quad (2.4)$$

where A_0 is the original (undeformed) cross-sectional area of the gauge region and ΔL is the change in sample gauge length ($L-L_0$) due to the deformation [22].

Figure 2.14 represents the stress-strain behavior over the entire strain range for a typical polymeric material.

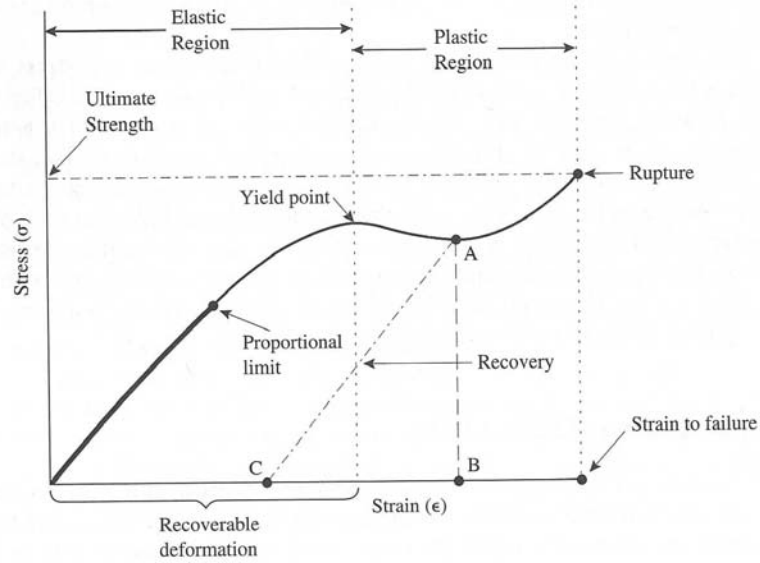


Figure 2.14 Stress-strain behavior over the entire strain range for a typical polymeric material [34]

Tensile stress (nominal), σ is the tensile load per unit area of minimum original cross-section, within the gauge boundaries, carried by the test specimen at any given moment. It is expressed in force per unit area, usually megapascals, (Equation 2.3).

Tensile strength (nominal), σ_m is the maximum tensile stress sustained by the specimen during a tension test. When the maximum stress occurs at the yield point, it is designated tensile strength at yield. When the maximum stress occurs at break, it is designated tensile strength at break.

Tensile strain, ϵ is the ratio of the elongation to the gauge length of the test specimen, that is, the change in length per unit of original length. It is expressed as a dimensionless ratio (Equation 2.4).

It is seen in Equation 2.5 that modulus of elasticity, E is the ratio of stress (nominal) to corresponding strain below the proportional limit of a material. It is expressed in force per unit area, usually megapascals. It is also known as elastic modulus or Young's modulus [35].

$$E = \sigma/\epsilon \tag{2.5}$$

2.7.1.2 Flexural Tests

ASTM D790M-92 test methods cover the determination of flexural properties of unreinforced and reinforced plastics and electrical insulating materials using a three-point or four-point loading system [36].

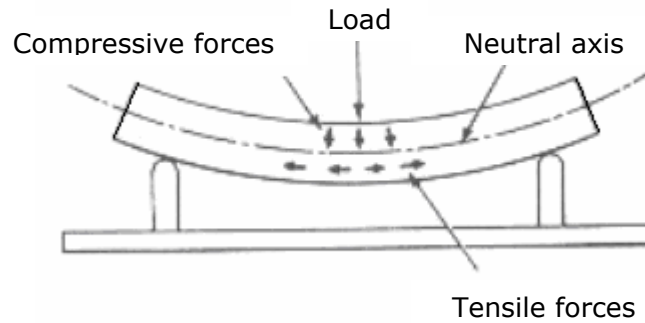


Figure 2.15 The stresses on the sample during flexural testing [37]

Three-point loading system utilizes center loading on a simply supported beam [36]. At the point of loading, the top surface of the specimen is placed in a state of compression, whereas the bottom surface is in tension (Figure 2.15). Stress is computed from the specimen thickness, the bending moment and the moment of inertia of the cross-section. The maximum tensile stress exists at the bottom specimen surface directly below the point of load application [21].

Flexural strength is equal to the maximum stress in the outer fibers at the moment of break. It is calculated by the following equation;

$$S = 3PL/2bd^2 \quad (2.6)$$

where S is the stress in the outer fibers at midspan (MPa), P is the load at a given point on the load-deflection curve (N), L is the support span (mm), b is width of beam tested (mm) and d is depth of beam tested (mm).

The maximum strain in the outer fibers occurs at midspan as well, and may be calculated as follows;

$$r = 6Dd/L^2 \quad (2.7)$$

where r is the maximum strain in the outer fibers (mm/mm), D is the maximum deflection of the center of the beam (mm), L is the support span (mm), and d is depth of beam tested (mm).

The tangent modulus of elasticity (flexural modulus) is the ratio, within the elastic limit of stress to corresponding strain and shall be expressed in megapascals. It is calculated by drawing a tangent to the steepest initial straight-line portion of the load-deflection curve and using Equation 2.8.

$$E_B = L^3m/4bd^3 \quad (2.8)$$

where E_B is modulus of elasticity in bending (MPa), L is support span (mm), b is width of beam tested (mm), d is depth of beam tested (mm), and m is slope of the tangent to the initial straight line portion of the load-deflection curve (N/mm) [36].

2.7.1.3 Impact Tests

Impact tests measure the energy required for failure when a standard specimen receives a rapid stress loading. The impact strength of a polymer can be measured employing a number of techniques including the Izod and the Charpy tests [33]. For both the Izod and Charpy tests a hammerlike weight strikes a specimen and the energy-to-break is determined from the loss in the kinetic energy of the hammer. Other variations include the falling ball or dart test, whereby the energy-to-break is determined from the weight of the ball and the height from which it is dropped [22].

The most popular impact tests are Izod and Charpy impact tests specified in ASTM D256-92 [38]. In this study, Charpy impact test was applied to the test specimens in order to determine their impact strengths.

2.7.2 Scanning Electron Microscopy (SEM)

Due to the great depth of focus, relatively simple image interpretation and ease of sample preparation, SEM is the preferred technique for viewing specimen detail at a resolution well exceeding that of the light microscope. The SEM

images vividly display the three-dimensional characteristics of the object surface under examination [39].

In SEM analysis, the surface of a specimen to be examined is scanned with an electron beam and the reflected (or back-scattered) beam of electrons is collected, then displayed at the same scanning rate on a cathode ray tube. The image on the screen, which may be photographed, represents the surface features of the specimen. The surface may or may not be polished and etched, but it must be electrically conductive; a very thin metallic surface coating must be applied to nonconductive materials. Magnifications ranging from 10 to in excess of 50000 diameters are possible [21].

2.7.3 X-Ray Diffraction (XRD)

The method of x-ray diffraction and scattering is one of the oldest and most widely used techniques available for the study of polymer structures. A beam of x-rays incident to a material is partly absorbed and partly scattered, and the rest is transmitted unmodified. The scattering of x-rays occurs as a result of interaction with electrons in the material. The x-rays scattered from different electrons interfere with each other and produce a diffraction pattern that varies with scattering angle. The variation of the scattered and diffracted intensity with angle provides information on the electron density distribution and hence the atomic positions within the material [39]. X-ray diffraction is used to determine the identity of crystalline phases in a multiphase sample and the atomic and molecular structures of single crystals. It can also be used to determine structural details of polymers, fibers, thin films and amorphous solids and to study stress, texture and particle size [16].

In the spectrum of electromagnetic radiation, x-rays lie between the ultraviolet rays and gamma rays. Those x-rays used for structure analysis have wavelengths λ in the range of 0.05-0.25 nm. Most work on polymers is done with the Cu $K\alpha$ emission line, a doublet with an average wavelength equal to 0.154nm [39].

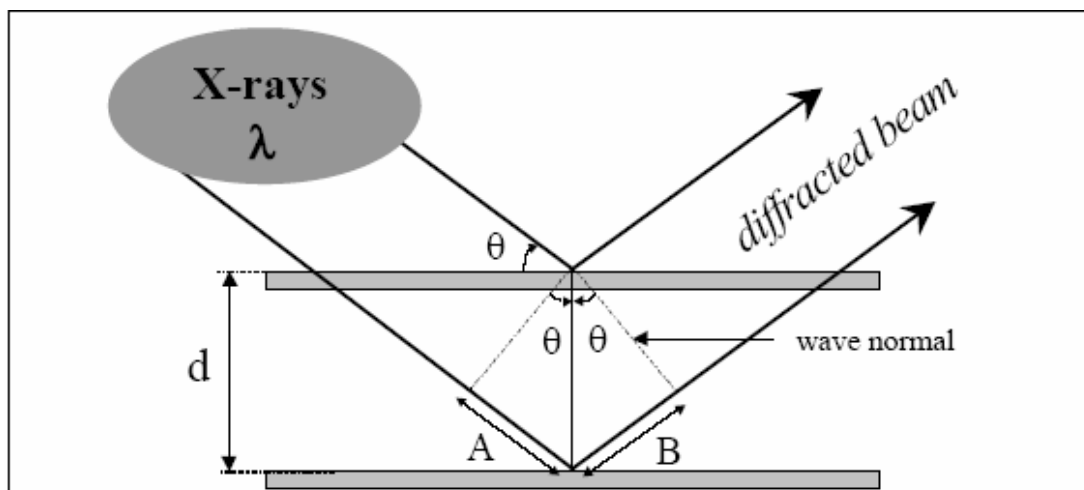


Figure 2.16 Principle of X-Ray diffraction

Figure 2.16 shows the diffraction from two scattering planes (i.e. two consecutive clay layers or other crystallographic planes of the layers themselves) that are separated by a distance d (i.e. interlamellar spacing or d -spacing) and intercept x-rays of wavelength λ at the incident angle θ . The experimental 2θ value is the angle between the diffracted and incoming x-ray waves. The wave normals connect points of identical phase for incident and diffracted waves. Since the direction of d is normal to the planes, and the wave normal is normal to the wavelets, the angles opposite A and B are also θ . Thus, $\sin \theta = A/d = B/d$ so that $(A+B) = 2d\sin\theta$. Thus, a constructive interference occurs when:

$$n\lambda = 2d\sin\theta \quad (2.9)$$

This equation is known as the Bragg Law. The integer n refers to the degree of the diffraction [30].

2.8 Previous Studies

In this study, we have focused on the nanocomposites based on unsaturated polyester resins from glycolized poly(ethylene terephthalate). A lot of studies have been reported in the literature on unsaturated polyesters. Previous studies on unsaturated polyester resins from PET waste and unsaturated polyester-clay nanocomposites are summarized in the following sections.

2.8.1 Unsaturated Polyester Resins from PET Waste

Vaidya and Nadkarni investigated the glycolysis of PET to synthesize unsaturated polyesters. They have many studies on this area. In one of their studies [40], the effect of amount of glycol (PG) on the extent of depolymerization and the nature of the glycolyzed PET were investigated. The processing characteristics like viscosity, gel time, and exotherm temperature of the resins were investigated with respect to the amounts of styrene monomer, initiator and accelerator. The resins were compared with the conventional general purpose resin and were found to be comparable in their processability. The mechanical and dynamic mechanical properties of the PET based resins were reported in the subsequent publication [41]. The mechanical properties (tensile strength, flexural strength, impact strength, hardness) and viscoelastic behavior of the PET waste based resins were found to be comparable with the ordinary grade of general purpose resin. These resins exhibited better heat distortion temperatures compared to the general purpose resin. In another study [42], kinetics of the polycondensation of maleic anhydride with glycolyzed PET waste was reported. It was found that the rates of polyesterification of PET based systems were higher than that of the general purpose resin.

Suh et al. [3] compared the properties of UP prepared by glycolysis of PET with propylene glycol (PG), diethylene glycol (DEG) and their mixture. The cure behaviour and the tensile properties of the cured resin based on glycolysed PET were investigated. It was seen that it was possible to control the extent of depolymerization, gelation time and brittleness of UP resin using different glycol compositions.

Öztürk and Güçlü [43] investigated the curing and mechanical properties of unsaturated polyester resins prepared from glycolysis products of waste PET obtained by using various glycol compounds and their mixture. Ethylene glycol (EG), propylene glycol (PG), diethylene glycol (DEG), triethylene glycol (TEG) and PG-TEG mixture was used in this study. The curing characteristics such as gel time and maximum curing temperatures, and mechanical properties such as hardness, tensile strength and elastic modulus of these resins were investigated. The waste PET resins were compared with the reference resins prepared with the same glycols and the properties of the resins were found to be compatible with the properties of the reference resins. The DEG and TEG based resins were found

to be more flexible than PG based resins. But, PG based resins had higher tensile strength and hardness than DEG and TEG based resins.

Curing behavior of unsaturated polyester resins based on recycled PET has been also studied by researchers. Lu and Kim [44] prepared a typical unsaturated polyester resin based on the glycolized PET products and studied the curing reaction with styrene by differential scanning calorimetry. Lee et al. [45] investigated the effects of recycled PET content and glycol type on the curing behavior. The curing behavior was interpreted from the viewpoint of change in double bond concentration, inherent reactivity and styrene/fumarate ratio of the unsaturated polyester resins.

2.8.2 Unsaturated Polyester-Clay Nanocomposites

Kornmann et al. [46] investigated the possibility to synthesize materials with nanocomposite structure based on montmorillonite (MMT) and unsaturated polyester (UP). The effect of MMT content on mechanical properties was studied. The X-ray and transmission electron microscopy data confirmed the formation of a nanocomposite material and the mechanical properties were improved even with 1.5 vol% MMT content.

Suh et al. [4] studied the property and formation mechanism of glycolised PET based UP-MMT nanocomposite by using two different mixing methods (simultaneous and sequential). In the simultaneous mixing process, the unsaturated polyester chains, styrene monomers and organophilic-treated MMTs were simultaneously mixed. In the sequential mixing process, at first step pre-intercalates of the UP and MMT nanocomposites were prepared. This mixture was then dissolved in styrene. The styrene monomer diffuses between silicate layers more easily than uncured UP chains. Therefore, in the simultaneous mixing method, the total crosslinking density of the samples decreased due to the low concentration of styrene in uncured UP chains. However, in the sequential mixing method, the crosslinking reaction took place homogeneously inside and outside of the silicate layers and crosslinking density reached the degree of the crosslinking density of the cured pure UP.

Bharadwaj et al. [47] investigated the structure-property relationships in crosslinked polyester-clay nanocomposites and found that although there was

firm evidence showing the formation of a nanocomposite structure, the tensile modulus, loss and storage modulus exhibited a progressively decreasing trend with increasing clay concentration due to the progressive decrease in the degree of crosslinking with increasing clay concentration.

İnceoğlu and Yilmazer [27] investigated the effects of unmodified and organically modified MMT on the mechanical properties of MMT/UP nanocomposites. Modified MMTs showed improvements on the mechanical properties with the maximum degree of exfoliation at approximately 3% - 5% clay content. The degree of exfoliation was lower in the unmodified one. It was also observed that ultrasonic bath after mechanical mixing had a positive effect on the Young's modulus, tensile and impact strength of the composites.

Zhang et al. [48] focused on the role of the polymerizable group of quaternary ammonium in improving interfacial interaction between the silicate layers and polymer chains and the mechanical properties of UP-MMT hybrids. The effects of organophilic MMTs obtained from different quaternary ammoniums on the mechanical properties and the structure of unsaturated polyester based nanocomposites were compared.

Fu and Qutubuddin [49] used two polymerizable cationic surfactants for functionalization of MMT and preparation of UP-clay nanocomposites. Characterization of samples was made using X-ray diffraction, transmission electron microscopy and dynamic mechanic analysis techniques.

Oleksy et al. [50] studied the unsaturated polyester compositions containing modified smectites. By using bentonites modified with quaternary ammonium salts as fillers of UP resins, a significant improvement of the stability of UP resins was observed with essentially no change in the reactivity of resins. Mechanical properties of cured composites were also improved, depending on the type of the bentonite used.

Mironi-Harpaz et al. [51] investigated the effects of various mixing processes by using several organically modified clay types. The incorporation of these organoclays resulted in an intercalated structure. Organoclays that exhibited the highest intercalation levels were further studied using a sequential mixing

method. Processing parameters such as mixing modes, applied shearing levels, clay contents and mixing temperatures were investigated.

Xu and Lee [52] studied the kinetic analysis and mechanical properties of nanoclay reinforced UP resins cured at low temperatures. A mechanistic kinetic model based on the free radical copolymerization mechanism was developed to simulate the reaction rate and conversion profiles of UP resins with various nanoclay contents.

CHAPTER 3

EXPERIMENTAL

3.1 Materials

3.1.1 Recycled PET

Recycled PET used in the experiments was supplied by Sasa Company, Adana. Recycled PET was in the form of randomly sized flakes and obtained from bottles. Some basic properties of recycled PET obtained from the producer are given in Table 3.1.

Table 3.1 Properties of recycled PET

Intrinsic Viscosity	0.75 dl/g
T _g	60 °C
T _m	255-260 °C

3.1.2 Glycols

All of the glycols, which were used during the glycolysis reaction of PET, were obtained from Solventaş Company.

3.1.2.1 Ethylene Glycol (EG)

Chemical structure of EG is shown in Figure 3.1 and some of its properties are given in Table 3.2.

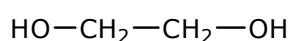


Figure 3.1 Chemical structure of Ethylene Glycol

Table 3.2 Physical properties of Ethylene Glycol

Molecular Weight	62.1 g/mol
Specific Gravity	1.11
Boiling Point	198 °C

3.1.2.2 Propylene Glycol (PG)

Chemical structure of PG is shown in Figure 3.2 and some of its properties are given in Table 3.3.

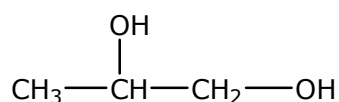


Figure 3.2 Chemical structure of Propylene Glycol

Table 3.3 Physical properties of Propylene Glycol

Molecular Weight	76.09 g/mol
Specific Gravity	1.04
Boiling Point	188.2 °C

3.1.2.3 Diethylene Glycol (DEG)

Chemical structure of DEG is shown in Figure 3.3 and some of its properties are given in Table 3.4.

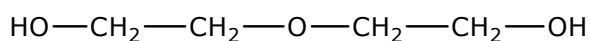


Figure 3.3 Chemical structure of Diethylene Glycol

Table 3.4 Physical properties of Diethylene Glycol

Molecular Weight	106.1 g/mol
Specific Gravity	1.12
Boiling Point	245 °C

3.1.3 Zinc Acetate

Zinc acetate was used as the transesterification catalyst in the glycolysis reaction of PET.

3.1.4 Maleic Anhydride (MA)

Maleic Anhydride used in this study was purchased from Poliya A.Ş. It is available as a white powder. It was used in the polyesterification reaction and provided the unsaturation sites which take part in the cross-linking reaction. Some of its physical properties are given in Table 3.5 and its chemical structure is shown in Figure 3.4.

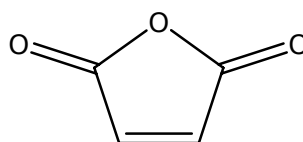


Figure 3.4 Chemical structure of Maleic Anhydride

Table 3.5 Physical properties of Maleic Anhydride

Molecular Weight	98.06 g/mol
Melting Point	52.6 °C
Boiling Point	200 °C

3.1.5 Organoclays

Experiments were carried out with natural montmorillonite organically modified with three different quaternary ammonium salts. These organoclays were purchased from Southern Clay Products. Figure 3.5 shows the organoclay (Cloisite® Nanoclays) selection chart based on polymer/monomer chemistry.

Cloisite® Nanoclays are surface treated to be compatible with a whole host of systems. These organoclays are prepared via ion exchange reaction between Na^+ montmorillonite and a quaternary ammonium salt by the manufacturer. The chart below indicated relative hydrophobicity of the products.

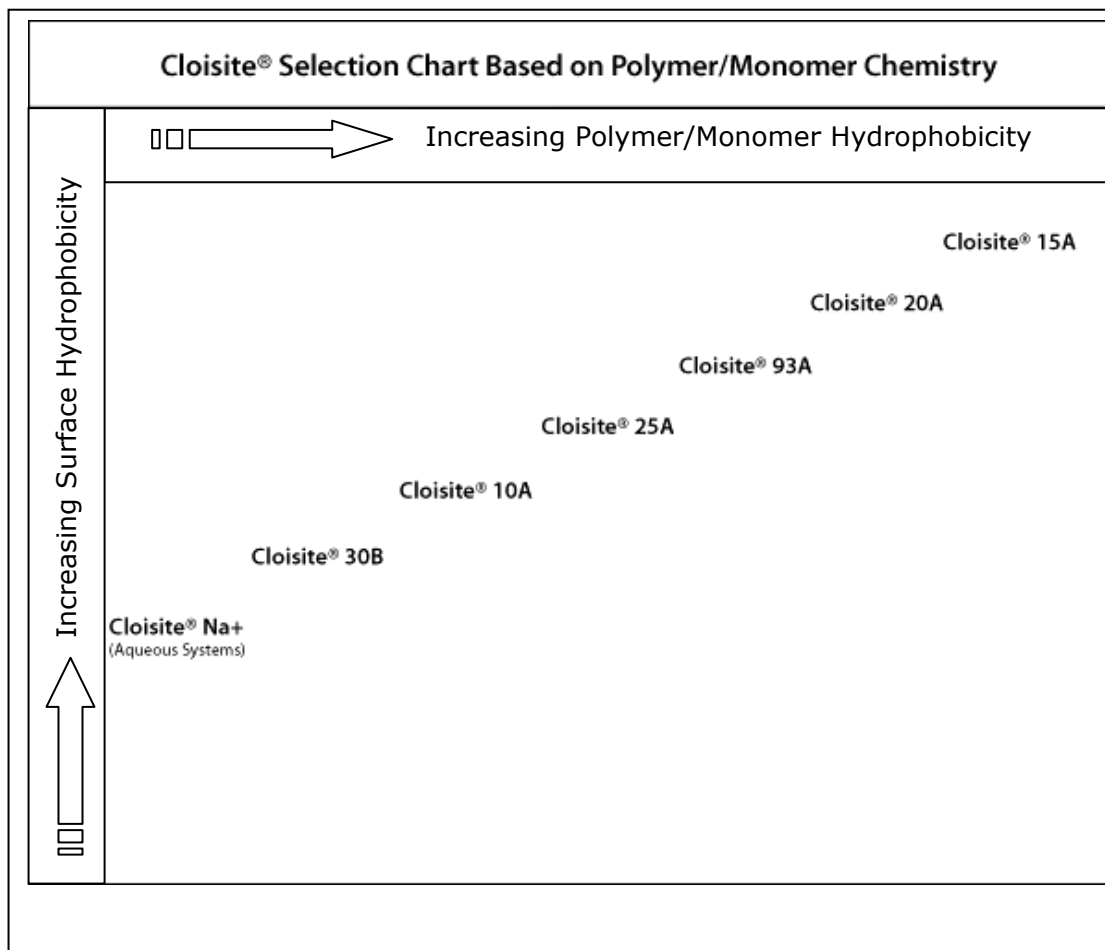


Figure 3.5 Cloisite® selection chart from Southern Clay Products

The structures of the organoclays used in this study are as follows.

3.1.5.1 Cloisite 30B

Figure 3.6 shows the chemical structure of the organic modifier of Cloisite 30B. Some of the physical properties of Cloisite 30B which obtained from the manufacturer are given in Table 3.6.

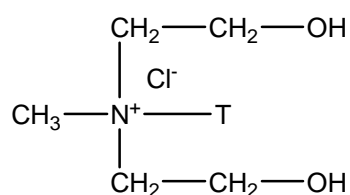


Figure 3.6 Chemical structures of the quaternary ammonium and the anion, chloride used in the manufacture of Cloisite 30B

Table 3.6 Physical data of Cloisite 30B

Organic Modifier	MT2EtOH*
Modifier Concentration	90meq/100g clay
Specific gravity	1.98 g/cm ³
Initial d-spacing	18.5 Å

* MT2EtOH: methyl, tallow, bis-2-hydroxyethyl, quaternary ammonium

T: Tallow (~65%C18; ~30%C16; ~5%C14),

3.1.5.2 Cloisite 25A

The chemical structure of the organic modifier is shown in Figure 3.7 and physical properties of Cloisite 25A are given in Table 3.7.

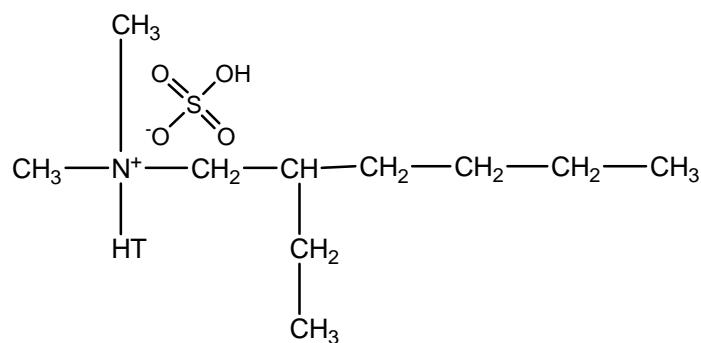


Figure 3.7 Chemical structures of the quaternary ammonium and the anion, methyl sulfate used in the manufacture of Cloisite 25A

Table 3.7 Physical data of Cloisite 25A

Organic Modifier	2MHTL8*
Modifier Concentration	95meq/100g clay
Specific gravity	1.87 g/cm ³
Initial d-spacing	18.6 Å

* 2MHTL8: dimethyl, hydrogenated tallow, 2-ethylhexyl quaternary ammonium
 HT: Hydrogenated tallow (~65%C18; ~30%C16; ~5%C14),

3.1.5.3 Cloisite 15A

The chemical structure of the organic modifier is shown in Figure 3.8 and some of the physical properties of Cloisite 15A are listed in Table 3.8.

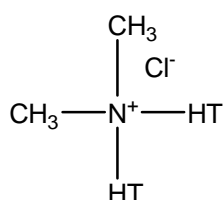


Figure 3.8 Chemical structures of the quaternary ammonium and the anion, chloride used in the manufacture of Cloisite 15A

Table 3.8 Physical data of Cloisite 15A

Organic Modifier	2M2HT*
Modifier Concentration	125meq/100g clay
Specific gravity	1.66 g/cm ³
Initial d-spacing	31.5 Å

* 2M2HT: dimethyl, dihydrogenated tallow, quaternary ammonium
HT: Hydrogenated tallow (~65%C18; ~30%C16; ~5%C14),

3.1.6 Styrene

Styrene, which is a polymerizable monomer, contains C-C reactive double bonds, acts as a curing agent by bridging adjacent polyester molecules at their unsaturation positions. In this study, styrene was supplied by Solventaş Company. Some of its physical properties are given in Table 3.9 and its chemical structure is shown in Figure 3.9.

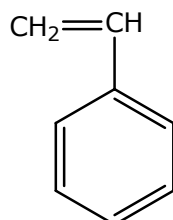


Figure 3.9 Chemical structure of Styrene

Table 3.9 Physical properties of Styrene

Molecular Weight	104.15 g/mol
Specific gravity	0.91
Boiling Point	145 °C

3.1.7 Hydroquinone

Hydroquinone was used to provide stability during the dissolution of the hot polyester resin in styrene as an inhibitor.

3.1.8 Cobalt Naphthenate

Cobalt Naphthenate was purchased from Poliya A.Ş. and is available as 1% solution. It was used as the accelerator in the cross-linking reaction of unsaturated polyester resin.

3.1.9 Methyl Ethyl Ketone Peroxide (MEKP)

Methyl Ethyl Ketone Peroxide was used as the initiator in the cross-linking reaction of the unsaturated polyester resin. It was purchased from Poliya A.Ş. and is available as liquid.

3.1.10 Release Agent

Polywax SV-6 from Poliya A.Ş. was used as the release agent in order to make it easy to take the cured specimens out of the molds.

3.2 Experimental Procedure

3.2.1 Glycolysis Reaction

In the experimental runs, the waste PET, a glycol (ratio of PET:glycol=1:4 mol/mol) and zinc acetate catalyst, 0.5% of PET weight, were mixed together and charged to a glass reactor. The reactor used was a four-necked, round-bottomed flask of 500ml capacity having a reflux condenser, gas bubbler, thermocouple and mechanical stirrer. The reactor was heated for 8h at 185°C for EG and PG, and at 205°C for DEG. The reaction was carried out under reflux in nitrogen atmosphere. After 8h, the glycolyzed products were allowed to cool to room temperature. The flowchart of the glycolysis of PET is shown in Figure 3.10.

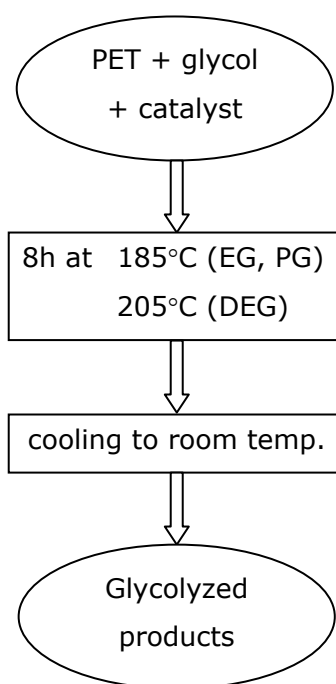


Figure 3.10 Flowchart of the glycolysis of PET

End-group analysis is one of the methods in the determination of the number average molecular weight of the polymers. Generally, the number average molecular weight of the hydroxyl terminated glycolyzed products is measured using the acetylation method. This method takes long time and there is one study that reports the theoretical and experimental hydroxyl values and molecular weights of different glycol based oligomers [53]. All the glycolysis reaction parameters are chosen same as the previous study, thus molecular weights reported in that study can be also used in this study.

Table 3.10 gives the theoretical and experimental molecular weights of oligomers based on different types of glycols. Experimental values were obtained after 8h glycolysis of PET at 185°C for EG and PG, and at 205°C for DEG. From Table 3.10, it is clearly seen that experimental values lie between the molecular weights of monomers and trimers. Thus, it can be concluded that mixtures of monomers, dimers and trimers may exist in the glycolyzed products.

Table 3.10 Theoretical and experimental molecular weights (g/mol) of different glycol based oligomers [53]

		Monomer	Dimer	Trimer
EG based	theoretical	254	446	638
	experimental	291		
PG based	theoretical	268	460	652
	experimental	399		
DEG based	theoretical	298	490	682
	experimental	594		

3.2.2 Preparation of UP-MMT Nanocomposites

The UP-MMT nanocomposites were prepared by reacting the glycolyzed products with maleic anhydride and MMT. The glycolyzed products, maleic anhydride (ratio of hydroxyl:carboxyl=1.1:1) and clay, 0, 1, 3 and 5% wt. with different modifiers, were mixed in the glass reactor having a partial condenser. The reactants were heated at 160°C in nitrogen atmosphere and maintained at that temperature to the end of the reaction. The reaction took nearly 14h. Each hour, 10ml toluene was used as an azeotropic solvent to assist water removal. During the reaction, the acid number of the polymer obtained was determined to monitor the progress of the reaction. When the acid number reached 50 mgKOH/g resin, vacuum was applied for 1 hour in order to remove the residual water from the reactor. 50 ppm hydroquinone was added to styrene, 20% of resin weight, to prevent premature gelation and styrene was heated up to 40-50°C to avoid sudden solidification of the resin. Then the prepolymer-clay mixture was dissolved in 20% wt. styrene. It was mechanically mixed for 3 hours. During mixing the styrene content in the resin was determined by a procedure which will be explained in the latter part of the experimental procedure section. After determining the styrene content, the amount of styrene to obtain 35% wt. of the resin was added to the mixture. An additional ultrasonic mixing with a frequency of 35 kHz was applied for 30min. After that cobalt naphthenate as the accelerator (0.1% wt. of the resin) was added to the resin and mixed for few minutes and vacuum was applied for 20min. Then MEKP, as the initiator, was added (0.1% wt. of the resin) and mixed for ~10s. Finally, after the release agent was applied to the aluminum mold surfaces, the resin was cast into the molds which are shaped according to ASTM standards.

Materials were cured for 4 h at 120°C. The temperature was gradually increased from room temperature to 120°C at the beginning and then cooled from 120°C to room temperature at the end of the curing stage in order to prevent craze and cracks due to sudden crosslinking and cooling. The flowchart of the UP-MMT nanocomposites preparation is shown in Figure 3.11.

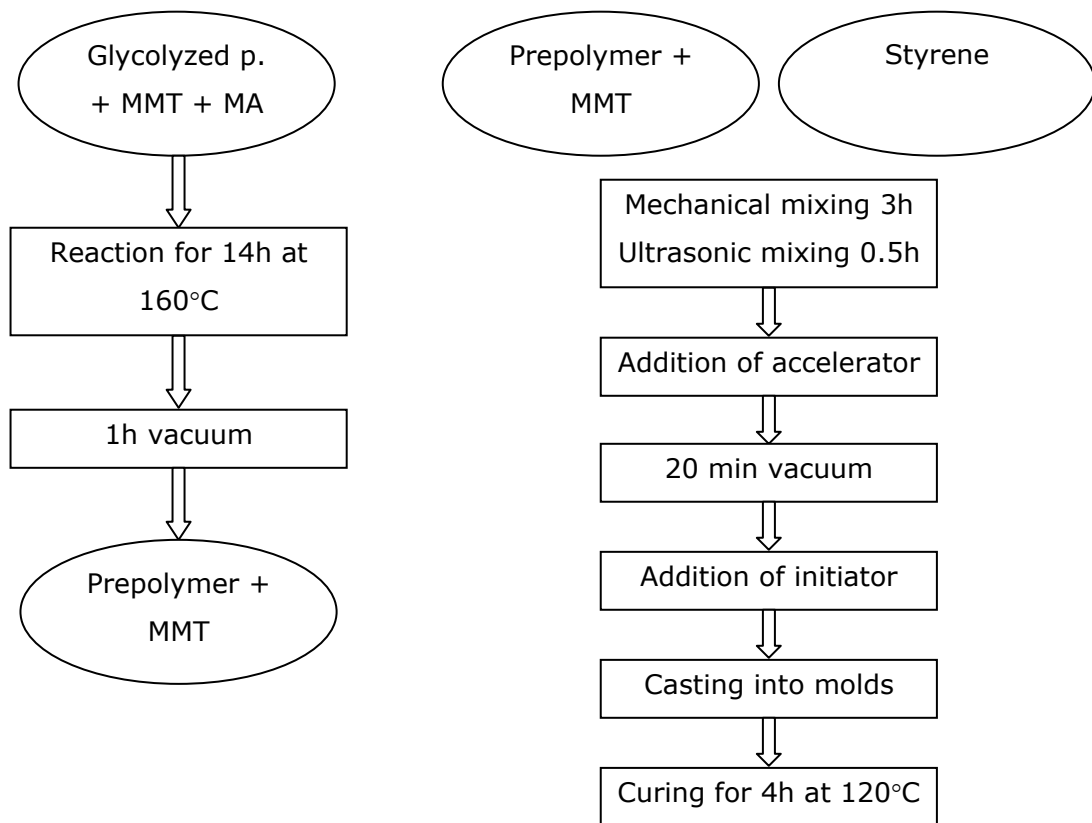


Figure 3.11 Flowchart of UP-MMT nanocomposites preparation

3.2.3 Acid Number Determination

Acid number of a resin is defined as the milligrams of potassium hydroxide (KOH) required to neutralize the free or unreacted carboxyl groups in 1 gram of the resin. It is determined by the following formula [54]:

$$AN = \frac{\text{ml. of KOH} \times \text{normality of KOH} \times 56.1}{\text{wt. of sample in grams}} \quad (3.1)$$

In order to determine the acid number of the resin, during the polycondensation reaction, ~1 g of the prepolymer was dissolved in 50ml, 1/2 (v/v) ethanol/toluene solution and titrated with 0.1N ethanolic KOH solution by using thymol blue indicator until the yellow color turned blue.

The molecular weights (MW_{av}) were calculated by the following formula [54];

$$MW_{av} \text{ (approx.)} = 56100 / \text{acid number} \quad (3.2)$$

3.2.4 Determination of Styrene Percentage in the Resin

The styrene in which the prepolymer would dissolve was calculated as 20 % of the resin. In order to determine the actual amount of styrene in the resin obtained, ~1 g of resin was taken on a watch glass and mixed with 0.2 ml 10% (w/w) hydroquinone/acetone solution by the help of a metal paper clip. The mixture was then heated at 150°C for 1 h. During 1 h time period styrene evaporated and at the end actual amount of styrene in the resin (S/R) was calculated by the Equation 3.3.

$$[(M_2 + M_1) - M_3] / M_2 = S/R \quad (3.3)$$

Since;

$$M_1 = m_{\text{watch glass}} + m_{\text{paper clip}}$$

$$M_2 = m_{\text{resin}} = \sim 1 \text{ g}$$

$$M_3 = (m_{\text{watch glass}} + m_{\text{paper clip}} + m_{\text{resin}}) \text{ after 1 h}$$

S = styrene

R = prepolymer + styrene

In this study, the effects of glycol type, clay type and clay content on the mechanical and structural properties of the nanocomposites produced from glycolized PET and organically modified clay was investigated. All the formulations applied in this study and acid numbers of the resins which determined at the end of the polyesterification reaction are shown in Table 3.11.

Table 3.11 Formulations and acid numbers of the resins

Glycol Type	Clay Type	Clay Content (wt. %)	Acid No.(mg KOH/g resin)
EG	-	0	41
EG	30B	1	35
EG	30B	3	38
EG	25A	1	33
EG	15A	1	44
PG	-	0	44
PG	30B	1	39
PG	30B	3	41
PG	30B	5	39
PG	25A	1	43
PG	15A	1	34
DEG	-	0	37
DEG	30B	1	39
DEG	30B	3	35
DEG	30B	5	38
DEG	25A	1	39
DEG	15A	1	41

During the polymerization reaction, when MMT was added to the system, the mixture began to foam due to motion of the stirrer and heat. At high clay concentrations it was more difficult to control the foam. For this reason, sample containing 5 wt. % Cloisite 30B was not prepared by using EG.

Before mixing, all the organically modified clays were dried under vacuum at 120°C for 4 hours to avoid hydrolytic degradation of materials.

3.3 Characterization

3.3.1 Mechanical Testing Procedure and Equipment

All mechanical tests were performed at room temperature. Ten specimens were tested for each set of experiment. For each series of tests, average results and standard deviations were calculated and reported.

3.3.1.1 Tensile Tests

Tensile tests were performed according to ASTM D638M-91a (Standard Test Method for Tensile Properties of Plastics) by a Lloyd LR 30 K Universal Testing Machine. The shape and the dimensions of the specimens were specified according to Type-II in this standard, which are given in Figure 3.12 and Table 3.12. The crosshead speed of the machine was set at 5 mm/min, which was calculated considering the specimen gauge length of 50 mm and strain rate of 0.1 min^{-1} . After strain-stress diagrams were obtained, tensile strength, tensile modulus and percent strain at break values were calculated.

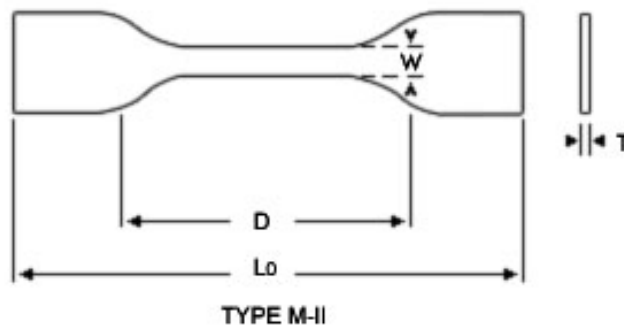


Figure 3.12 Tensile test specimen

Table 3.12 Tensile test specimen dimensions

D – distance between grips	50 mm
L_0 – length overall	115 mm
T – thickness	4 mm
W – width of narrow section	6 mm

3.3.1.2 Flexural Tests

Three-point bending tests were performed according to Test Method-I Procedure A of ASTM D790M-92 (Standard Test Methods for Flexural Properties of Unreinforced and Reinforced Plastics and Electrical Insulating Materials) on rectangular specimens by using a Lloyd 30K Universal Testing Machine. The three-point loading diagram is shown in Figure 3.13.

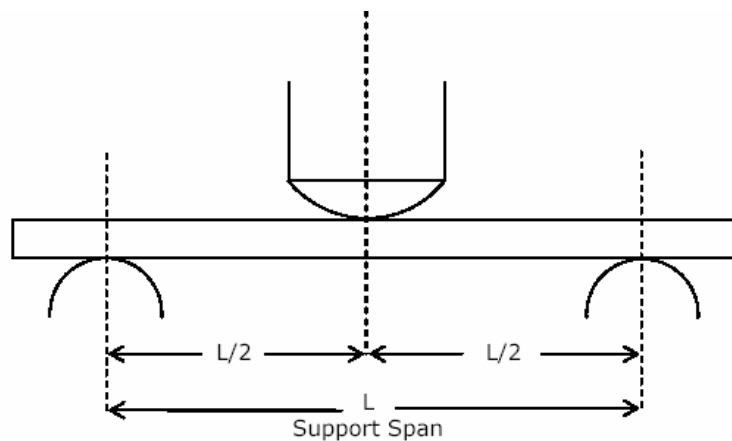


Figure 3.13 Three-point loading diagram

The dimensions of the specimens were $80 \times 11 \times 4$ mm and the support span was 50 mm. The rate of cross-head motion was calculated as 10.42 mm/min according to ASTM standards. For this value of crosshead motion, corresponding strain rate was 0.1 min^{-1} .

3.3.1.3 Impact Tests

Charpy impact tests were performed by using a Pendulum Impact Tester of Coesfeld Material Test, according to the Test Method-I Procedure A in ASTM D256-91a (Standard Test Methods for Impact Resistance of Plastics and Electrical Insulating Materials). Dimensions of the unnotched samples were $50 \times 6 \times 4$ mm. During the test, the sample is supported at both ends and the pendulum of the impact testing machine strikes the sample as shown in Figure 3.14.

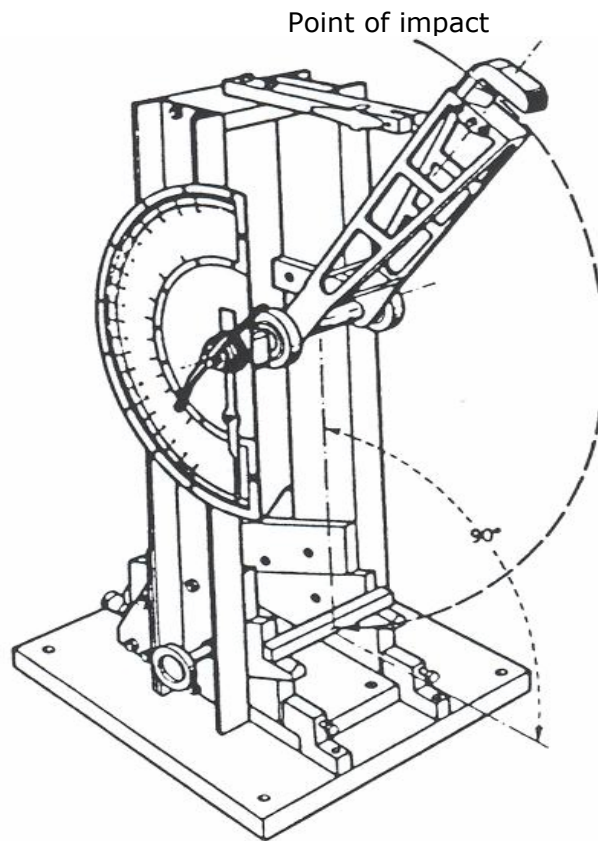


Figure 3.14 Charpy-type impact instrument

3.3.2 Morphological Analysis

3.3.2.1 Scanning Electron Microscopy (SEM) Analysis

A low voltage SEM (JEOL JSM-6400) was used to analyze the impact fractured surfaces of the composites. The fracture surfaces were coated with a thin layer of gold prior to viewing with the scanning electron microscope. The SEM photographs were taken at $\times 250$ and $\times 3000$ magnifications.

3.3.2.2 X-Ray Diffraction (XRD) Analysis

The composites were analyzed by using a RIGAKU D/MAX 2200/PC X-ray diffractometer. $\text{Cu K}\alpha$ ($\lambda = 1.54\text{\AA}$) radiation, generated at a voltage of 40 kV and current of 40mA was used as the X-Ray source. The diffraction angle 2θ was scanned from 1° to 10° at a scanning rate of $1^\circ/\text{min}$ and a step size of 0.01° .

CHAPTER 4

RESULTS AND DISCUSSION

4.1 Morphological Analysis

4.1.1 X-Ray Diffraction (XRD) Analysis

X-ray diffraction analysis is the most straightforward method to characterize the structure of nanocomposites. By monitoring the position, shape and intensity of the basal reflections from the silicate layers, the nanocomposite structure can be identified [29].

Three types of the clay structures are used to describe the dispersion of the clay in a nanocomposite. These are phase separated microcomposites, intercalated nanocomposites and exfoliated nanocomposites. In XRD analysis, microcomposite materials have no change in d-spacing, meaning that no polymer has entered the galleries and that the spacing between the clay layers is unchanged. Intercalated nanocomposites have an increased d-spacing, indicating that polymer has entered the galleries, expanding the layers. Exfoliated nanocomposites show no peak in XRD, suggesting that a great amount of polymer has entered the gallery space, expanding the clay layers randomly [55].

The d-spacing and 2θ values obtained from the XRD analysis of the Cloisite 30B containing samples are given in Table 4.1 with respect to glycol type and clay loading.

Table 4.1 X-ray diffraction results of all compositions prepared by Cloisite 30B*

Glycol Type	Organoclay wt. %	d-spacing (Å)	2θ (deg)
EG	1	exfoliated	-
	3	37.23	2.37
PG	1	41.43	2.13
	3	40.29	2.19
	5	39.39	2.24
DEG	1	39.93	2.21
	3	exfoliated	-
	5	35.73	2.47

* The original d-spacing of Cloisite 30B is 17.94 Å and 2θ value is 4.92 deg.

Figure 4.1 shows XRD patterns of nanocomposites synthesized by using ethylene glycol and organoclay Cloisite 30B. The y-axis is shifted for clarity. As seen in the figure, no peak is observed in the XRD pattern of the nanocomposite containing 1 wt. % organoclay. This is the evidence of the exfoliation of the organoclay particles in the polymer matrix. It can be stated that the optimum organoclay concentration for this combination is 1 wt. % in terms of obtaining an exfoliated structure. On the other hand, at 3 wt. % clay loading two peaks are observed. The first peak at $2\theta=2.37^\circ$ shows the intercalated structure of the nanocomposite. The d-spacing is increased from 17.94 Å for pure Cloisite 30B to 37.23 Å. Second peak is closer to the characteristic peak of Cloisite 30B. It can be concluded that a partially intercalated structure is obtained. Some of the clay particles are unaffected by the UP matrix and the basal spacing remains the same.

Figures 4.2 and 4.3 show the XRD patterns of nanocomposites synthesized by propylene glycol and diethylene glycol, respectively. In Figure 4.2, at 3 and 5 wt. % clay loadings XRD patterns contain diffraction peaks which show partially intercalated structures. However, at 1 wt. % clay loading the sample show a faint peak at $2\theta=2.13^\circ$ ($d=41.43$ Å), suggesting that a small part of organoclay is intercalated by UP resin. From Table 4.1 a slight decrease in the d-spacing is observed when organoclay loading is increased. This decrease can be attributed to decreased tendency of clay particles to intercalate at high clay contents.

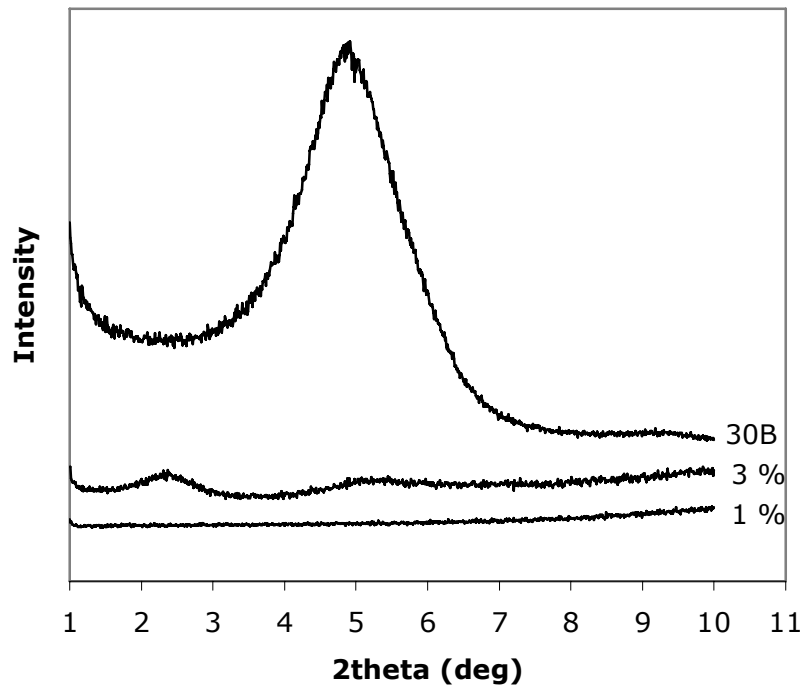


Figure 4.1 X-ray diffraction patterns of nanocomposites synthesized by ethylene glycol containing 1 and 3 wt. % organoclay (Cloisite 30B)

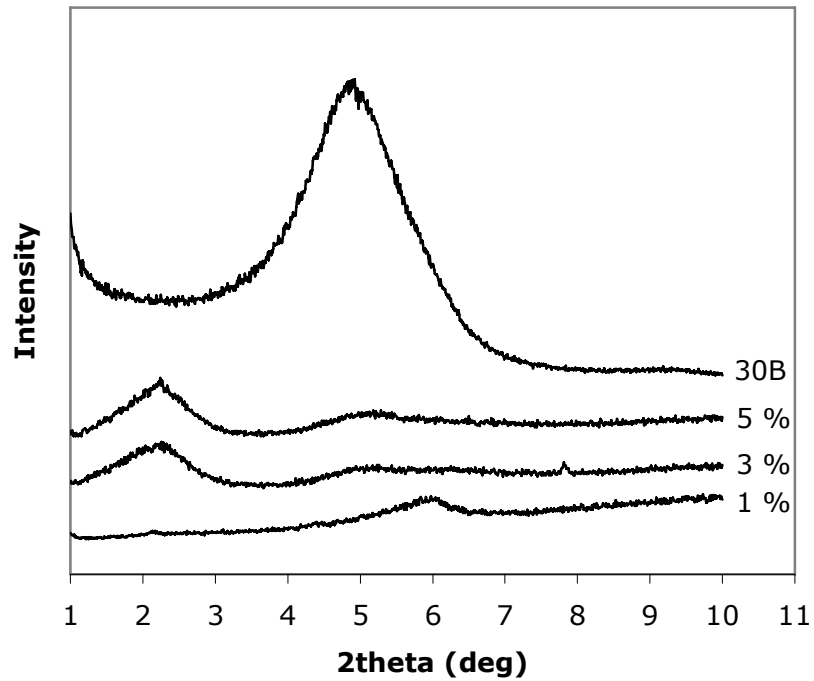


Figure 4.2 X-ray diffraction patterns of nanocomposites synthesized by propylene glycol containing 1, 3 and 5 wt. % organoclay (Cloisite 30B)

In Figure 4.3, samples containing 1 and 5 wt. % organoclay show partially intercalated structures. At 3 wt. % clay content, no peak is detected by XRD, which suggests that it has an exfoliated structure. Many factors such as concentration and order of the clay can influence the XRD patterns of layered silicates. For example, samples where the clay is not well ordered will fail to produce a Bragg diffraction peak, and that is the correct conclusion drawn from the data. It is not the fault of the technique that leads to the incorrect conclusion of a nanocomposite being exfoliated when in reality it is highly disordered. Therefore, XRD analysis does not prove or disprove the existence of exfoliated clay platelets in the nanocomposite [55]. Other morphological analysis techniques (SEM and TEM analysis) should also be used to filling in gaps of information that XRD cannot obtain.

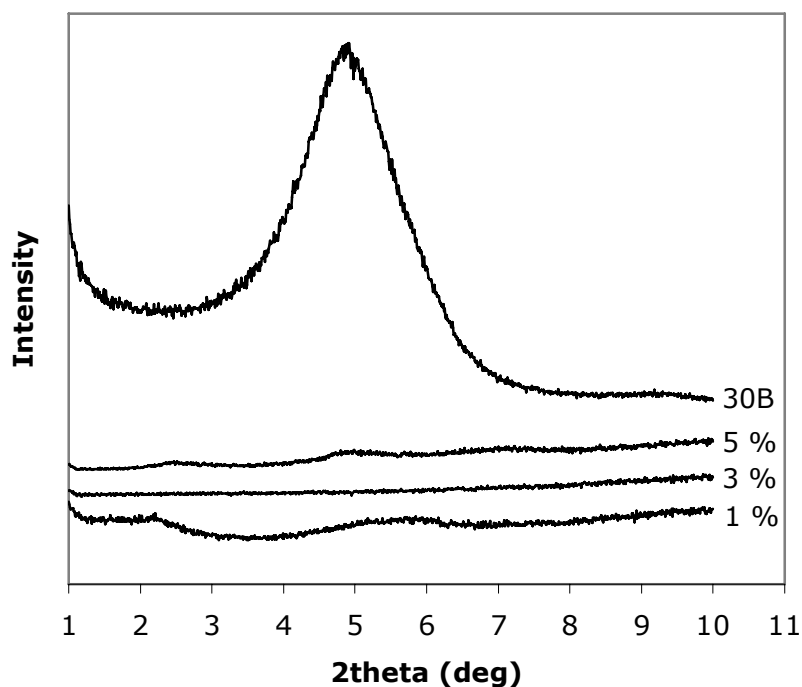


Figure 4.3 X-ray diffraction patterns of nanocomposites synthesized by diethylene glycol containing 1, 3 and 5 wt. % organoclay (Cloisite 30B)

Figures 4.4 through 4.6 show the glycol effect on the nanocomposites containing 1, 3 and 5 wt. % organoclay, respectively. In Figure 4.4 samples prepared by PG and DEG show peaks, which verify the formation of a partially intercalated structure. From Table 4.1, it can be seen that d-spacing of the PG based sample is larger than DEG based sample. EG based sample shows no peak, suggesting

exfoliation. It can be stated that, polymer synthesized by EG shows the highest compatibility with organoclay and polymer synthesized by DEG shows the lowest compatibility with organoclay. The main reason for that is the chemical structure of glycols. EG has the shortest chain length. Because of this, during in-situ polymerization EG molecules can easily enter the galleries between the clay platelets and thus increase the d-spacing. On the other hand, DEG has the longest chain length and DEG molecules hardly intercalate between the clay layers.

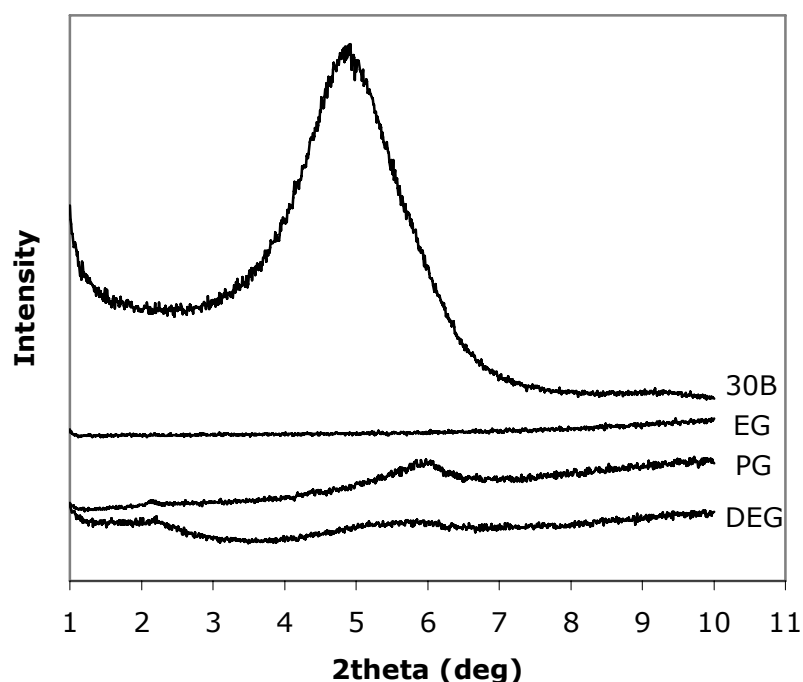


Figure 4.4 X-ray diffraction patterns of nanocomposites prepared by different types of glycols containing 1 wt. % organoclay (Cloisite 30B)

XRD patterns of nanocomposites prepared by 5 wt. % organoclay show similar behavior as 1 wt. % organoclay containing nanocomposites. However, at 3 wt. % nanocomposites completely opposite behavior is observed. In the pattern of the nanocomposite prepared by DEG, no peak is detected by XRD, which indicates further delamination of the silicate layers and formation of an exfoliated structure. EG and PG based nanocomposites exhibit partially intercalated structures characteristics in the XRD patterns.

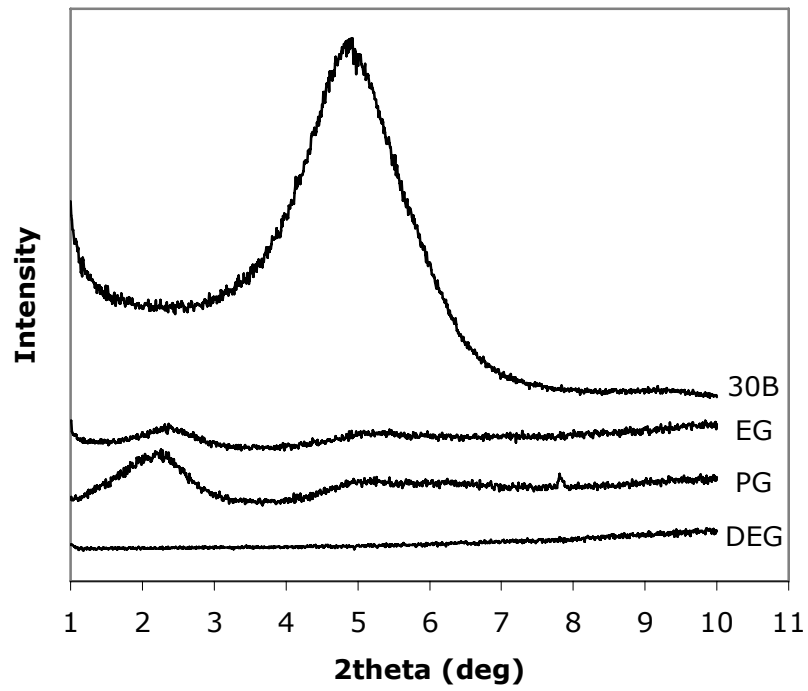


Figure 4.5 X-ray diffraction patterns of nanocomposites prepared by different types of glycols containing 3 wt. % organoclay (Cloisite 30B)

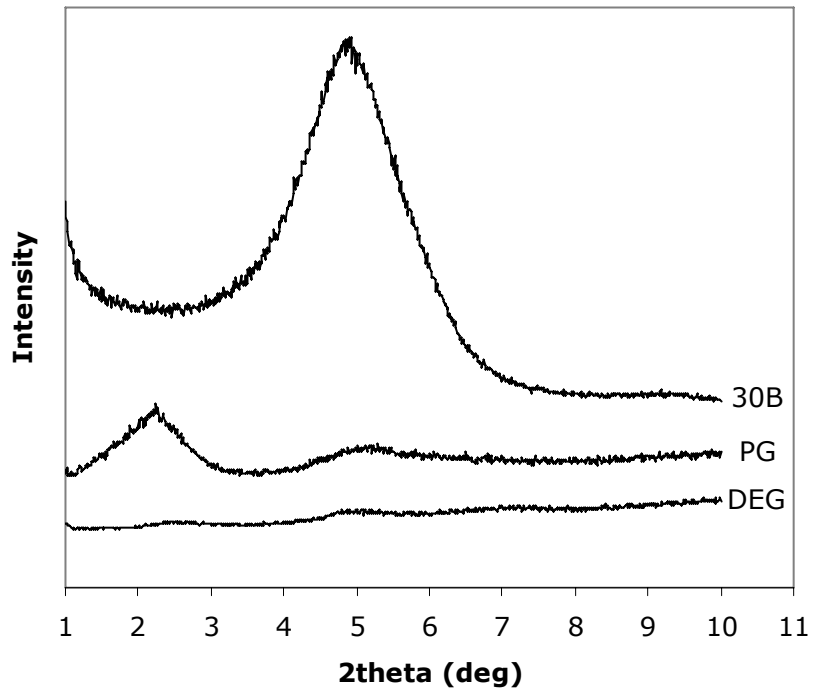


Figure 4.6 X-ray diffraction patterns of nanocomposites prepared by different types of glycols containing 5 wt. % organoclay (Cloisite 30B)

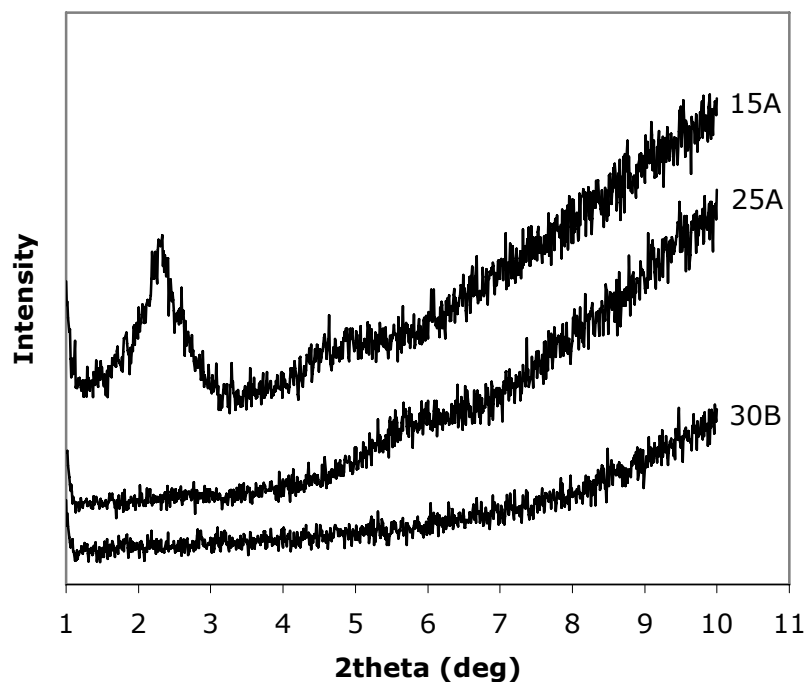


Figure 4.7 X-ray diffraction patterns of nanocomposites prepared by ethylene glycol and different types of organoclays (1 wt. % organoclay)

Figures 4.7 through 4.9 show the effect of organoclay type on the nanocomposites synthesized by EG, PG and DEG, respectively. In Figure 4.7 the XRD patterns of nanocomposites prepared by EG are seen. In the pattern of nanocomposite prepared by Cloisite 30B, formation of an exfoliated structure is confirmed with the absence of a basal reflection. In the pattern of nanocomposite prepared by Cloisite 15A, two basal reflections are detected by XRD. These suggest a partially intercalated structure. However, sample prepared by Cloisite 25A shows only one peak at $2\theta = 5.85$. This peak indicates the unaffected clay platelets. Their basal spacing remains the same. According to Table 4.3, PG and DEG based samples, which prepared by Cloisite 25A exhibit 93 % increase in gallery size. In the light of these results, in the case of EG based samples, it may be stated that some of the organoclay particles are exfoliated and some of them are unaffected by the polymer matrix.

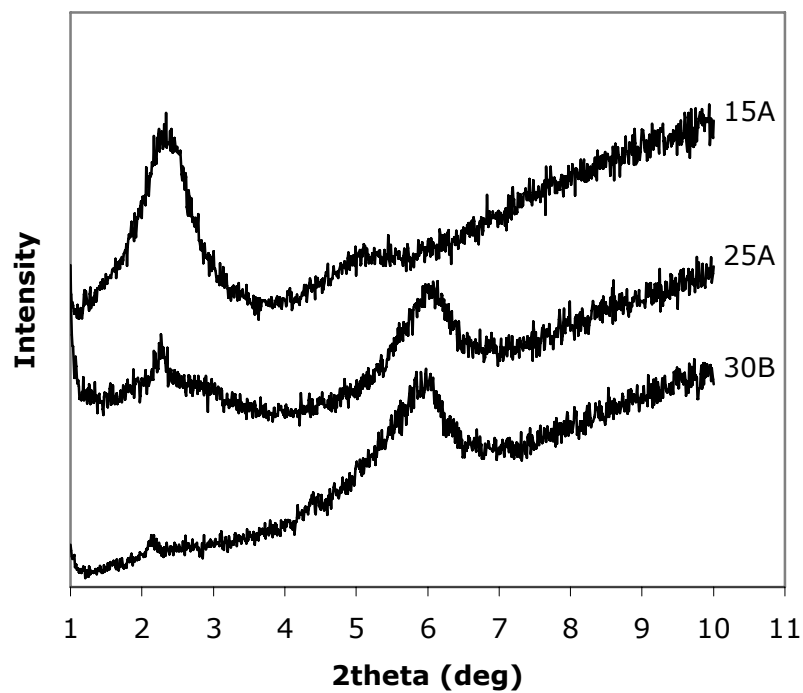


Figure 4.8 X-ray diffraction patterns of nanocomposites prepared by propylene glycol and different types of organoclays (1 wt. % organoclay)

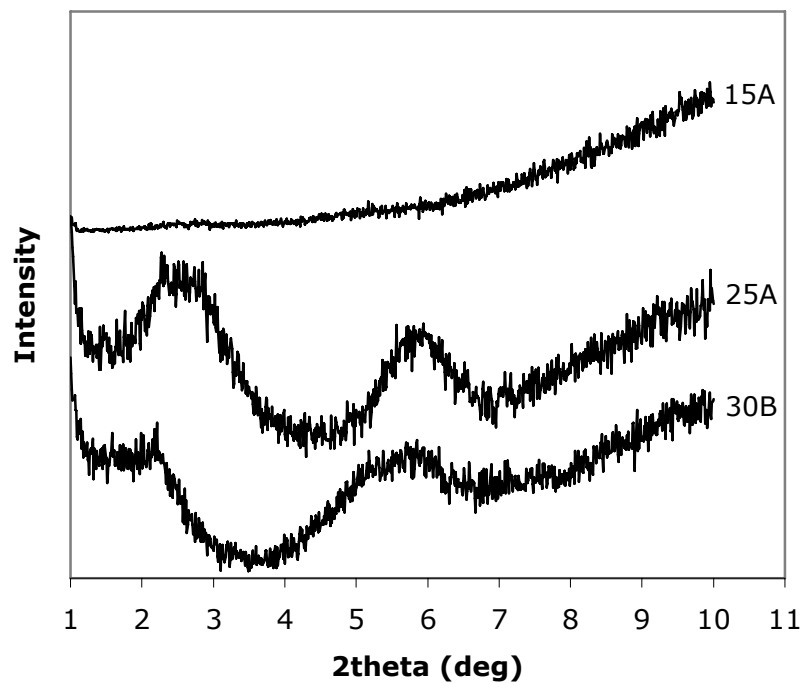


Figure 4.9 X-ray diffraction patterns of nanocomposites prepared by diethylene glycol and different types of organoclays (1 wt. % organoclay)

In Figure 4.8, the XRD patterns of nanocomposites synthesized by PG are seen. All of the nanocomposites exhibit partially intercalated structures. From Table 4.3 the % increase in the d-spacings are 131%, 93% and 18% for organoclays Cloisite 30B, 25A and 15A, respectively.

In Figure 4.9, although nanocomposites synthesized by Cloisite 30B and 25A show partially intercalated structure, no peak is detected in the XRD pattern of sample prepared by Cloisite 15A. Exfoliated structures show no peak by XRD, suggesting that a great amount of polymer has entered the gallery space, expanding the clay layers so far apart that diffraction cannot be observed with wide-angle ($2\theta > 1^\circ$) XRD techniques. Furthermore, the clay layers are sufficiently disordered such that they no longer give a coherent XRD signal [55]. However, in this sample organoclay agglomerates can be seen even with naked eye. Because of that, this sample strongly suggests undispersed clay particles.

In Table 4.2, the final d-spacings of the silicate sheets are given with respect to the glycol and clay type. Table 4.3 gives the percent increase in the d-spacings of organoclays with respect to organoclay types.

Table 4.2 X-ray diffraction results of compositions prepared by different types of organoclays* (1 wt. % organoclay)

Glycol Type	Organoclay Type	d-spacing (Å)	2θ (deg)
EG	Cloisite 30B	exfoliated	-
	Cloisite 25A	partially exfoliated	-
	Cloisite 15A	37.87	2.33
PG	Cloisite 30B	41.43	2.13
	Cloisite 25A	38.87	2.27
	Cloisite 15A	37.71	2.34
DEG	Cloisite 30B	39.93	2.21
	Cloisite 25A	38.70	2.28
	Cloisite 15A	undispersed	-

*The original d-spacing of Cloisite 30B is 17.94 Å and 2θ value is 4.92 deg.
 The original d-spacing of Cloisite 25A is 20.1 Å and 2θ value is 4.39 deg.
 The original d-spacing of Cloisite 15A is 31.97 Å and 2θ value is 2.76 deg.

Table 4.3 % increase in the d-spacings of organoclays with respect to organoclay types (1 wt. % organoclay)

Glycol Type	Organoclay Type		
	Cloisite 30B	Cloisite 25A	Cloisite 15A
EG	exfoliated	partially exfoliated	18%
PG	131%	93%	18%
DEG	123%	93%	undispersed

From Table 4.2, it can be clearly seen that Cloisite 30B containing samples give the highest d-spacing value. Although, Cloisite 30B has the lowest original d-spacing among the other organoclay types, maximum increase in the gallery size is obtained with Cloisite 30B.

According to the manufacturers Cloisite selection chart based on polymer/monomer chemistry, Cloisite 15A is the most hydrophobic and Cloisite 30B is the least hydrophobic organoclay. Since unsaturated polyester is not a hydrophobic polymer, Cloisite 30B is the most compatible organoclay with UP matrix. From Table 4.3, it can be seen that the maximum increase in the gallery size is obtained with Cloisite 30B and minimum increase in the gallery size is obtained with Cloisite 15A. These results prove that Cloisite 30B is the most compatible organoclay with unsaturated polyester system. However, glycol type does not significantly affect the gallery size, in the intercalated systems.

All the XRD data including that of the Cloisite powders and unfilled polyesters are given in Appendix A.

4.1.2 Scanning Electron Microscopy (SEM) Analysis

In order to investigate the effect of the glycol type, clay content and the clay type on the morphological structure of the impact fractured surfaces; Scanning Electron Microscopy (SEM) analysis was performed. SEM images of all the formulations will be presented here with the same magnifications of $\times 250$ and $\times 3000$.

Figure 4.10 shows the impact fractured surfaces of neat unsaturated polyesters synthesized by different glycol types. It is obvious that the impact surfaces of these materials are smooth and few straight crack propagation lines are observed.

In Figures 4.11 through 4.13, SEM micrographs of UP nanocomposites prepared by different glycol types containing 1, 3 and 5 wt. % organoclay are shown, respectively. It is seen that featureless structures of pure unsaturated polyesters disappear. In Figures 4.11 and 4.12 it is obviously seen that nanocomposites prepared by DEG have the most tortuous crack propagation path. This results in highest impact strength of the samples prepared by DEG. The reason for that is the chemical structure of DEG. DEG has the longest chain length among the glycols studied, which gives flexibility to the polymer.

As seen in figures, SEM micrographs of EG and PG based samples are almost the same. Small agglomerates are seen in these micrographs and the amount and size of the agglomerates increase with increasing organoclay concentration. The agglomerations of the clay particles decrease the impact strength, since they act as stress concentrators. On the other hand, the crack propagation lines are exhibiting a shorter and closer structure with increasing clay loading. In Figures 4.13 (a) and 4.13 (b), PG based nanocomposite exhibit a tortuous crack propagation path and a small increase in the impact strength is observed.

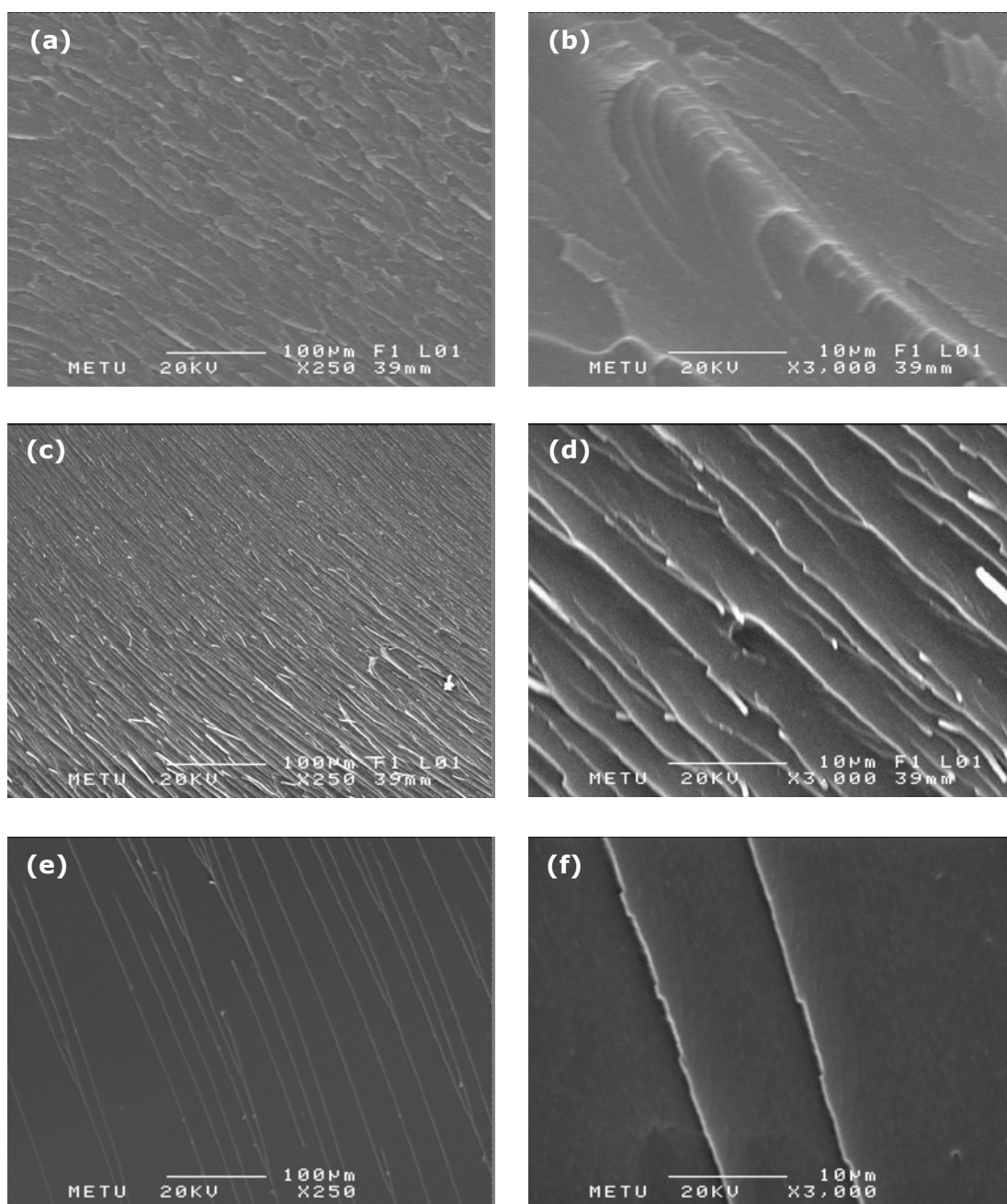


Figure 4.10 SEM micrographs of pure unsaturated polyesters synthesized by (a) EG $\times 250$, (b) EG $\times 3000$, (c) PG $\times 250$, (d) PG $\times 3000$, (e) DEG $\times 250$, (f) DEG $\times 3000$.

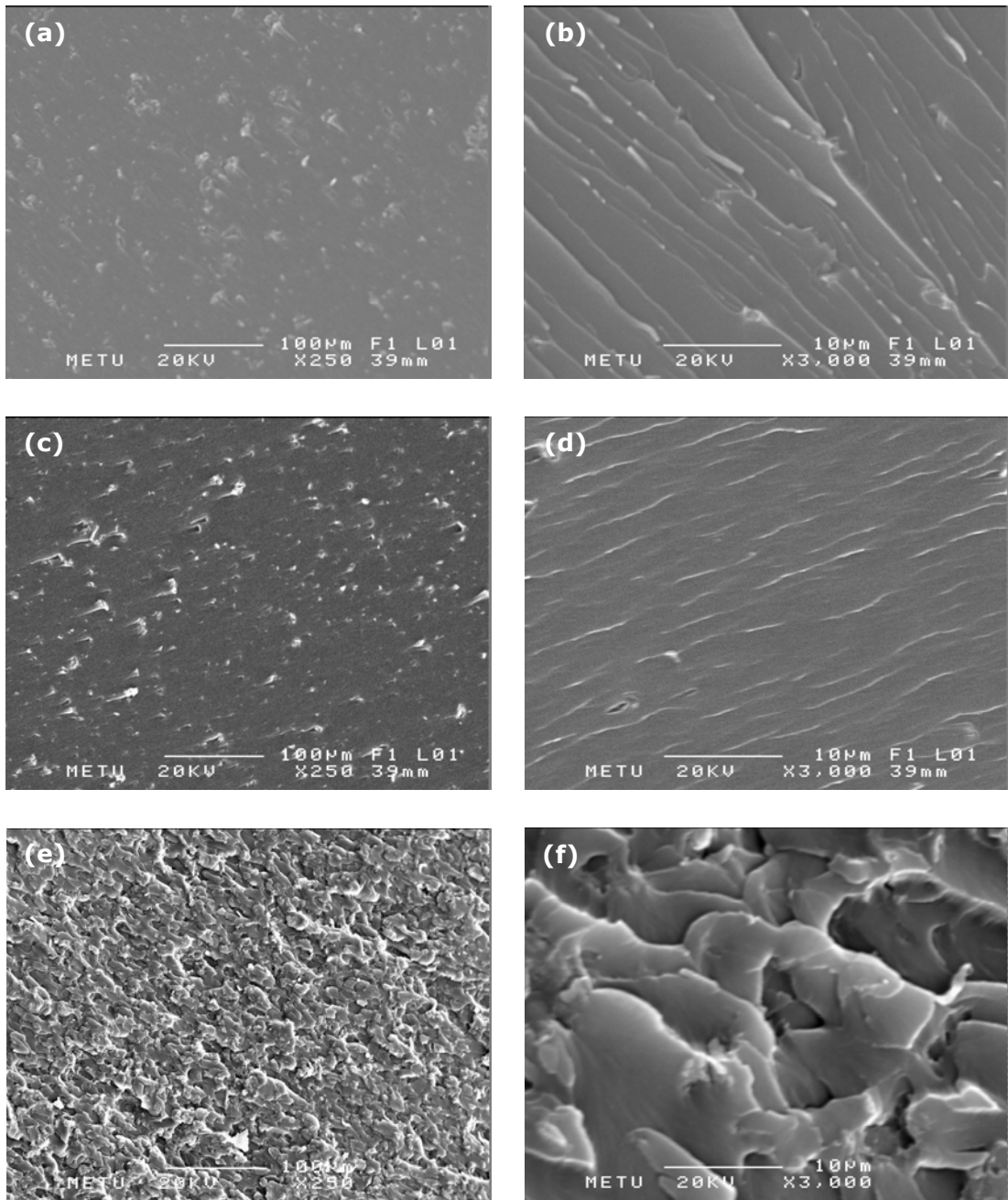


Figure 4.11 SEM micrographs of unsaturated polyester nanocomposites containing 1 wt. % Cloisite 30B synthesized by (a) EG $\times 250$, (b) EG $\times 3000$, (c) PG $\times 250$, (d) PG $\times 3000$, (e) DEG $\times 250$, (f) DEG $\times 3000$.

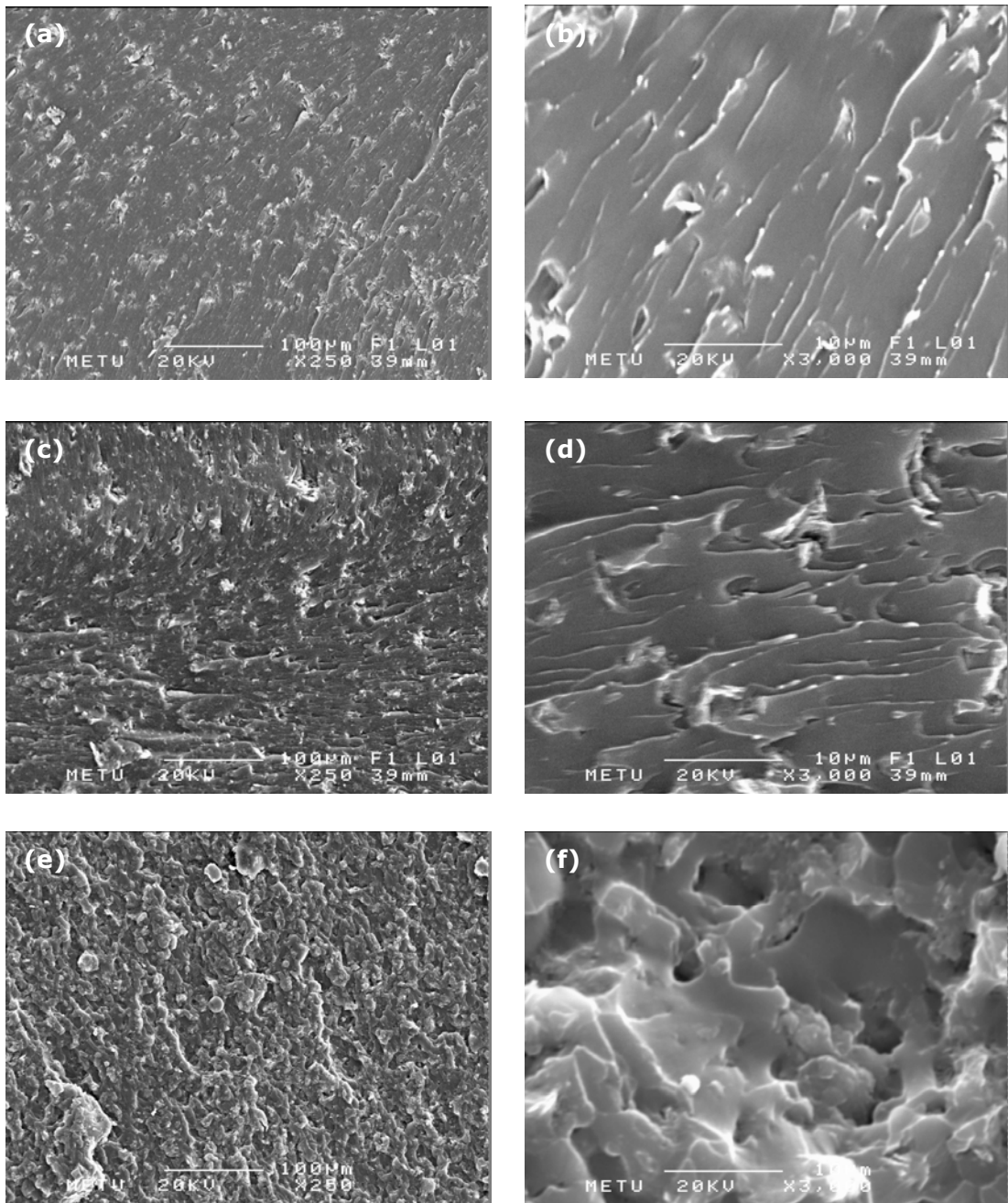


Figure 4.12 SEM micrographs of unsaturated polyester nanocomposites containing 3 wt. % Cloisite 30B synthesized by (a) EG $\times 250$, (b) EG $\times 3000$, (c) PG $\times 250$, (d) PG $\times 3000$, (e) DEG $\times 250$, (f) DEG $\times 3000$.

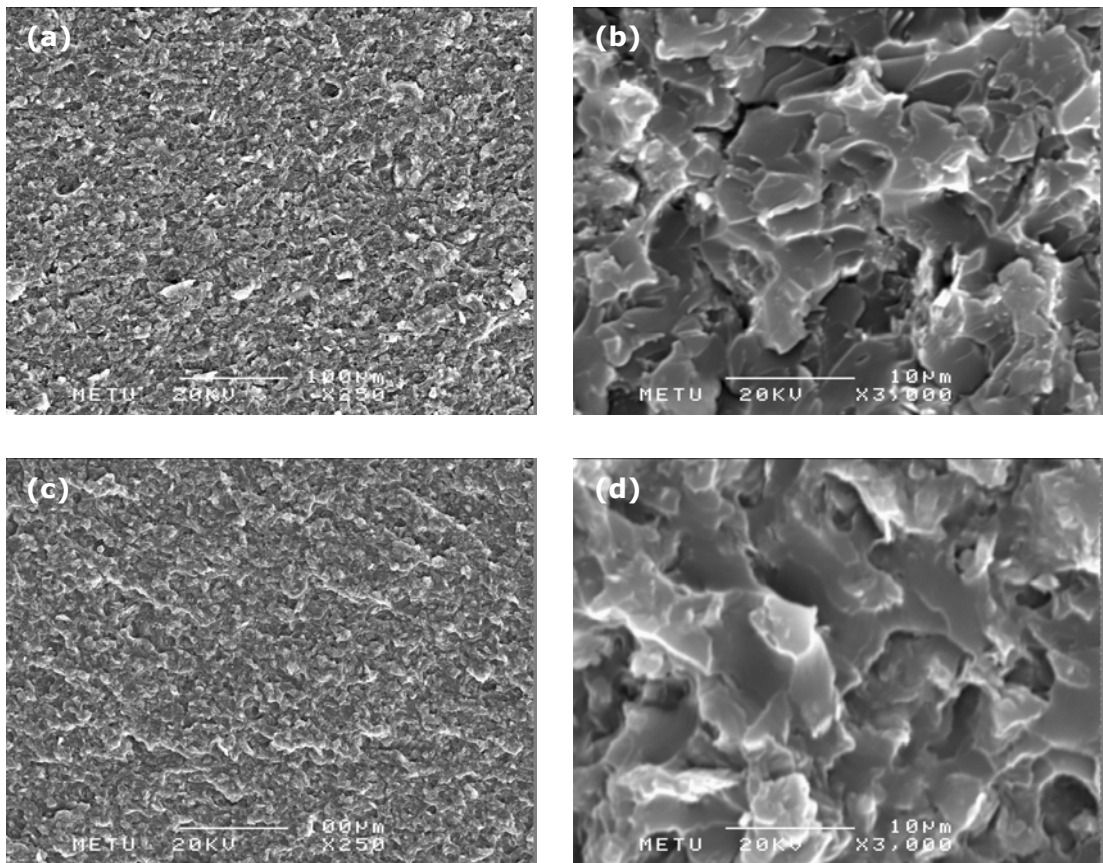


Figure 4.13 SEM micrographs of unsaturated polyester nanocomposites containing 5 wt. % Cloisite 30B synthesized by (a) PG $\times 250$, (b) PG $\times 3000$, (c) DEG $\times 250$, (d) DEG $\times 3000$.

Figures 4.14, 4.15 and 4.16 show the impact fractured surfaces of unsaturated polyester nanocomposites synthesized by varying organoclay types and using EG, PG and DEG, respectively. However, it is very difficult to interpret the effect of clay type on the morphological structure of the nanocomposites. These micrographs exhibit similar structures, except for Figure 4.16. In Figures 4.16 (a) and 4.16 (b), the tortuous crack propagation paths of sample containing Cloisite 30B are clearly seen. Figures 4.16 (c) and 4.16 (d) show agglomerated Cloisite 25A particles in the polymer matrix and sample containing Cloisite 15A has a smooth structure as shown in Figures 4.16 (e) and 4.16 (f). These results are in good agreement with the XRD and impact strength results discussed later. However, these should be supported by Transmission Electron Microscopy (TEM) analysis. TEM is a more powerful technique to study structures at and below the

nanometer scale. It allows a precise observation of nanostructures with an exceptional resolution (about 0.2 nm) [30].

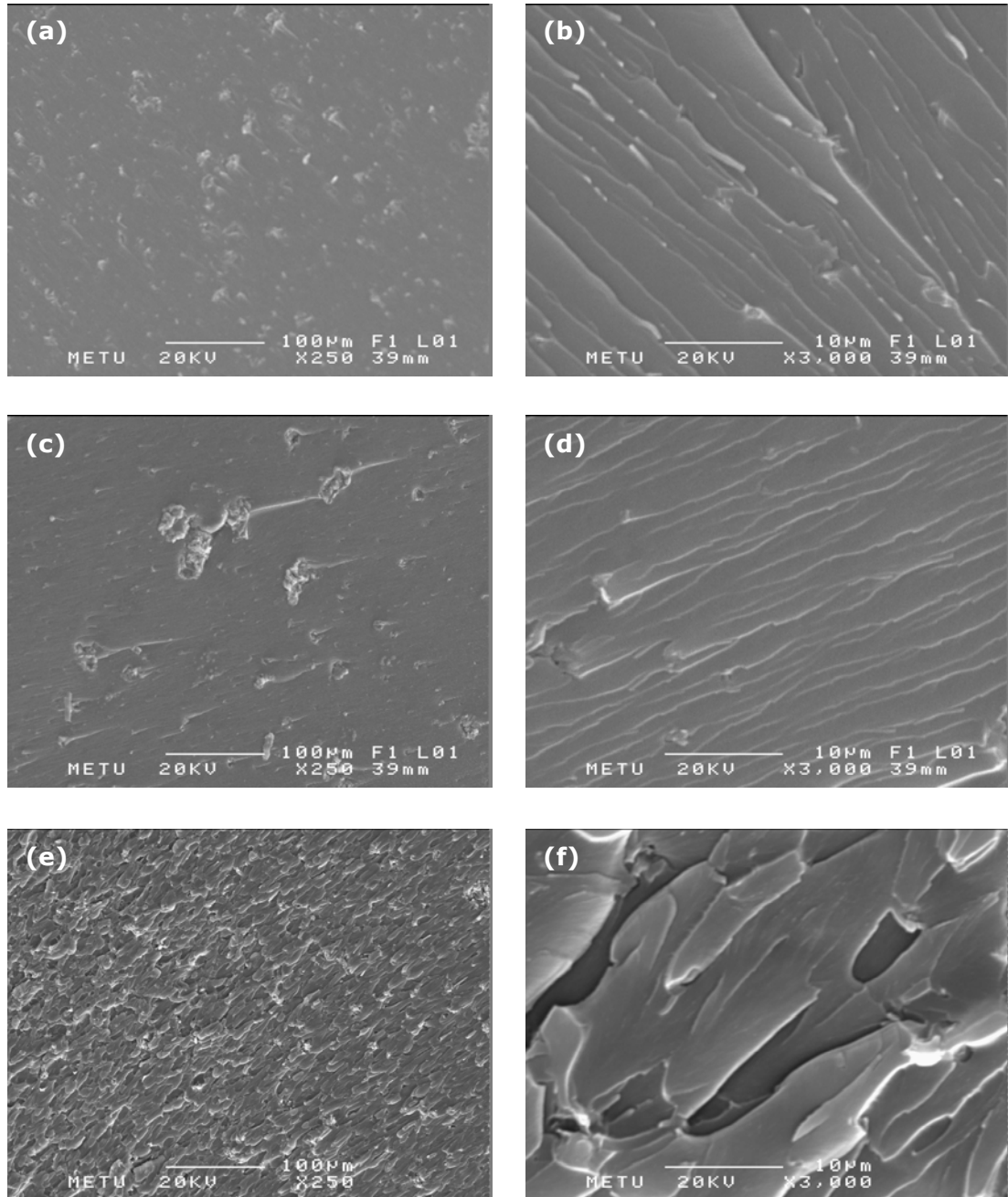


Figure 4.14 SEM micrographs of unsaturated polyester nanocomposites synthesized by EG containing 1 wt. % organoclay; (a) Cloisite 30B $\times 250$, (b) Cloisite 30B $\times 3000$, (c) Cloisite 25A $\times 250$, (d) Cloisite 25A $\times 3000$, (e) Cloisite 15A $\times 250$, (f) Cloisite 15A $\times 3000$.

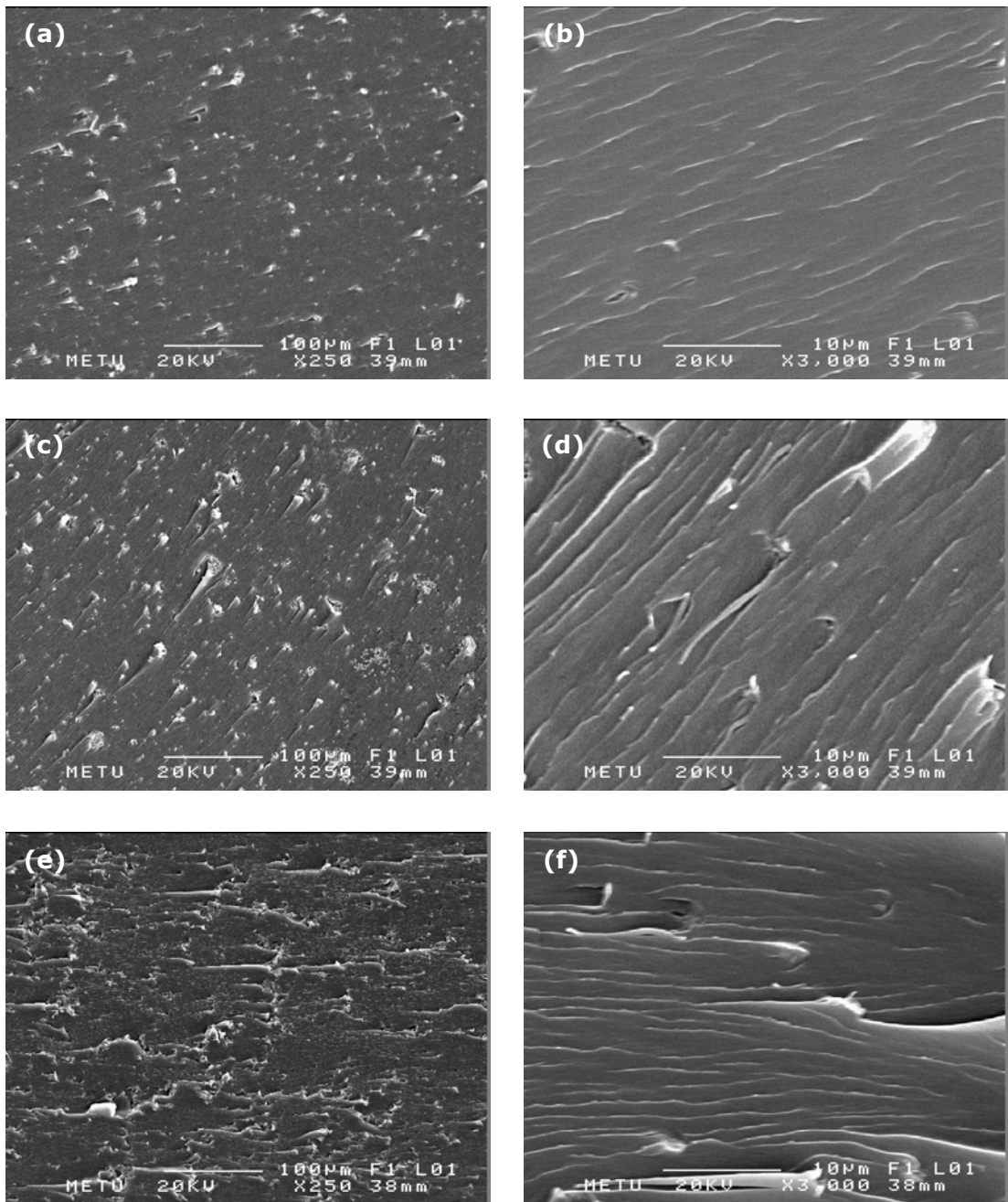


Figure 4.15 SEM micrographs of unsaturated polyester nanocomposites synthesized by PG containing 1 wt. % organoclay; (a) Cloisite 30B $\times 250$, (b) Cloisite 30B $\times 3000$, (c) Cloisite 25A $\times 250$, (d) Cloisite 25A $\times 3000$, (e) Cloisite 15A $\times 250$, (f) Cloisite 15A $\times 3000$.

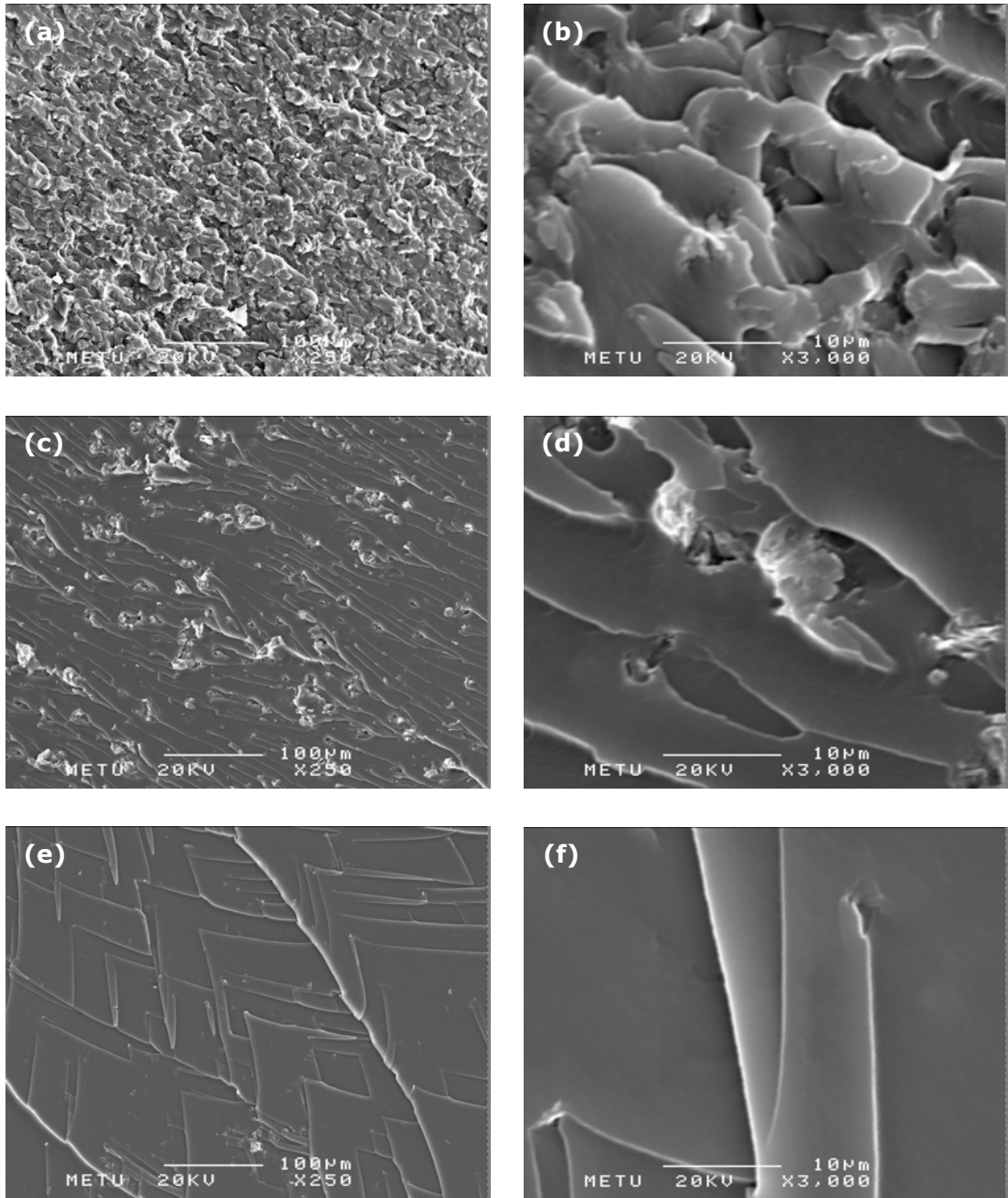


Figure 4.16 SEM micrographs of unsaturated polyester nanocomposites synthesized by DEG containing 1 wt. % organoclay; (a) Cloisite 30B $\times 250$, (b) Cloisite 30B $\times 3000$, (c) Cloisite 25A $\times 250$, (d) Cloisite 25A $\times 3000$, (e) Cloisite 15A $\times 250$, (f) Cloisite 15A $\times 3000$.

4.2 Mechanical Analysis

Mechanical analysis included the investigation of tensile strength, tensile modulus, tensile strain at break, flexural strength, flexural modulus, flexural strain at maximum stress and impact strength. Arithmetic means and standard deviations of tensile, flexural and impact results are given in Appendix B.

4.2.1 Tensile Test Analysis

Figures 4.18 through 4.21 show the effect of glycol type on the stress-strain curves of samples obtained from tensile tests. It can be clearly seen from the figures that PG based samples indicate the highest tensile modulus and DEG based samples indicate the highest strain at break values. This is a result of the chemical structure of the glycols and the side reactions that occur during the polymerization reaction. As mentioned earlier, EG has the shortest chain length and DEG has the longest chain length. Because of that, DEG gives great flexibility and toughness and EG gives rigidity to the material [56]. On the other hand, due to the presence of the pendant methyl group, the PG resulting resins are less crystalline and more compatible with styrene than those obtained using EG and DEG [13].

Side reactions also take place during the polyesterification reaction. One of them is maleate to fumarate transition (Figure 4.17). The esterified maleic (cis-maleate ester) isomerizes to the trans isomer (trans-fumarate).

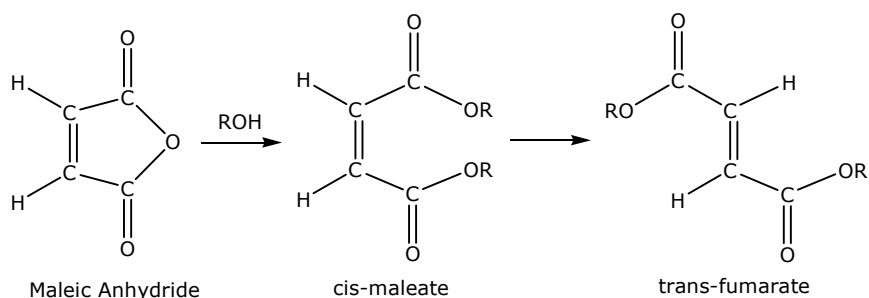


Figure 4.17 Isomerization of maleate to fumarate [16]

The reactivity of the polymer with styrene depends on the degree of isomerization. Maleate polymers in the cis form create strain across the double

bond, causing some displacement from a planar configuration; fumarate polymers in the trans configuration are influenced less by steric effects and the double bond can assume a planar configuration conducive to addition copolymerization reactions with styrene. Branched asymmetric reactants like PG create sufficient steric interference to promote isomerization to the trans-fumarate polymers, whereas linear glycols such as EG and DEG produce resins that have higher levels of the maleate polymer. Fumarate polymers show higher reactivity rates with styrene, and lead to a complete cross-linking reaction [16].

In the light of this information, it can be stated that glycol type is very effective on the mechanical properties of the final cured product. Samples prepared by PG are the most brittle ones, due to the maleate-fumarate isomerization and high compatibility of PG based resins with styrene monomer. Therefore, samples synthesized by PG have higher crosslink density and they show highest tensile modulus and lowest tensile strain at break values. Generally, EG based samples show the highest tensile strength and samples prepared by DEG show the most flexible structure.

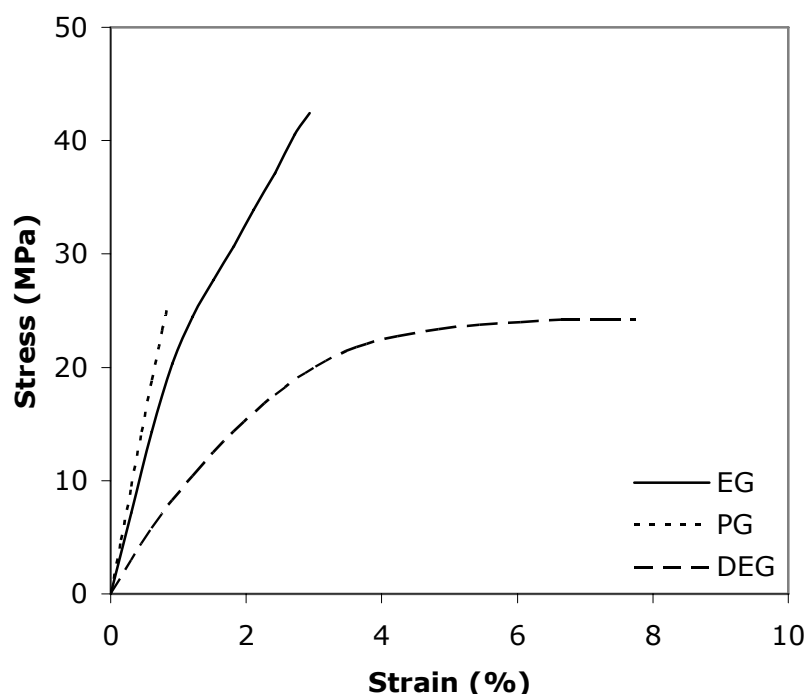


Figure 4.18 Effect of glycol type on the stress-strain curves of pure unsaturated polyesters

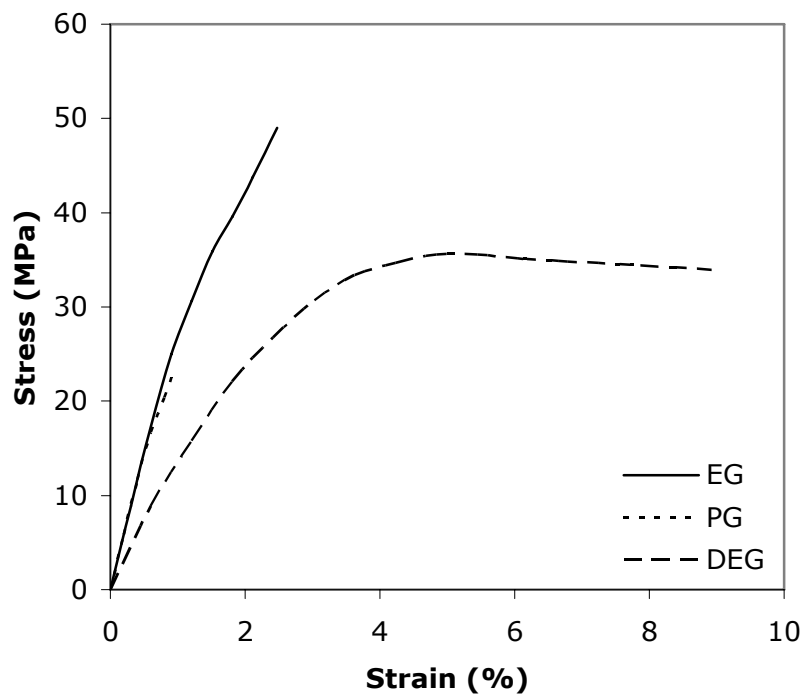


Figure 4.19 Effect of glycol type on the stress-strain curves of nanocomposites containing 1 wt. % organoclay (Cloisite 30B)

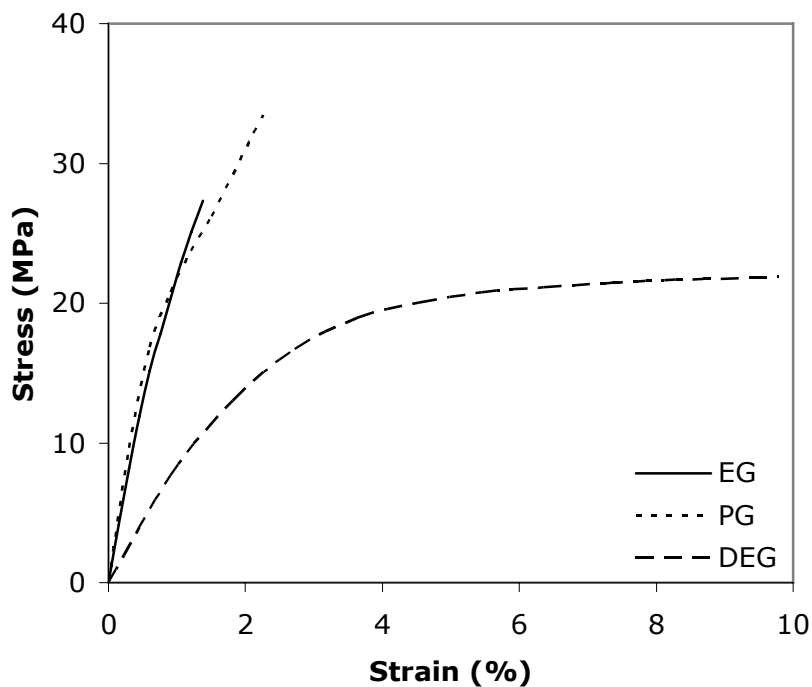


Figure 4.20 Effect of glycol type on the stress-strain curves of nanocomposites containing 3 wt. % organoclay (Cloisite 30B)

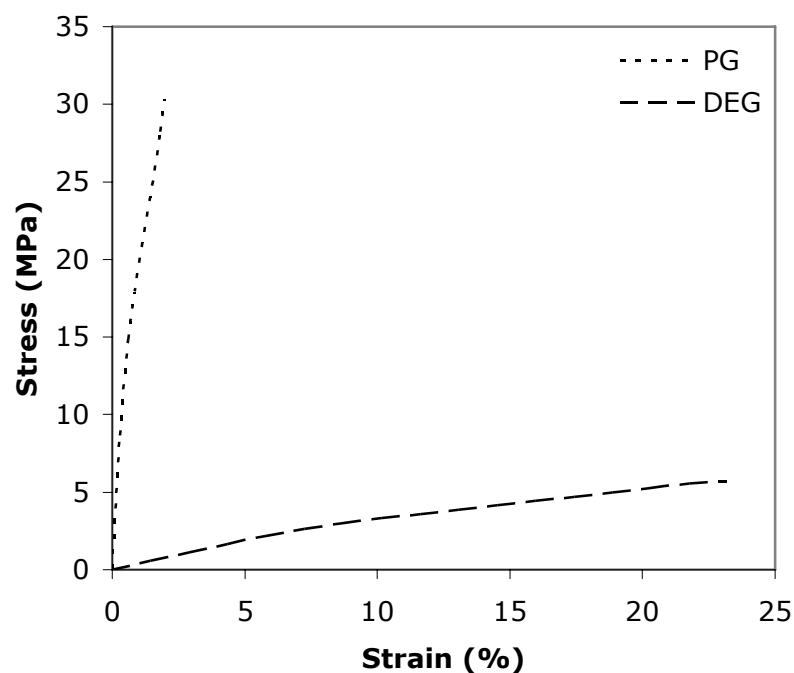


Figure 4.21 Effect of glycol type on the stress-strain curves of nanocomposites containing 5 wt. % organoclay (Cloisite 30B)

The effect of organoclay concentration can be seen from Figures 4.22 through 4.27. Figures 4.22, 4.23 and 4.24 show the stress-strain curves of nanocomposites prepared by EG, PG and DEG, respectively. It is seen from the graphs that samples synthesized by EG and DEG generally give maximum tensile strength and tensile modulus values at 1 wt. % organoclay loading. This is a result of the adhesion between the polymer and the layered silicate surfaces. Degree of delamination of the clay in the polymer matrix and the interaction between the clay layers and the polymer strongly influences the mechanical properties of nanocomposites [30]. The polymer molecules at the surface of the nanoscale particles are completely immobilized and there is a neighboring region of partially immobilized molecules. Due to the high surface area of nanoscale particles, the effects from reduced molecular mobility become significant, improving tensile strength and tensile modulus values of nanocomposites [46]. As seen from the Figure 4.23 that, PG based samples are different from the others and exhibit the maximum strength at 3 wt. % organoclay loading.

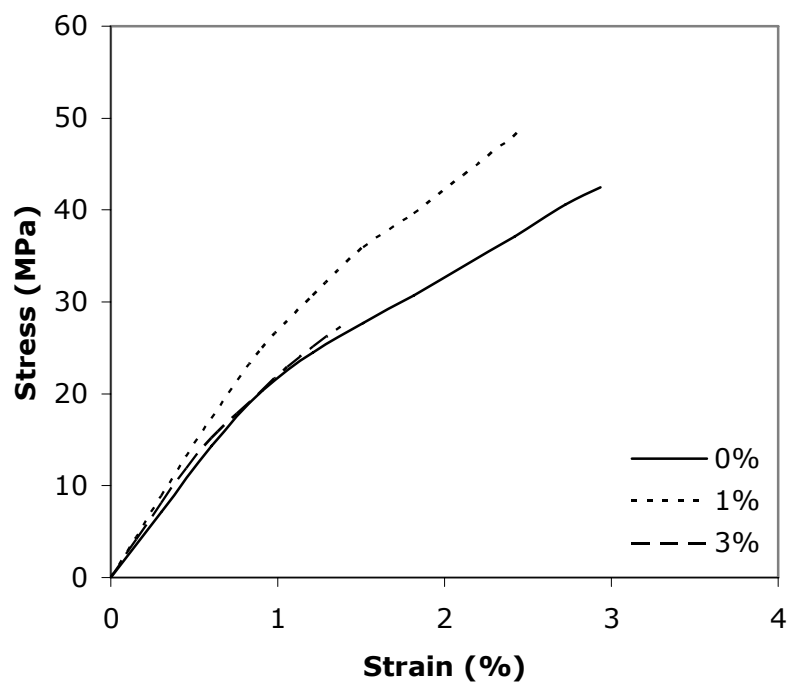


Figure 4.22 Effect of organoclay (Cloisite 30B) content on the stress-strain curves of nanocomposites prepared by EG

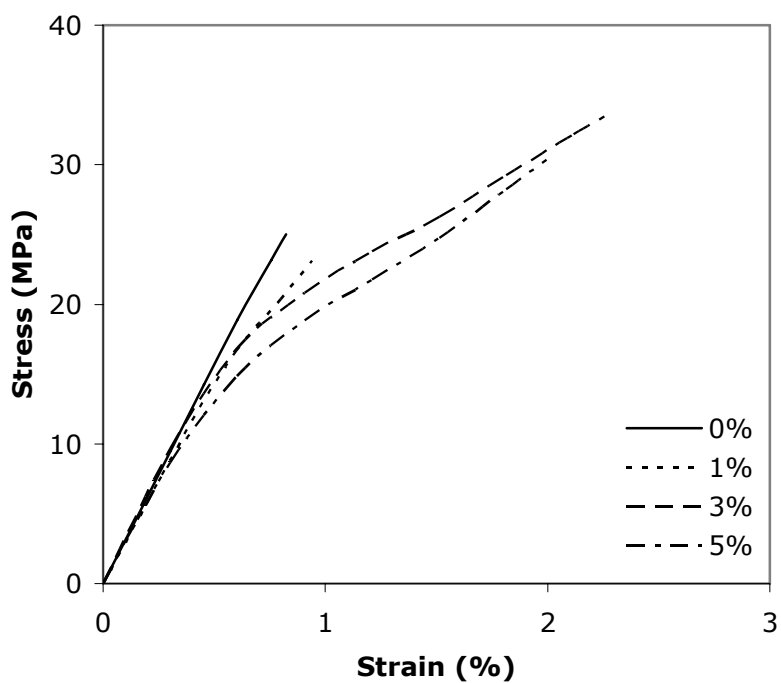


Figure 4.23 Effect of organoclay (Cloisite 30B) content on the stress-strain curves of nanocomposites prepared by PG

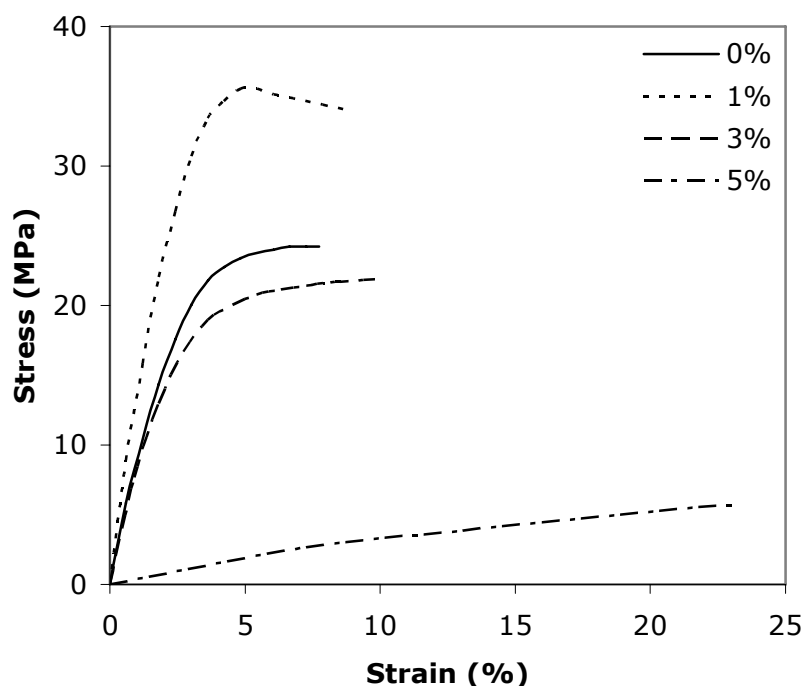


Figure 4.24 Effect of organoclay (Cloisite 30B) content on the stress-strain curves of nanocomposites prepared by DEG

Figures 4.25 and 4.26 display the tensile strength and tensile modulus of the samples with respect to the organoclay concentration. Nanocomposites prepared by EG give maxima at 1 wt. % organoclay content. This result is also in good agreement with the XRD results. XRD pattern of nanocomposite prepared by EG containing 1 wt. % Cloisite 30B shows an exfoliated structure. Beyond 1 wt. % clay content, tensile strength and tensile modulus values start to decrease with the clay concentration. The reason for the decrease can be explained by the agglomeration of the clay particles at higher clay contents. Degree of clay-polymer interactions is decreased at higher clay loadings. This is the cause of interfacial debonding during tensile testing. Thus, reduction in tensile properties are observed [27]. Moreover, clay particles act as stress concentrators initiating the cracks at high clay loadings. SEM micrographs of EG based samples also support these results. At high clay loadings larger organoclay agglomerates are observed in these micrographs.

PG based nanocomposites show maximum tensile strength at 3 wt. % organoclay concentration. However, there is no improvement on tensile modulus. They show a different behavior than EG and DEG based

nanocomposites. Samples prepared by PG are the most brittle, thus experimental errors may occur during the mechanical testing.

Nanocomposites synthesized by DEG also give a maximum point at 1 wt. % clay content in both tensile strength and modulus. At higher clay loadings, sharp decreases are observed in Figures 4.25 and 4.26. This can be attributed to the decrease in the crosslink density of the material. Organoclay content is inversely related to the crosslink density. Clay particles consume free radicals. Thus, crosslink density is decreased with increasing clay content, leading to lower tensile strength and modulus.

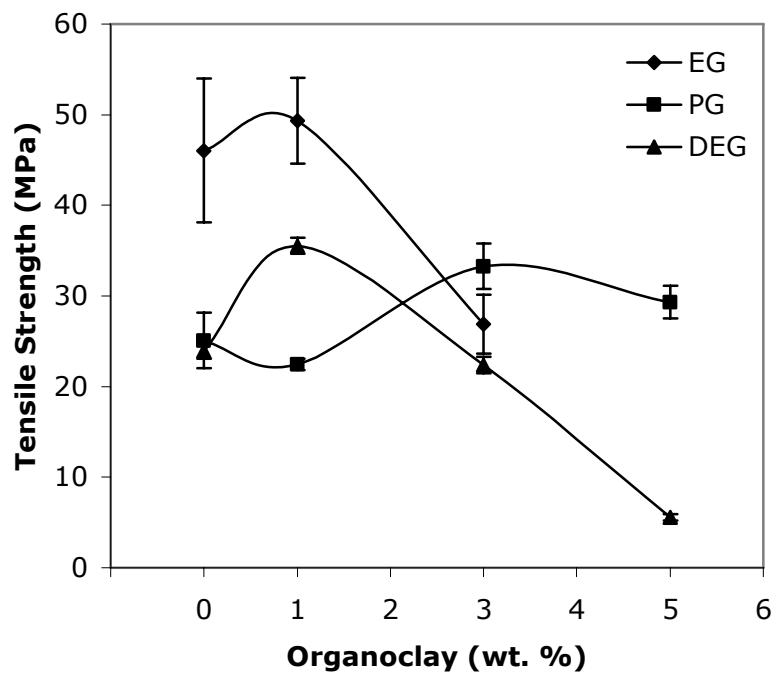


Figure 4.25 Effect of organoclay (Cloisite 30B) content on the tensile strength values of nanocomposites prepared by different glycol types

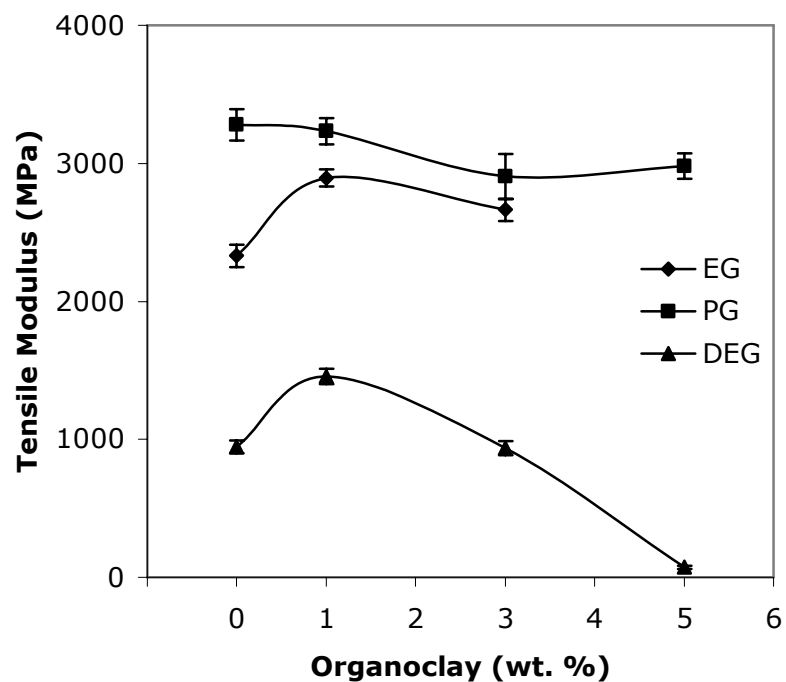


Figure 4.26 Effect of organoclay (Cloisite 30B) content on the tensile modulus values of nanocomposites prepared by different glycol types

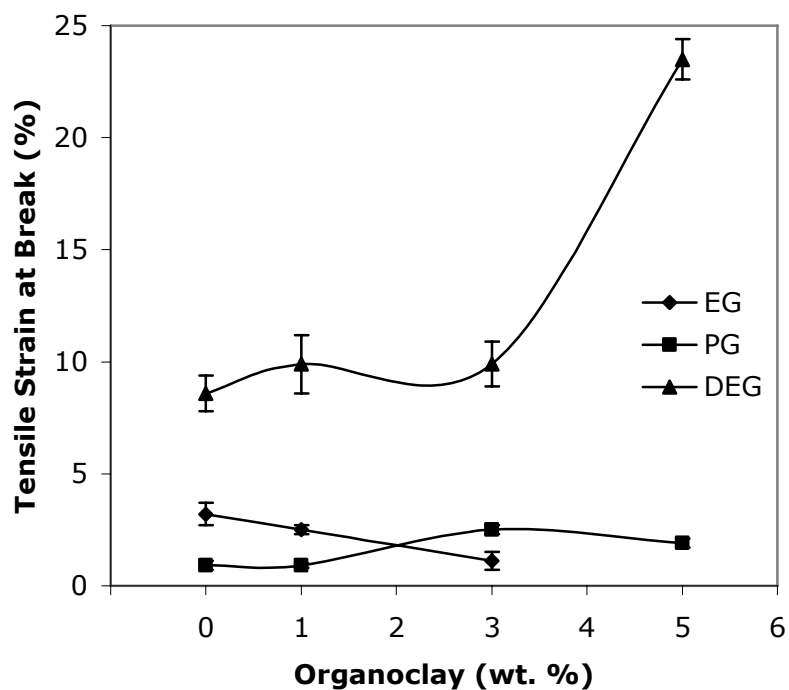


Figure 4.27 Effect of organoclay (Cloisite 30B) content on the tensile strain at break values of nanocomposites prepared by different glycol types

Figure 4.27 shows the strain at break values of nanocomposites with respect to organoclay content. EG based samples show a slight decrease. The decrease in the strain at break value arises from the fact that the material consists of unsaturated polyester and organoclay, and all the elongation is due to the unsaturated polyester since the organoclay is a rigid filler. Thus, the actual elongation experienced by the unsaturated polyester is much greater than the measured elongation of the composite [23]. On the other hand, addition of organoclay causes an increase in strain at break values of PG and DEG based samples. The main reason for that is the reduced crosslink density. This effect of the clay particles is clearly seen at 5 wt. % clay containing samples prepared by DEG.

Stress-strain curves of nanocomposites synthesized by different types of organoclays are seen in Figures 4.28 through 4.30. EG and DEG based samples, again exhibit similar behavior. Samples containing Cloisite 30B show highest and samples containing Cloisite 15A show the lowest tensile strength. However, nanocomposites prepared by PG give the smallest tensile strength value with Cloisite 30B. This may be due to the brittle structure of PG based samples, as mentioned earlier.

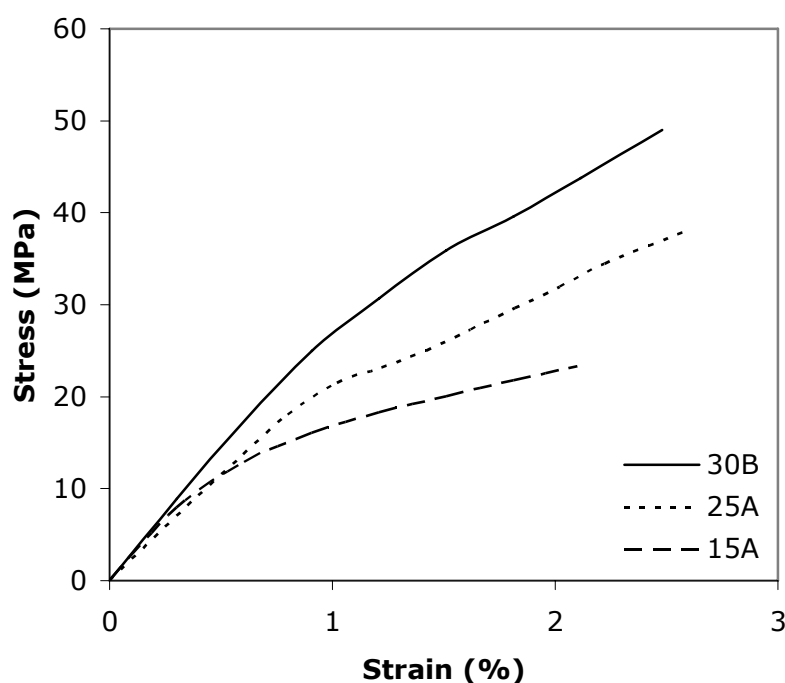


Figure 4.28 Effect of organoclay type (1 wt. %) on the stress-strain curves of nanocomposites prepared by EG

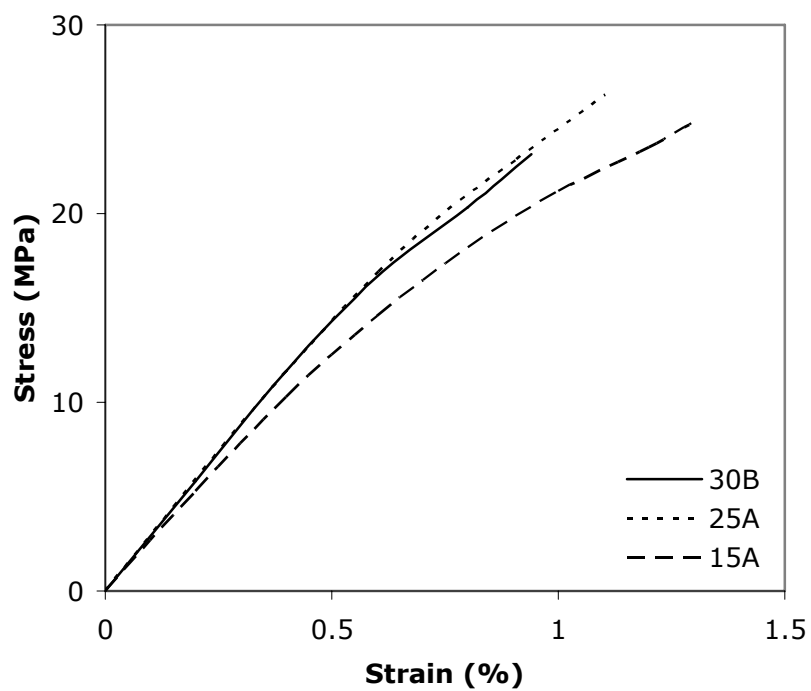


Figure 4.29 Effect of organoclay type (1 wt. %) on the stress-strain curves of nanocomposites prepared by PG

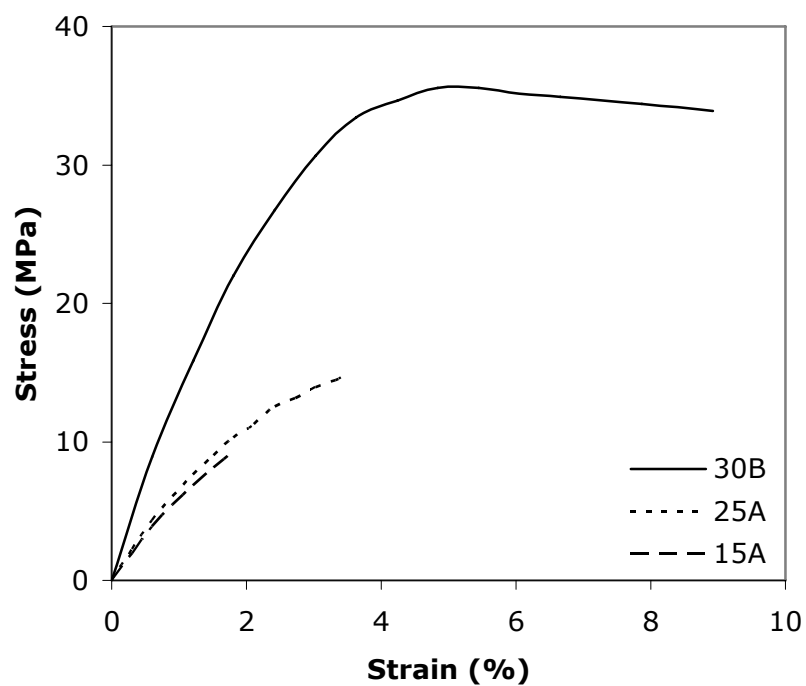


Figure 4.30 Effect of organoclay type (1 wt. %) on the stress-strain curves of nanocomposites prepared by DEG

For a better understanding, comparisons of clay types are given in the Figures 4.31 through 4.33. Figures 4.31 and 4.32 display the tensile strength and tensile modulus of the nanocomposites with respect to organoclay type. EG and DEG based samples containing Cloisite 30B show the highest strength and modulus. Cloisite 25A and Cloisite 15A containing samples follow Cloisite 30B containing samples but there is no improvement of strength and modulus values when compared with the neat polyesters. From the XRD patterns of these samples, maximum degree of intercalation and exfoliation is always obtained by using Cloisite 30B, leading to maximum tensile strength and tensile modulus owing to higher level of polymer-clay adhesion and possible reactions between the clay modifier and the unsaturated polyester resin [37]. In samples containing Cloisite 25A and Cloisite 15A, unintercalated clay particles form agglomerates and because of that clay-polymer interactions are lower. On the other hand, nanocomposites prepared by PG show no significant change in tensile properties by the addition of different types of organoclays.

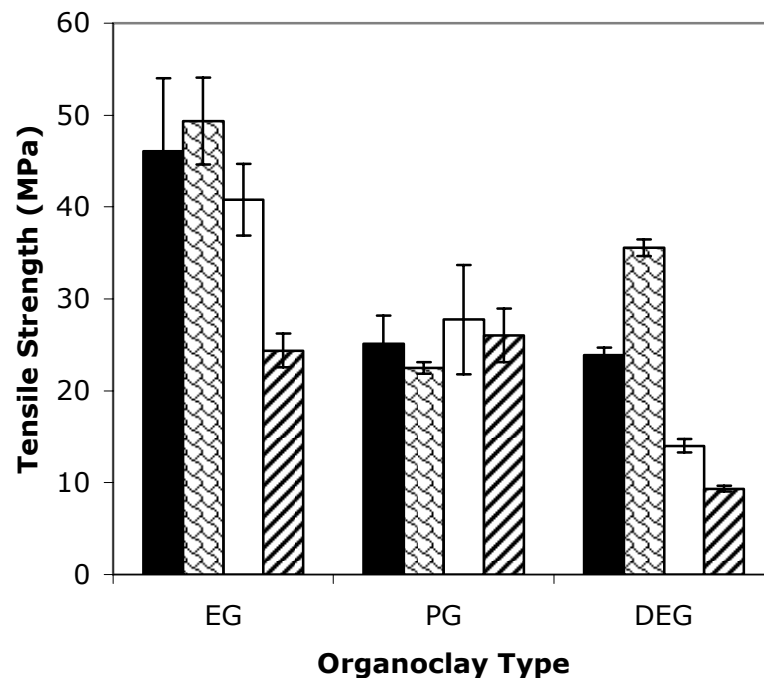


Figure 4.31 Effect of organoclay type (1 wt. %) on the tensile strength values of nanocomposites prepared by different glycol types (From left to right: pure UP, Cloisite 30B, Cloisite 25A, Cloisite 15A)

Another factor that influences the polymer clay interaction is the organic modifier of the clay. Functionalized organic cations (carboxylic acid and hydroxyl groups) which are used to modify the montmorillonite, can strongly interact with the matrix during curing [29]. Cloisite 30B has two hydroxyl groups, that can react with the carboxyl groups and the tensile strength and tensile modulus results confirm the importance of strong interaction between the matrix and clay.

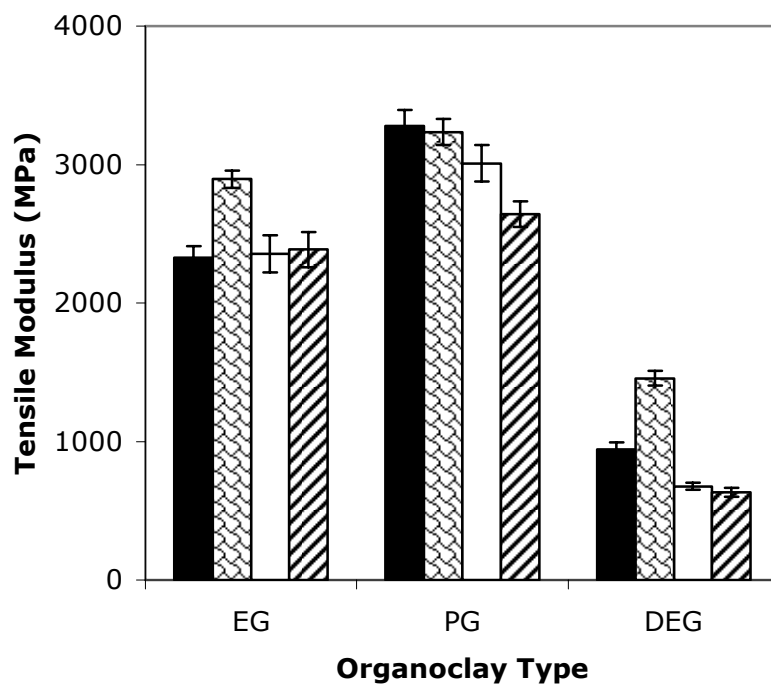


Figure 4.32 Effect of organoclay type (1 wt. %) on the tensile modulus values of nanocomposites prepared by different glycol types (From left to right: pure UP, Cloisite 30B, Cloisite 25A, Cloisite 15A)

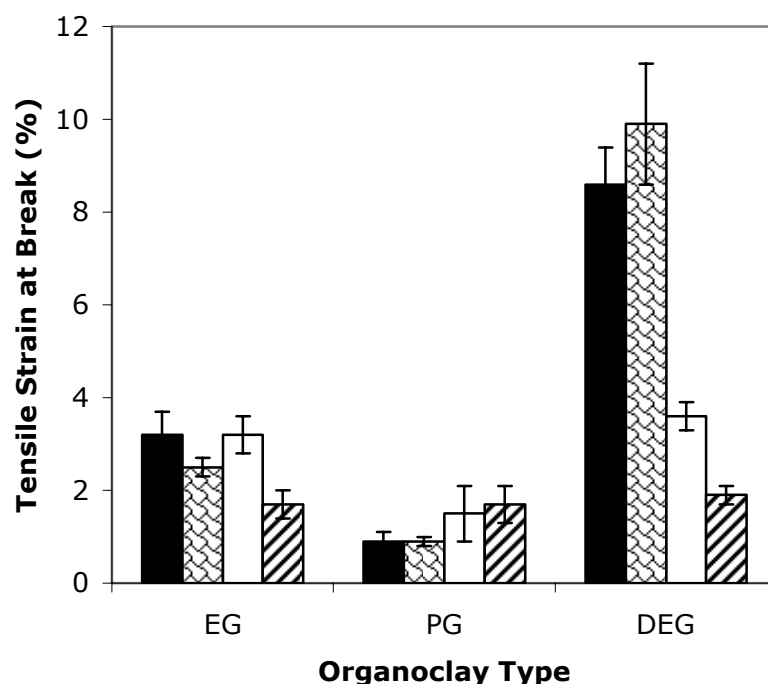


Figure 4.33 Effect of organoclay type (1 wt. %) on the tensile strain at break values of nanocomposites prepared by different glycol types (From left to right: pure UP, Cloisite 30B, Cloisite 25A, Cloisite 15A)

Figure 4.33 shows the tensile strain at break (%) values of the samples with respect to the organoclay type. As Figure 4.33 shows, there is no significant difference between the tensile strain at break values of the samples, except for nanocomposites prepared by DEG. Samples containing Cloisite 25A and Cloisite 15A exhibit a decreasing trend. This result can be attributed to the agglomeration of the silicate sheets which are obviously seen in SEM micrographs and XRD patterns. This is caused by poor adhesion between the polymer and the clay. Addition of rigid particulate fillers to a polymer matrix decreases the elongation at break since a more brittle structure is obtained. On the other hand, samples based on DEG that contain Cloisite 30B exhibit an increasing trend. Only in rare instances, if there is a good adhesion between the polymer and the filler, the fracture goes from particle to particle rather than following a direct path; in this case the filled polymers have higher elongations at break compared to neat resin [57]. SEM micrographs of this sample show a tortuous crack propagation path supporting this analysis.

4.2.2 Flexural Test Analysis

In this part, flexural properties of nanocomposites are presented. Flexural strength, flexural modulus and flexural strain at maximum stress values are discussed with respect to the glycol type, clay concentration and clay type. As mentioned before, samples synthesized by DEG are the most flexible. Owing to the highest flexibility of these samples, flexural tests continued beyond the maximum stress point. Furthermore, at 5 wt. % clay loading, the samples did not break at the end of the test. In order to compare all the compositions on the same basis, flexural strain at maximum stress values are used in the figures.

The effect of glycol type on the nanocomposites is shown in Figures 4.34 through 4.37. These graphs are in similar trend with the stress-strain graphs obtained by tensile test. DEG based samples give the highest flexural strain at maximum stress value and the lowest flexural strength and modulus values. These result show that the DEG units impart flexibility to the cured product. This can be attributed to the increase of the distance between the crosslink points in the cured resin and the flexible long linear ether linkages, which enable the chains to move more freely. It is observed that DEG based samples have lower crosslink density [3].

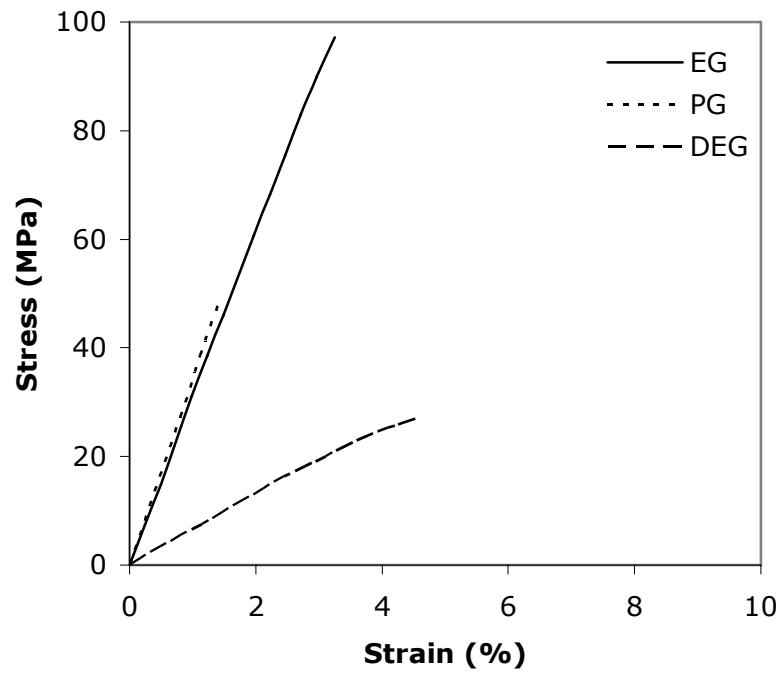


Figure 4.34 Effect of glycol type on the flexural stress-strain behavior of pure unsaturated polyesters

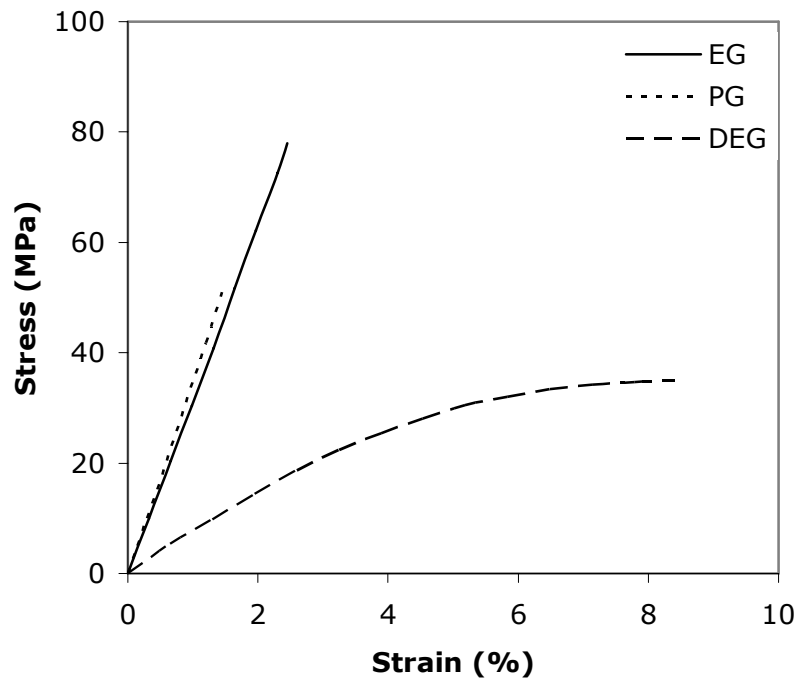


Figure 4.35 Effect of glycol type on the flexural stress-strain behavior of nanocomposites containing 1 wt. % organoclay (Cloisite 30B)

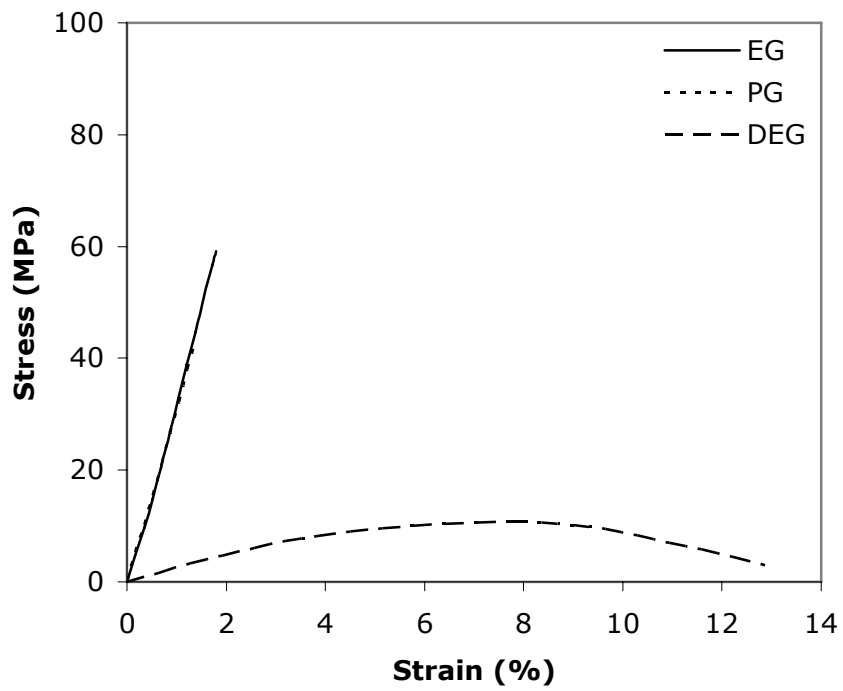


Figure 4.36 Effect of glycol type on the flexural stress-strain behavior of nanocomposites containing 3 wt. % organoclay (Cloisite 30B)

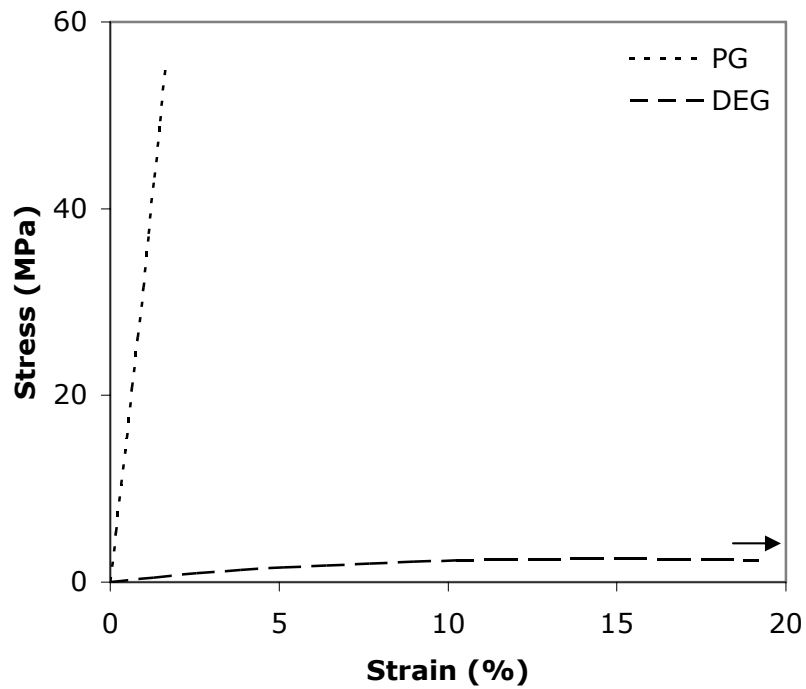


Figure 4.37 Effect of glycol type on the flexural stress-strain behavior of nanocomposites containing 5 wt. % organoclay (Cloisite 30B)

Because of the shortest chain length, EG units give rigidity to the cured products. Highest flexural strength values are obtained with EG based samples. As discussed in the previous part, PG based resins are more compatible with styrene. Therefore, samples synthesized by PG have higher crosslink density and they show highest flexural modulus and lowest flexural strain at maximum stress values.

Figures 4.38 through 4.40 display the flexural stress-strain behavior of the nanocomposites with respect to the organoclay content. Although, tensile strength and modulus values of EG based samples give maxima at 1 wt. % clay content and XRD results suggest an exfoliated structure, no improvement is shown in the flexural properties with respect to organoclay concentration. Moreover, in stress-strain curves of the samples synthesized by PG, no significant change is observed in the flexural properties. On the other hand, samples prepared by DEG give the maximum flexural strength and modulus values at 1 wt. % clay content. However, beyond 1 wt. % clay content, flexural strength and modulus values sharply decrease and flexural strain at maximum stress values significantly increase. As a matter of fact, 5 wt. % clay content samples did not break during the flexural test.

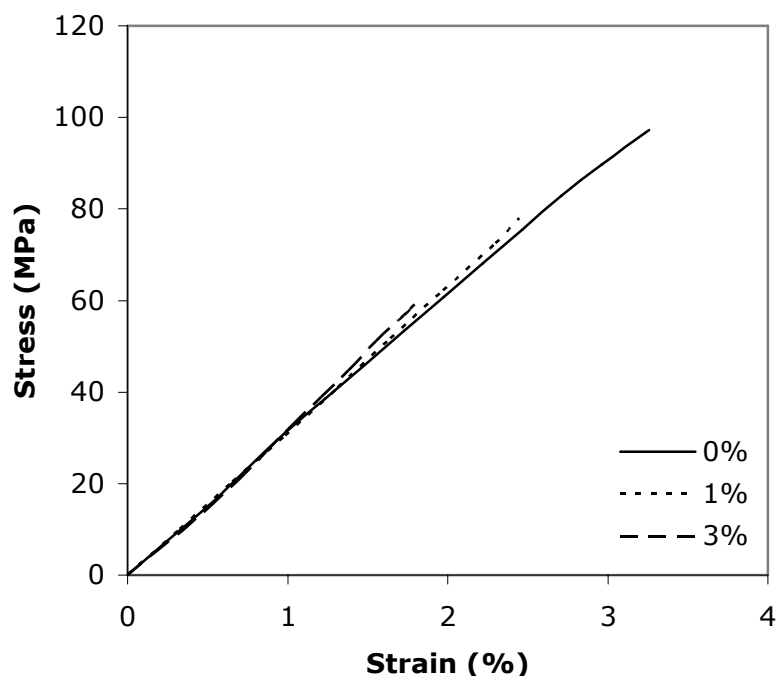


Figure 4.38 Effect of organoclay (Cloisite 30B) content on the flexural stress-strain behavior of nanocomposites prepared by EG

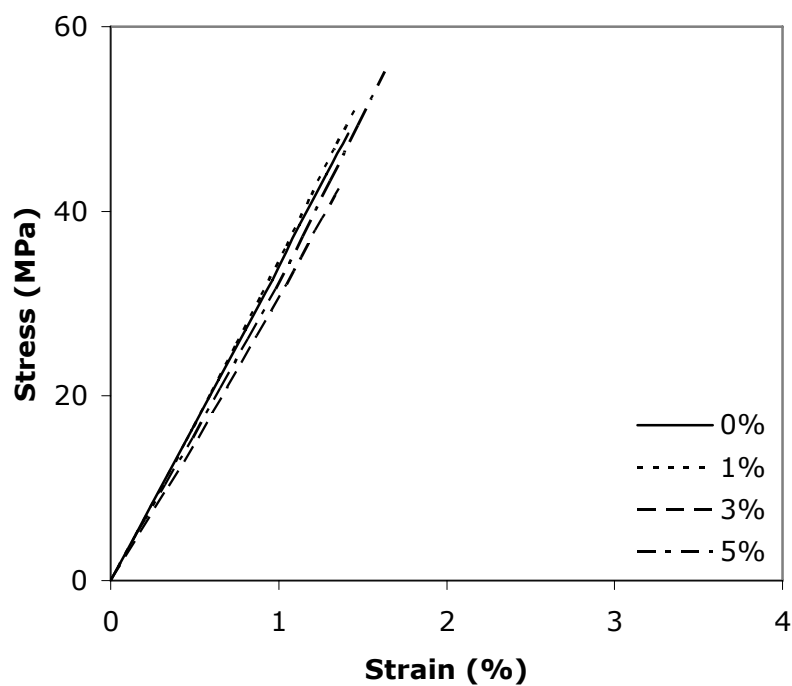


Figure 4.39 Effect of organoclay (Cloisite 30B) content on the flexural stress-strain behavior of nanocomposites prepared by PG

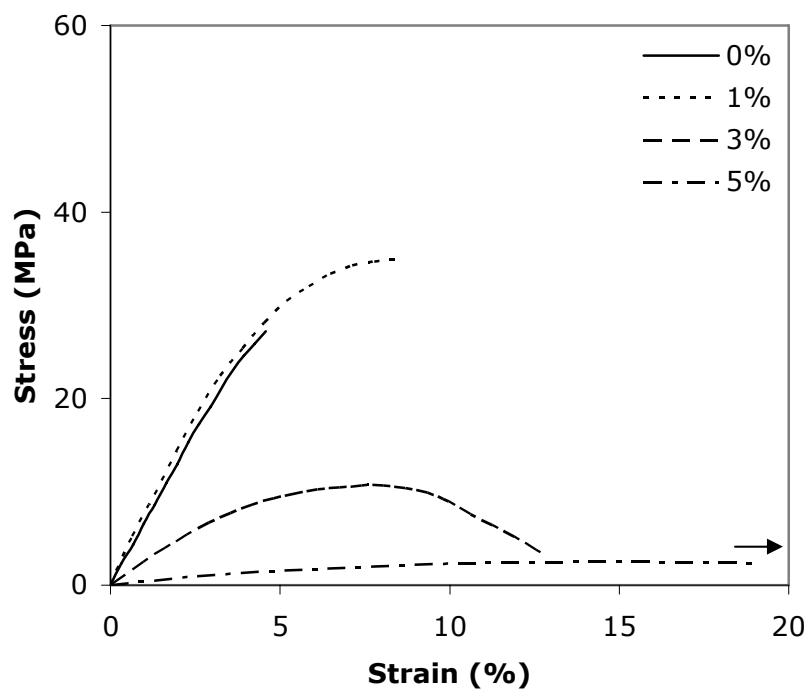


Figure 4.40 Effect of organoclay (Cloisite 30B) content on the flexural stress-strain behavior of nanocomposites prepared by DEG

As shown in Figures 4.25 and 4.41, flexural strength values are significantly greater than the tensile strength values due to the nature of the flexural test. Flexural test involves both tension and compression. The crack forms at the bottom of the specimen, which is under tension and grows up to the compression part. At this point, crack can not propagate easily towards the upper part because this part is in compression and prevents the propagation of the crack [23].

Even though rigid particulate fillers increase the flexural modulus, at high clay contents flexural modulus values show a decreasing trend as seen in Figure 4.42. The reason for that is the agglomeration of the clay particles and poor adhesion between polymer and clay at high clay concentrations. Agglomerates are weak points in the material and break easily when stress is applied. Then, they behave as strong stress concentrators [57]. Also, the crosslink density decreases with increasing clay content.

Clay concentration is highly effective on flexural strain at maximum stress values (Figure 4.43), especially on DEG based samples. This can be attributed to the decrease in the crosslink density of the material. As discussed in the tensile test part, high clay concentrations lower the crosslink density of the cured product.

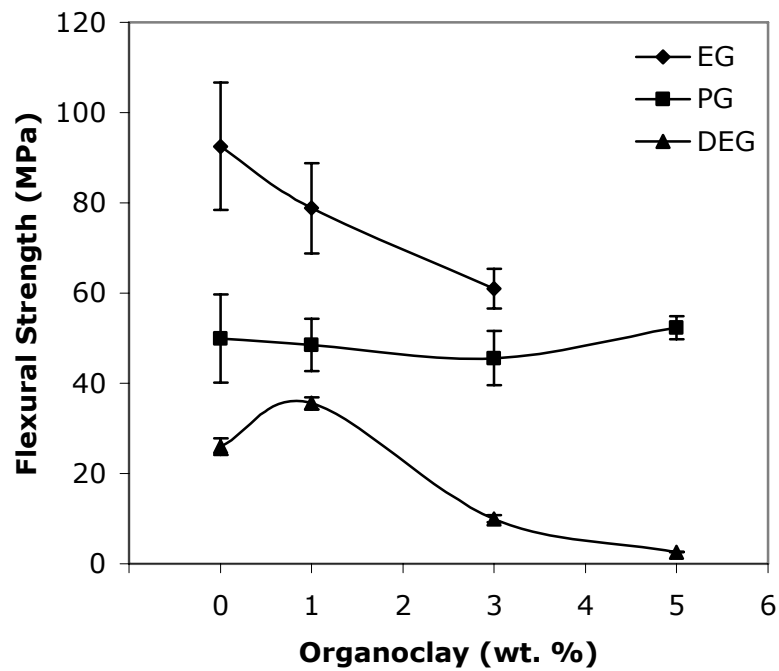


Figure 4.41 Effect of organoclay (Cloisite 30B) content on the flexural strength values of nanocomposites prepared by different glycol types

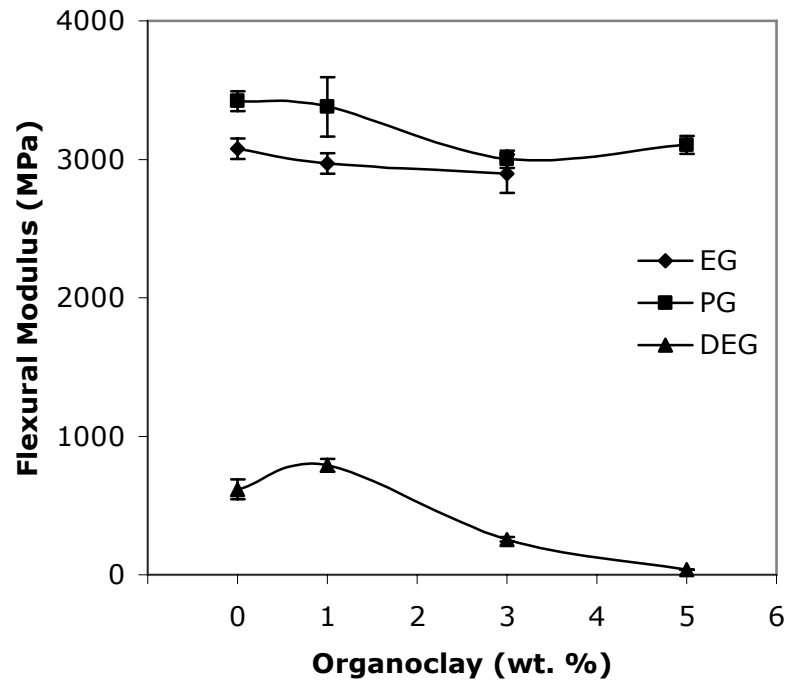


Figure 4.42 Effect of organoclay (Cloisite 30B) content on the flexural modulus values of nanocomposites prepared by different glycol types

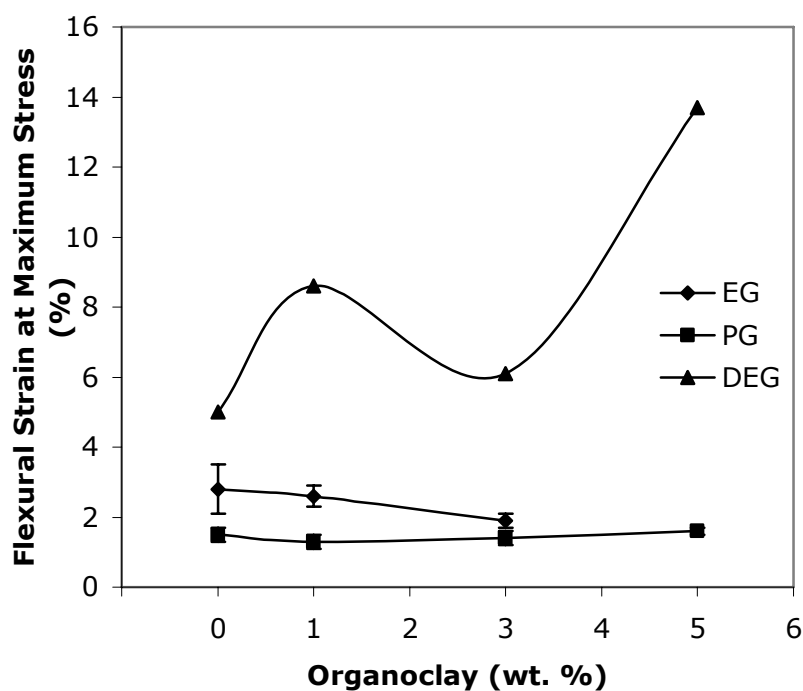


Figure 4.43 Effect of organoclay (Cloisite 30B) content on the flexural strain at maximum stress values of nanocomposites prepared by different glycol types

Flexural stress-strain curves of nanocomposites synthesized by different types of organoclays are seen in Figures 4.44 through 4.46. In samples based on DEG, Cloisite 30B show highest flexural properties. Samples containing Cloisite 25A and Cloisite 15A follow these results, which are in good agreement with the tensile test results. However, in EG and PG based samples, Cloisite 25A show the highest flexural strength and flexural strain at maximum stress values.

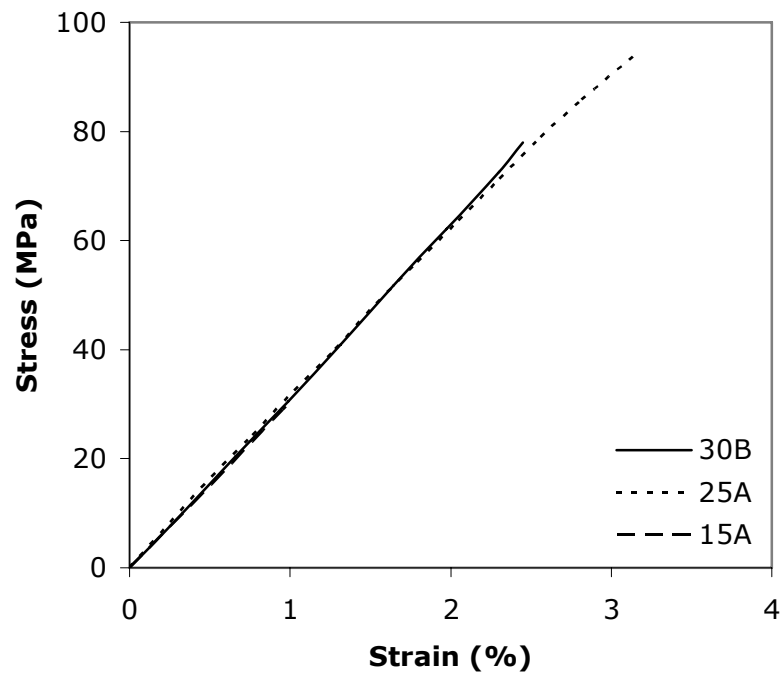


Figure 4.44 Effect of organoclay type (1 wt. %) on the flexural stress-strain behavior of nanocomposites prepared by EG

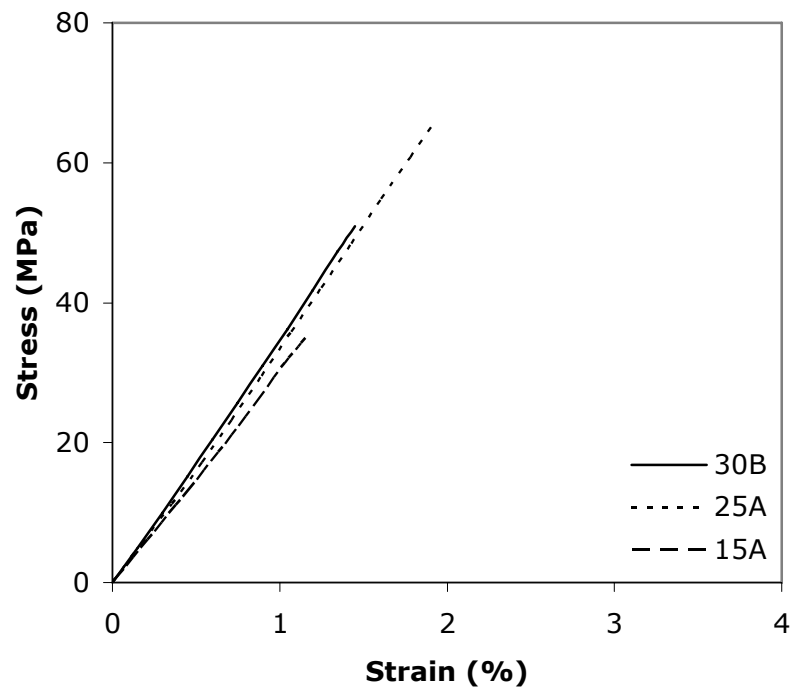


Figure 4.45 Effect of organoclay type (1 wt. %) on the flexural stress-strain behavior of nanocomposites prepared by PG

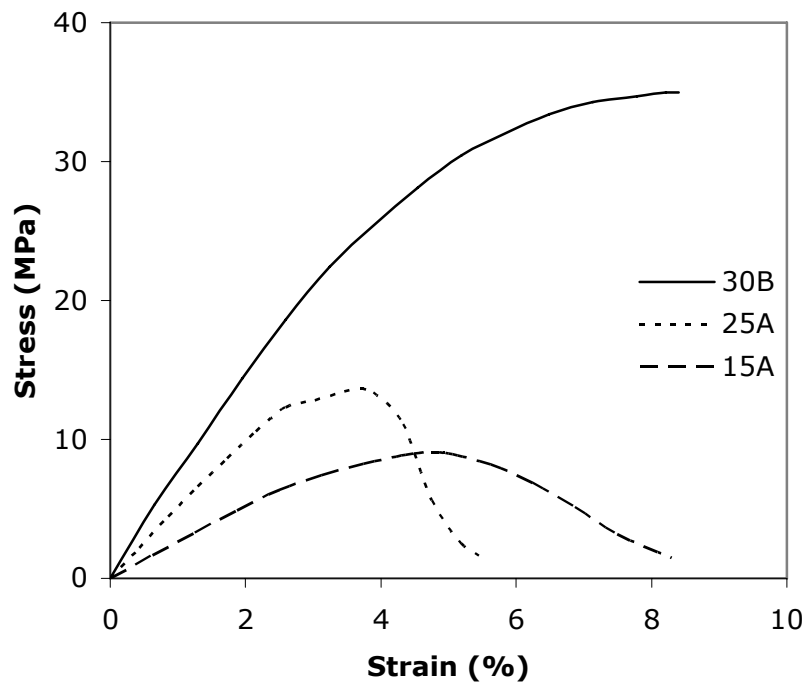


Figure 4.46 Effect of organoclay type (1 wt. %) on the flexural stress-strain behavior of nanocomposites prepared by DEG

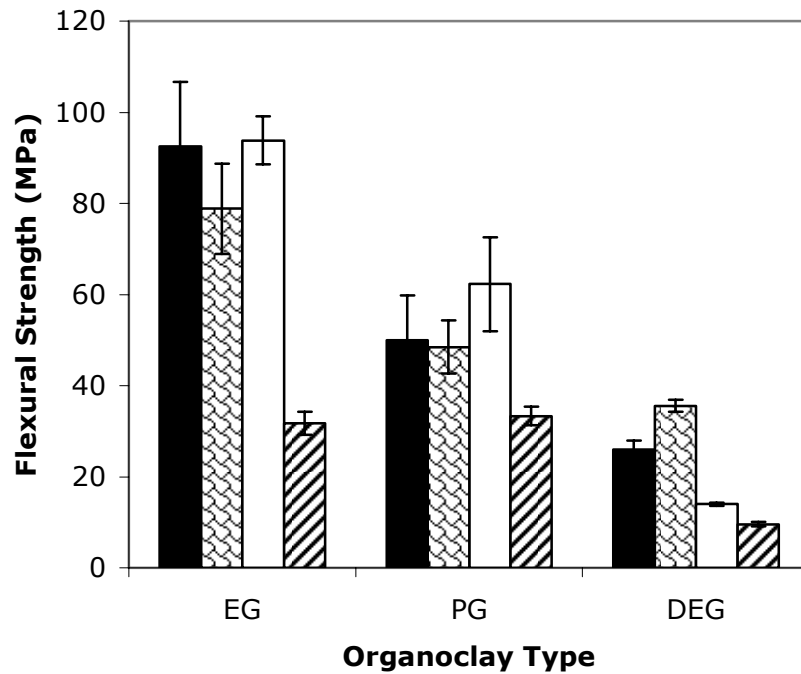


Figure 4.47 Effect of organoclay type (1 wt. %) on the flexural strength values of nanocomposites prepared by different glycol types (From left to right: pure UP, Cloisite 30B, Cloisite 25A, Cloisite 15A)

Figures 4.47 through 4.49 display the flexural strength, flexural modulus and flexural strain at maximum stress values with respect to organoclay type, respectively. As shown in these figures, DEG based samples containing Cloisite 30B exhibit the highest flexural properties owing to reactions between the hydroxyl groups within the clay modifier and the unsaturated polyester resin during curing. On the other hand, EG and PG based samples show no significant improvement in flexural properties with respect to the neat unsaturated polyesters. The reason for that could be the highly brittle structure of these samples.

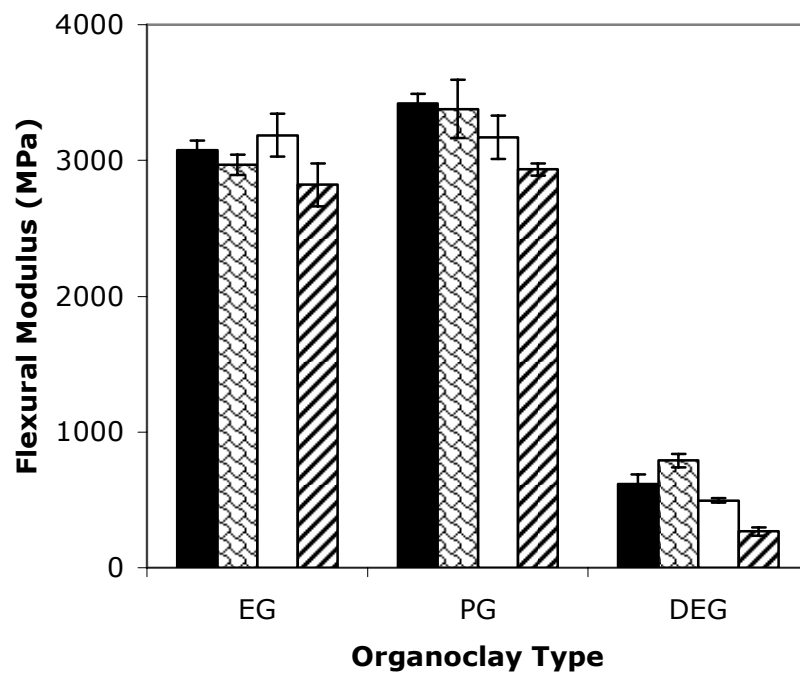


Figure 4.48 Effect of organoclay type (1 wt. %) on the flexural modulus values of nanocomposites prepared by different glycol types (From left to right: pure UP, Cloisite 30B, Cloisite 25A, Cloisite 15A)

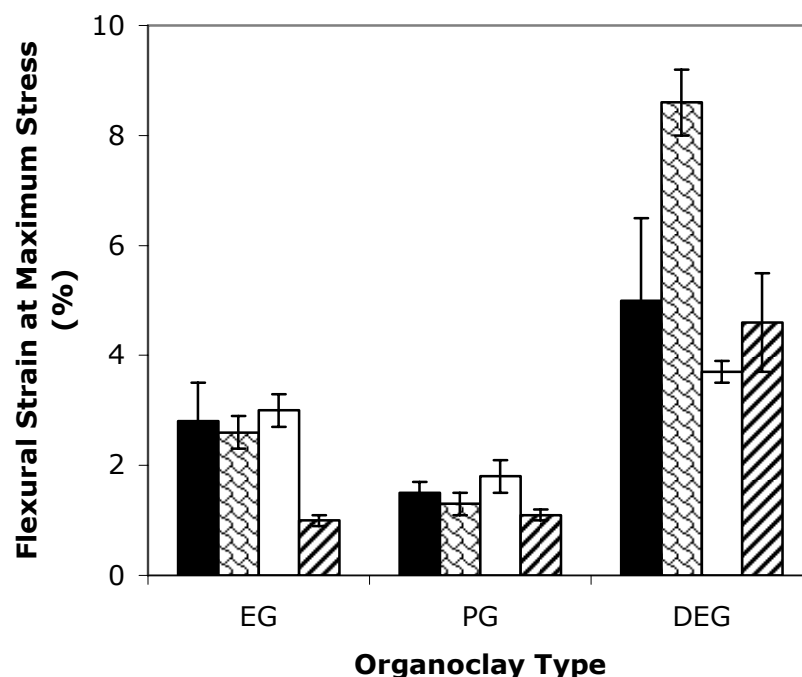


Figure 4.49 Effect of organoclay type (1 wt. %) on the flexural strain at maximum stress values of nanocomposites prepared by different glycol types (From left to right: pure UP, Cloisite 30B, Cloisite 25A, Cloisite 15A)

4.2.3 Impact Test Analysis

The impact strength is defined in terms of the area under the stress-strain curve or as energy to break. High impact strength and toughness are generally obtained by large strain at break values and large areas under the stress-strain curve [57].

Figure 4.50 shows the impact strength of the samples with respect to the organoclay content and glycol type. With respect to the glycol type, DEG based samples have the highest impact strength values due to the highest strain at break values. Furthermore, in all SEM micrographs of DEG based samples tortuous crack propagation path is seen, supporting these results. EG based samples follow DEG based samples. Finally, PG based samples show the lowest impact strength values. As mentioned in the previous parts, chemical structure of the glycols and their compatibility with styrene monomer highly affected the mechanical properties.

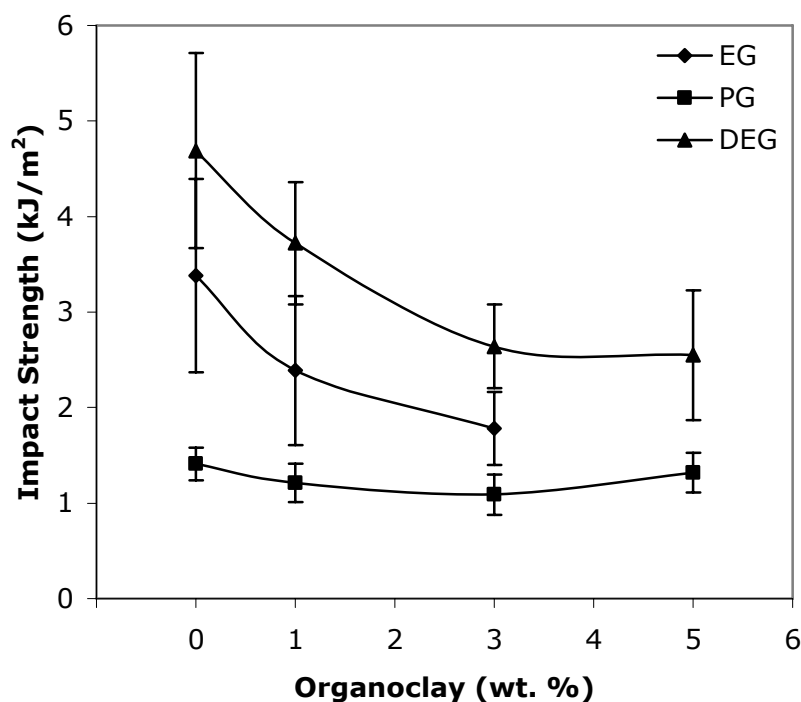


Figure 4.50 Effect of organoclay (Cloisite 30B) content on the impact strength values of nanocomposites prepared by different glycol types

Rigid fillers in a rigid polymer generally decrease the impact strength of a polymer. Impact strength is determined by the dewetting and crazing phenomena. The addition of rigid dewetting particles is the cause of the production of cracks. The crack propagates readily, so the particle acts as a crack initiator and lowers the impact strength. If there is no agglomeration of the particle, impact strength increases as particle size decreases [57].

As seen in Figure 4.50, impact strength decreases with the increase in the clay content. As discussed above, rigid particles decrease the impact strength values. Besides, at high clay concentrations, clay agglomerates are seen in the SEM micrographs, which act as stress concentrators and cause decrease in impact strength. On the other hand, PG based samples show an increasing trend beyond 3 wt. % clay loading. SEM micrographs of the PG based samples with 5 wt. % clay content exhibit a tortuous crack propagation path, which explain the slight increase in the impact strength. But this value is still smaller than the impact strength of neat unsaturated polyester.

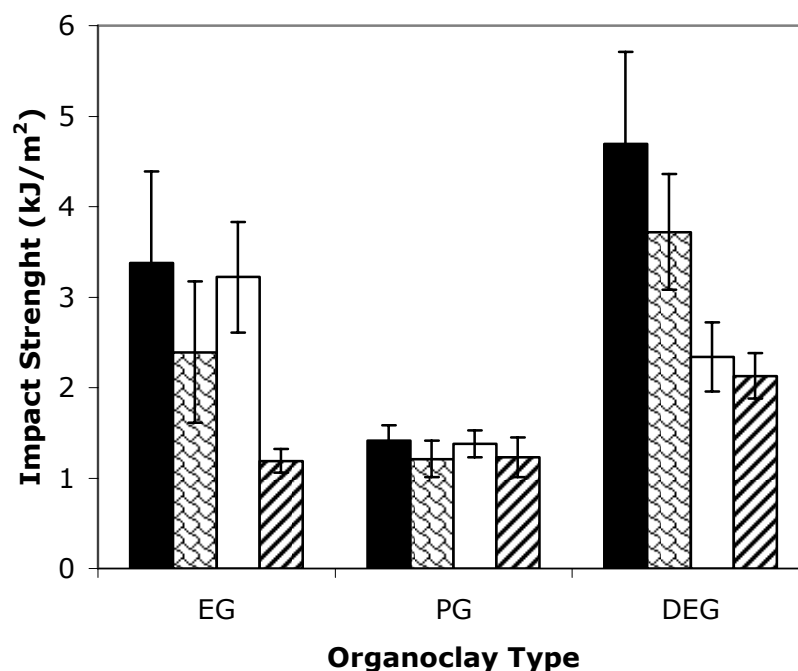


Figure 4.51 Effect of organoclay type (1 wt. %) on the impact strength values of nanocomposites prepared by different glycol types (From left to right: pure UP, Cloisite 30B, Cloisite 25A, Cloisite 15A)

The effect of organoclay type on the impact strength values are given in Figure 4.51. The effect of glycol type can also be seen in this figure. Impact values of samples prepared by PG show no significant difference owing to the brittle nature of the material. Surprisingly, EG based samples containing Cloisite 25A give the highest impact strength value among the other organoclay types. This result is completely different from the XRD and tensile test results. Experimental errors may occur during the mechanical testing, since samples synthesized by EG are also very brittle.

DEG based samples are the most flexible. Because of that, the effect of organoclay type is clearly seen in the figure. The only difference between organoclays are the organic modifiers used to render their structure from hydrophilic to organophilic and increase the distance between the platelets so that polymer molecules can easily get intercalated through the gap [37]. Although, Cloisite 15A has the maximum d-spacing, samples containing Cloisite 15A show the lowest impact strength value. Since unsaturated polyester is not a hydrophobic polymer, Cloisite 30B is the most compatible organoclay with

unsaturated polyester according to Figure 3.5. Moreover, Cloisite 30B has two hydroxyl groups that can strongly react with the UP resin. Thus, clay particles homogeneously disperse in the matrix and higher adhesion is obtained between the polymer and clay. The impact strength of the samples containing Cloisite 30B is the highest. However, Cloisite 25A and Cloisite 15A containing samples indicate low impact strength values. This is due to the agglomeration of the clay particles. As discussed above, clay agglomerates decrease the impact strength. These results are also in good agreement with the SEM micrographs of DEG based samples.

CHAPTER 5

CONCLUSIONS

In XRD analysis, in EG based samples containing 1 wt. % organoclay (Cloisite 30B) and in DEG based samples containing 3 wt. % organoclay, no peak is detected by XRD, which suggests that exfoliated structures are obtained. For samples synthesized by PG, the characteristic interlayer spacing of Cloisite 30B is increased to 41.43 Å at 1 wt. % clay loading, indicating the intercalation of the polymer chains between the silicate sheets. At high clay loadings a slight decrease in the d-spacings is observed. On the other hand, nanocomposite based on EG exhibits the highest compatibility with organoclay and shows an exfoliated structure. However, nanocomposites synthesized by DEG exhibit the lowest compatibility with organoclay and give smallest d-spacing values among other compositions. With respect to the organoclay type, maximum increase in the gallery size is obtained by Cloisite 30B. Cloisite 15A containing samples exhibit the minimum increase in the d-spacing. XRD analyses show that, clay type is much more effective than the other parameters.

SEM micrographs show that, the impact fractured surfaces of neat unsaturated polyesters are smooth and few straight crack propagation lines are observed. It is seen that featureless structures of pure unsaturated polyesters disappear with increasing organoclay content. Samples prepared by DEG have the most tortuous crack propagation path. EG and PG based samples show agglomerates of clay. The amount and size of the agglomerates increase with increasing organoclay concentration. However, at high clay contents PG based samples exhibit a tortuous crack propagation path. Only in DEG based samples, the influence of organoclay type is clearly seen. Sample containing Cloisite 30B shows a tortuous crack propagation path. Agglomeration is seen in the sample containing Cloisite 25A and smooth structure is observed in the sample containing Cloisite 15A. These results are in good agreement with both XRD and impact test results.

It is obviously seen that, for all mechanical properties, glycol type is the most effective experimental parameter. Mechanical behavior of nanocomposites indicate that, DEG based samples are the most flexible and PG based samples are the least flexible.

In tensile tests, samples synthesized by EG exhibit the maximum tensile strength and tensile modulus values at 1 wt. % organoclay loading. This sample also displays an exfoliated structure according to XRD pattern. Stiffness of the materials is improved by the addition of relatively low amounts of organoclay. At high clay loadings, a sudden increase in the strain at break values of DEG based nanocomposites is observed. In the comparison of the clay types, Cloisite 30B is found to exhibit the highest and Cloisite 15A is found to exhibit the lowest tensile strength values in all glycol types.

In terms of flexural behavior, in samples prepared by PG no significant changes are observed with respect to clay content. EG based samples show a decreasing trend in flexural properties with increasing clay content. On the other hand, DEG based samples give 36% rise in flexural strength and 28% increment in flexural modulus at 1 wt. % clay content. Besides, strain at maximum stress values increase at high clay loadings. These results support the tensile test results. As for the effect of organoclay type, EG and PG based samples show no significant improvement in flexural properties with respect to the neat unsaturated polyesters. However, in nanocomposites based on DEG, Cloisite 30B containing samples exhibit the best flexural properties.

DEG based samples have the highest impact strength values and these samples also exhibit a tortuous crack propagation path as seen from the SEM micrographs. Although, all the samples give a decreasing trend in the impact strength with the addition of organoclay, sample based on PG and 5 wt. % Cloisite 30B show a slight increase in impact strength. Samples prepared by EG and DEG show the highest impact strength values with Cloisite 25A and Cloisite 30B, respectively.

REFERENCES

- [1] Giannelis E.P., "Polymer Layered Silicate Nanocomposites", *Advanced Materials*, vol.8, p.29-35, (1996)
- [2] Giannelis E.P., "Polymer-Layered Silicate Nanocomposites: Synthesis, Properties and Applications", *Applied Organometallic Chemistry*, vol.12, p.675-680, (1998)
- [3] Suh D.J., Park O.O., Yoon K.H., "The Properties of Unsaturated Polyester Based on the Glycolized Poly(ethylene terephthalate) with Various Glycol Compositions", *Polymer*, vol.41, p.461-466, (2000)
- [4] Suh D.J., Lim Y.T., Park O.O., "The Property and Formation Mechanism of Unsaturated Polyester-Layered Silicate Nanocomposite Depending on the Fabrication Methods", *Polymer*, vol.41, p.8557-8563, (2000)
- [5] Akovali G., "Handbook of Composite Fabrication", Rapra Technology Limited, Shawbury, (2001)
- [6] Brandrup J., Bittner M., Michaeli W., Menges G., "Recycling and Recovery of Plastics", Carl Hanser Verlag, New York, (1996)
- [7] Mantia F., "Handbook of Plastics Recycling", Rapra Technology Limited, Shawbury, (2002)
- [8] Nadkarni V., "Polyester Waste Recycling: Sources, Processing Methods and End Uses", *International Fiber Journal*, vol.14, issue 3, (1999)
- [9] Ehrig R.J., "Plastics Recycling, Products and Processes", Hanser Publishers, New York, (1992)
- [10] Post Consumer Products Archives, <http://www.nrcan.gc.ca/mms/canmet-mtb/mmsl-lmsm/rnet/postarte.htm>, last accessed July 2005
- [11] Plastic / Polymer Recycling, <http://www.lotfi.net/recycle/plastic.html>, last accessed July 2005
- [12] Paszun D., Spychaj T., "Chemical Recycling of Poly(ethylene terephthalate)", *Industrial and Engineering Chemistry Research*, vol.36, p.1373-1383, (1997)

- [13] Malik M., Choudhary V., Varma I.K., "Current Status of Unsaturated Polyester Resins", *Rev. Macromol. Chem. Phys.*, c40(2&3), p.139-165, (2000)
- [14] Gamstedt E.K., Skrifvars M., Jacobsen T.K., Pyrz R., "Synthesis of Unsaturated Polyesters for Improved Interfacial Strength in Carbon Fibre Composites", *Composites: Part A* 33, p.1239-1252, (2002)
- [15] Boenig H.V., "Unsaturated Polyesters: Structure and Properties", Elsevier Publishing Company, Amsterdam, (1964)
- [16] "Kirk-Othmer Encyclopedia of Chemical Technology", 4th ed., John Wiley and Sons, Inc., New York, (1993)
- [17] Strong A.B., "Fundamentals of Composites Manufacturing: Materials, Methods and Applications", Society of Manufacturing Engineers, Publications Development Department, Reference Publications Division, Dearborn, (1989)
- [18] Hsu C.P., Lee L.J., "Free-radical Crosslinking Copolymerization of Styrene/Unsaturated Polyester Resins: 3. Kinetics-Gelation Mechanism", *Polymer*, vol.34, no.21, p.4516-4523, (1993)
- [19] "Polymeric Materials Encyclopedia", vol.11, 8469-8475, CRC Press, New York, (1996)
- [20] Lubin G., "Handbook of Composites", Van Norstrand Reinhold, New York, (1982)
- [21] Callister W.D., "Materials Science and Engineering: An Introduction", 4th ed., John Wiley and Sons, Inc., New York, (1997)
- [22] Fried J.R., "Polymer Science and Technology", 2nd ed., Prentice Hall PTR, USA, (2003)
- [23] İnceoglu A.B., "Synthesis and Mechanical Properties of Unsaturated Polyester Based Nanocomposites", M.S. Thesis, Department of Chemical Engineering, METU, Ankara, (2001)
- [24] Tolle T.B., Anderson D.P., "Morphology Development in Layered Silicate Thermoset Nanocomposites", *Composites Science and Technology*, vol.62, p.1033-1041, (2002)

- [25] Alexandre M., Dubois P., "Polymer-Layered Silicate Nanocomposites: Preparation, Properties and Uses of a New Class of Materials", *Materials Science and Engineering*, vol.28, p.1-63, (2000)
- [26] LeBaron P.C., Wang Z., Pinnavaia T.J., "Polymer-Layered Silicate Nanocomposites: An Overview", *Applied Clay Science*, vol.15, p.11-29, (1999)
- [27] İnceoglu A.B., Yilmazer Ü., "Synthesis and Mechanical Properties of Unsaturated Polyester Based Nanocomposites", *Polymer Engineering and Science*, vol.43, no.3, p.661-669, (2003)
- [28] Schmidt D., Shah D., Giannelis E.P., "New Advances in Polymer/Layered Silicate Nanocomposites", *Current Opinion in Solid State and Materials Science*", vol.6, p.205-212, (2002)
- [29] Ray S.S., Okamoto M., "Polymer/Layered Silicate Nanocomposites: A Review from Preparation to Processing", *Progress in Polymer Science*, vol.28, p.1539-1641, (2003)
- [30] Kornmann X., "Synthesis and Characterization of Thermoset-Clay Nanocomposites", Ph. D. Thesis, Lulea University of Technology, Sweden, (2000)
- [31] Pinnavaia T.J., Beall G.W., "Polymer-Clay Nanocomposites", John Wiley and Sons, Ltd., England, (2000)
- [32] Rotheron R.N., "Particulate-Filled Polymer Composites", 2nd ed., Rapra Technology Limited, Shawbury, (2003)
- [33] Seymour R.B., Carraher C.E., "Structure-Property Relationships in Polymers", Plenum Press, New York, (1984)
- [34] Kılınc M., "Processing and Characterization of Poly(ethylene terephthalate) Based Composites", M.S. Thesis, Department of Chemical Engineering, METU, Ankara, (2004)
- [35] ASTM D638M-91a, Standard Test Method for Tensile Properties of Plastics, "Annual Book of ASTM Standards", vol.08.01, p.174-182, Philadelphia, USA, (1993)
- [36] ASTM D790M-92, Standard Test Methods for Flexural Properties of Unreinforced and Reinforced Plastics and Electrical Insulating Materials, "Annual Book of ASTM Standards", vol.08.01, p.284-292, Philadelphia, USA, (1993)

- [37] Toprak P., "A New Route to the Synthesis of Nanocomposites by Using an Unsaturated Polyester Matrix", M.S. Thesis, Department of Chemical Engineering, METU, Ankara, (2004)
- [38] ASTM D256-92, Standard Test Methods for Impact Resistance of Plastics and Electrical Insulating Materials, "Annual Book of ASTM Standards", vol.08.01, p.58-74, Philadelphia, USA, (1993)
- [39] "Concise Encyclopedia of Polymer Science and Engineering", John Wiley and Sons, Inc., New York, (1990)
- [40] Vaidya U.R., Nadkarni V.M., "Unsaturated Polyester Resins from Poly(ethylene terephthalate) Waste. 1. Synthesis and Characterization", Industrial and Engineering Chemistry Research, vol.26, p.194-198, (1987)
- [41] Vaidya U.R., Nadkarni V.M., "Unsaturated Polyester Resins from Poly(ethylene terephthalate) Waste. 2. Mechanical and Dynamic Mechanical Properties", Industrial and Engineering Chemistry Research, vol.27, p.2056-2060, (1988)
- [42] Vaidya U.R., Nadkarni V.M., "Unsaturated Polyesters from PET Waste: Kinetics of Polycondensation", Journal of Applied Polymer Science, vol.34, p.235-245, (1987)
- [43] Öztürk Y., Güçlü G., "Unsaturated Polyester Resins Obtained from Glycolysis Products of Waste PET", Polymer-Plastics Technology and Engineering, vol.43, no.5, p.1539-1552, (2004)
- [44] Lu M., Kim S., "Unsaturated Polyester Resins Based on Recycled PET: Preparation and Curing Behavior", Journal of Applied Polymer Science, vol.80, p.1052-1057, (2001)
- [45] Lee D.S., Lee S.H., Kim J.H., "Curing Behavior of Unsaturated Polyester Resins Based on Recycled Poly(ethylene terephthalate) (RPET): Effects of RPET Content and Glycol Type", Polymer International, vol.44, p.143-148, (1997)
- [46] Kornmann X., Berglund L.A., Sterte J., Giannelis E.P., "Nanocomposites Based on Montmorillonite and Unsaturated Polyester", Polymer Engineering and Science, vol.38, no.8, p.1351-1358, (1998)
- [47] Bharadwaj R.K., Mehrabi A.R., Hamilton C., Trujillo C., Murga M., Fan R., Chavira A., Thompson A.K., "Structure-Property Relationships in Cross-linked Polyester-Clay Nanocomposites", Polymer, vol.43, p.3699-3705, (2002)

- [48] Zhang Y., Cai Q., Jiang Z., Gong K., "Preparation and Properties of Unsaturated Polyester-Montmorillonite Intercalated Hybrid", *Journal of Applied Polymer Science*, vol.92, p.2038-2044, (2004)
- [49] Fu X., Qutubuddin S., "Synthesis of Unsaturated Polyester-Clay Nanocomposites Using Reactive Organoclays", *Polymer Engineering and Science*, vol.44, no.2, p.345-351, (2004)
- [50] Oleksy M., Heneczkowski M., Galina H., "Chemosetting Resins Containing Fillers. I. Unsaturated Polyester Resin Compositions Containing Modified Smectites", *Journal of Applied Polymer Science*, vol.96, p.793-801, (2005)
- [51] Mironi-Harpaz I., Narkis M., Siegmann A., "Nanocomposite Systems Based on Unsaturated Polyester and Organo-Clay", *Polymer Engineering and Science*, vol.45, p.174-186, (2005)
- [52] Xu L., Lee L.J., "Kinetic Analysis and Mechanical Properties of Nanoclay Reinforced Unsaturated Polyester (UP) Resins Cured at Low Temperatures", *Polymer Engineering and Science*, vol.45, p.496-509, (2005)
- [53] Aghdampour M., "Tertiary Recovery of Polyethyleneterephthalate", M.S. Thesis, Department of Chemical Engineering, METU, Ankara, (1993)
- [54] Curtis L.G., Edwards D.L., Simons R.M., Trent P.J., Von Bramer P.T., "Investigation of Maleate-Fumarate Isomerization in Unsaturated Polyesters by Nuclear Magnetic Resonance", *I&EC Product Research and Development*, vol.3, no.3, p.218-221, (1964)
- [55] Morgan A.B., Gilman J.W., "Characterization of Polymer-Layered Silicate (Clay) Nanocomposites by Transmission Electron Microscopy and X-Ray Diffraction: A Comparative Study", *Journal of Applied Polymer Science*, vol.87, p.1329-1338, (2003)
- [56] Goodman S.H., "Handbook of Thermoset Plastics", 2nd ed., Noyes Publications, Westwood, (1998)
- [57] Nielsen L. E., Landel R.F., "Mechanical Properties of Polymers and Composites", 2nd ed., Marcel Dekker Inc., New York, (1994)

APPENDIX A

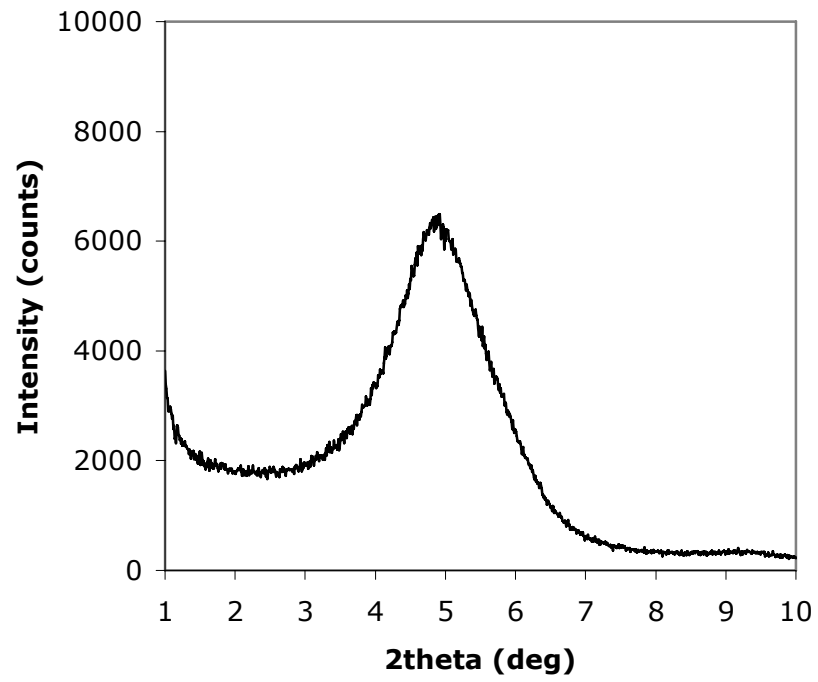


Figure A.1 X-ray diffraction pattern of Cloisite 30B

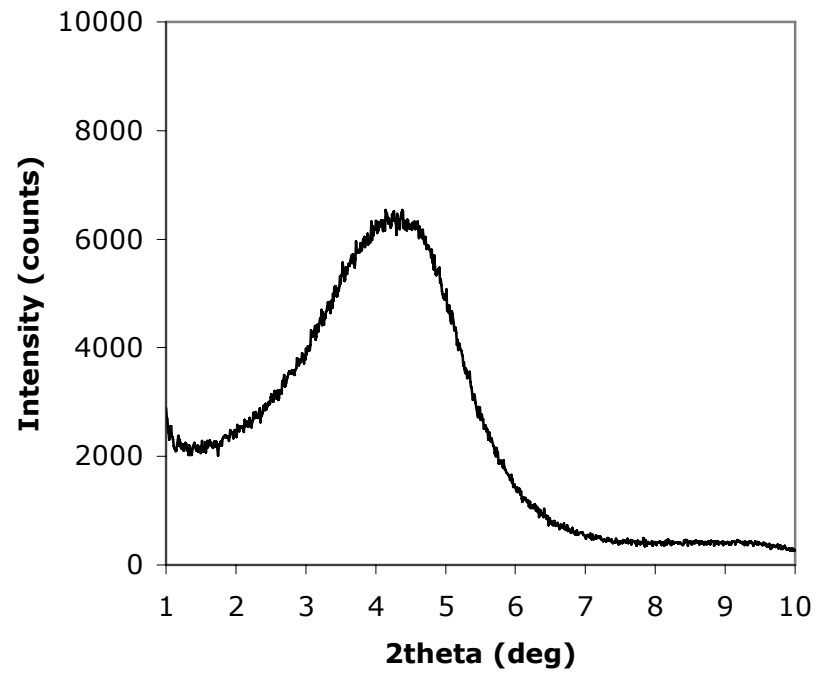


Figure A.2 X-ray diffraction pattern of Cloisite 25A

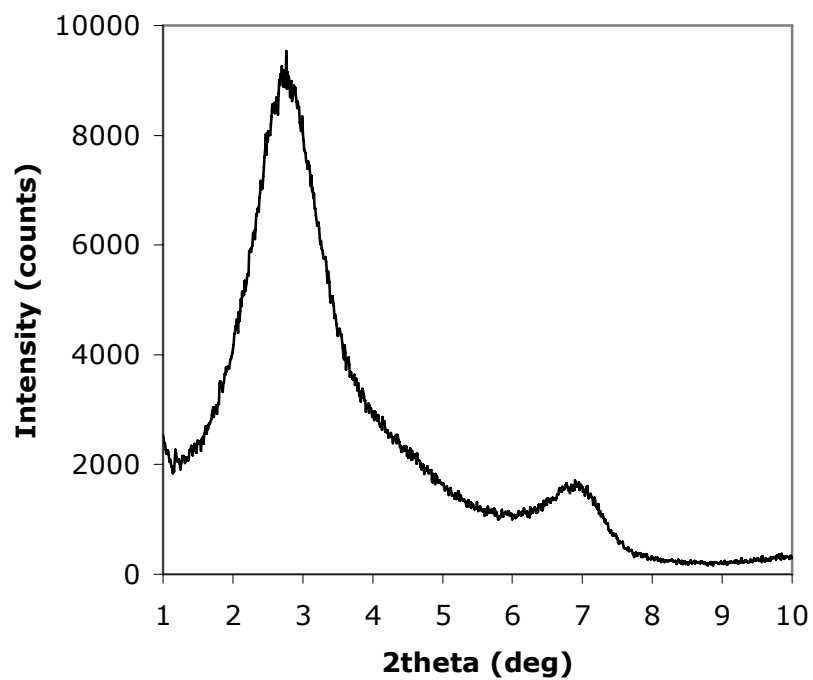


Figure A.3 X-ray diffraction pattern of Cloisite 15A

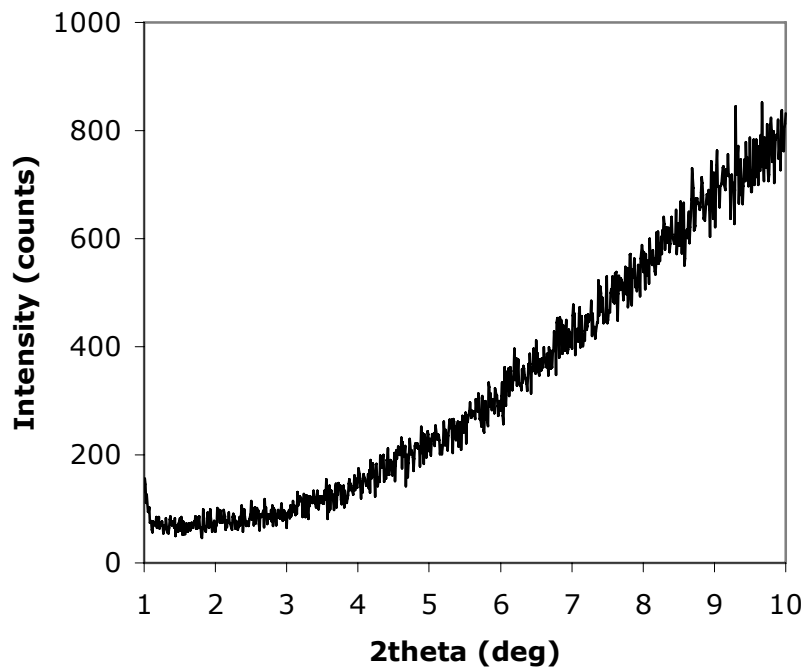


Figure A.4 X-ray diffraction pattern of pure unsaturated polyester synthesized by ethylene glycol

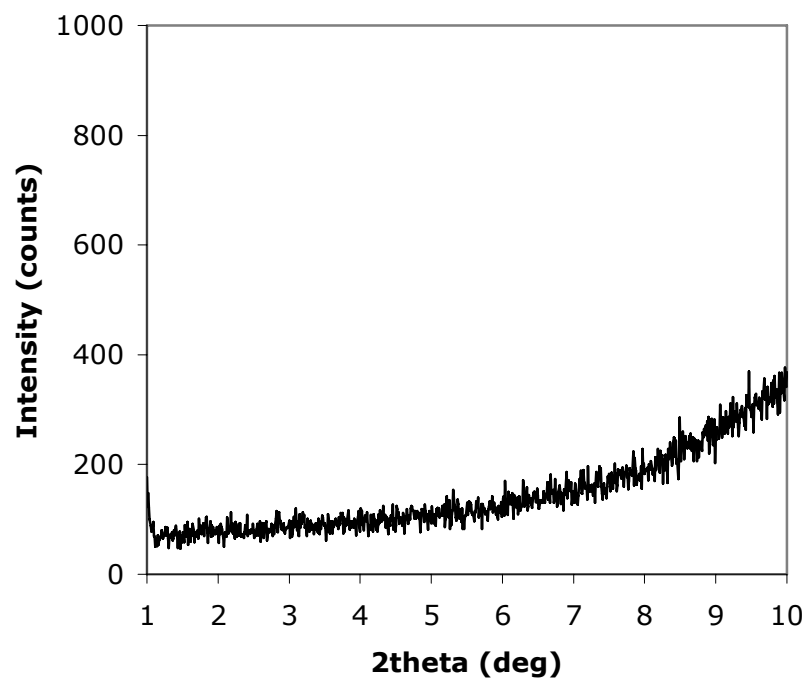


Figure A.5 X-ray diffraction pattern of nanocomposite synthesized by ethylene glycol containing 1 wt. % Cloisite 30B

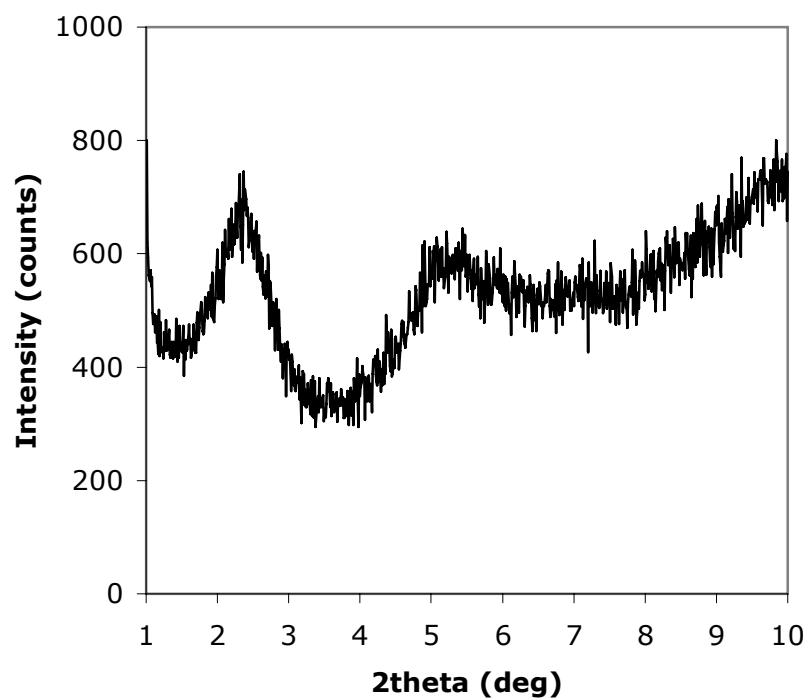


Figure A.6 X-ray diffraction pattern of nanocomposite synthesized by ethylene glycol containing 3 wt. % Cloisite 30B

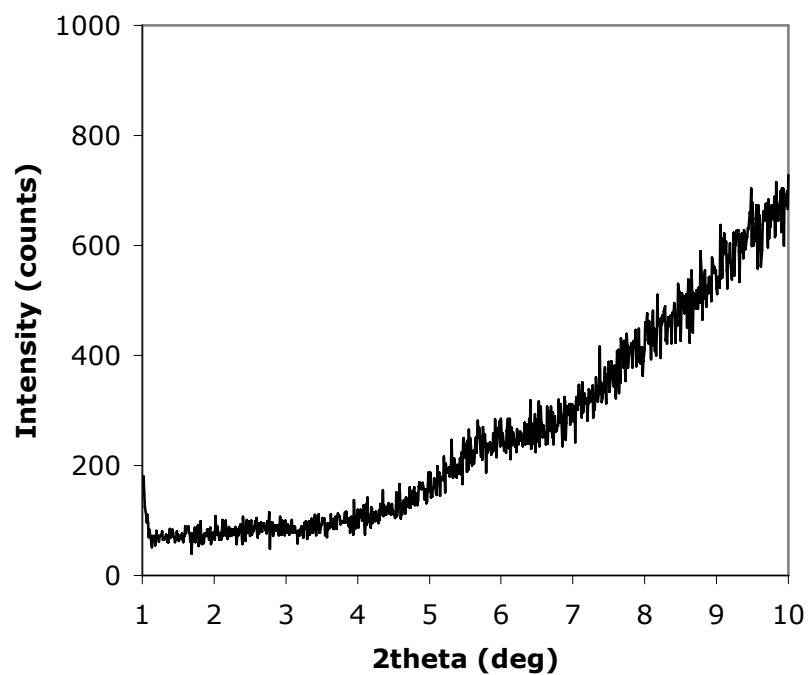


Figure A.7 X-ray diffraction pattern of nanocomposite synthesized by ethylene glycol containing 1 wt. % Cloisite 25A

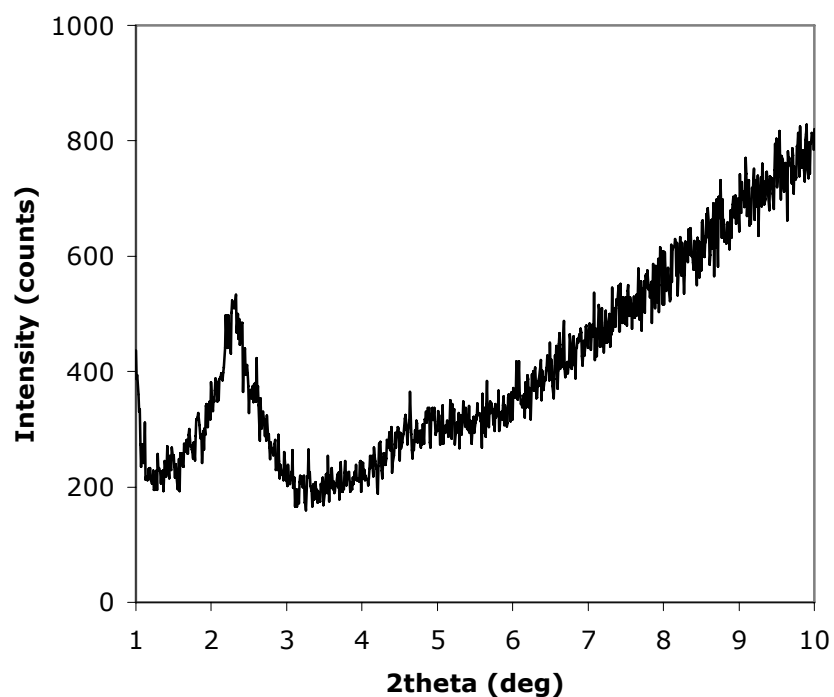


Figure A.8 X-ray diffraction pattern of nanocomposite synthesized by ethylene glycol containing 1 wt. % Cloisite 15A

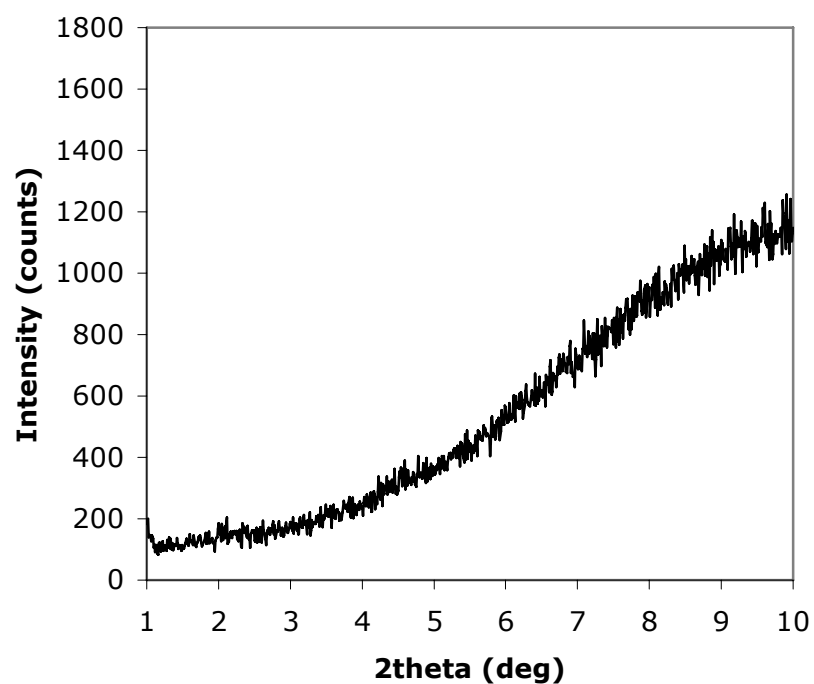


Figure A.9 X-ray diffraction pattern of pure unsaturated polyester synthesized by propylene glycol

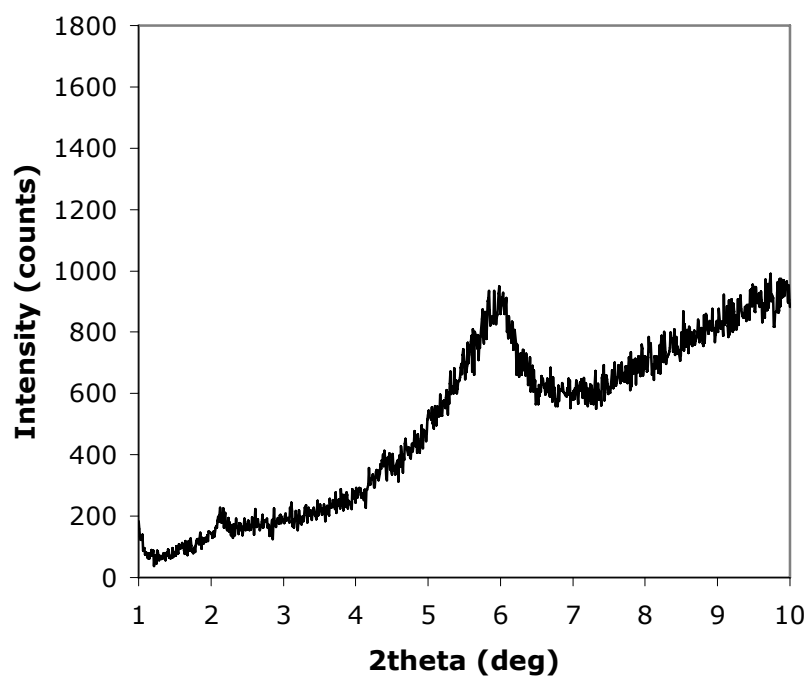


Figure A.10 X-ray diffraction pattern of nanocomposite synthesized by propylene glycol containing 1 wt. % Cloisite 30B

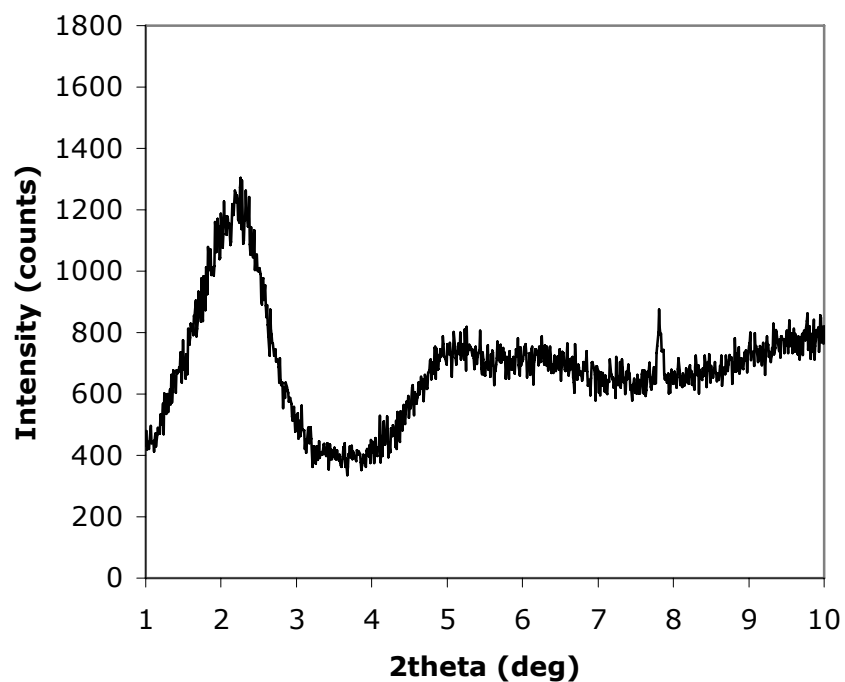


Figure A.11 X-ray diffraction pattern of nanocomposite synthesized by propylene glycol containing 3 wt. % Cloisite 30B

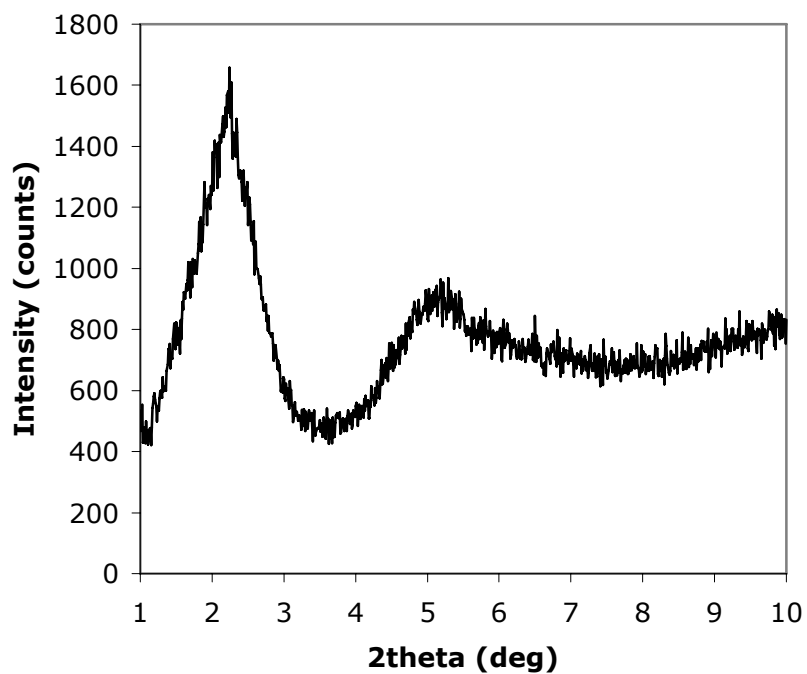


Figure A.12 X-ray diffraction pattern of nanocomposite synthesized by propylene glycol containing 5 wt. % Cloisite 30B

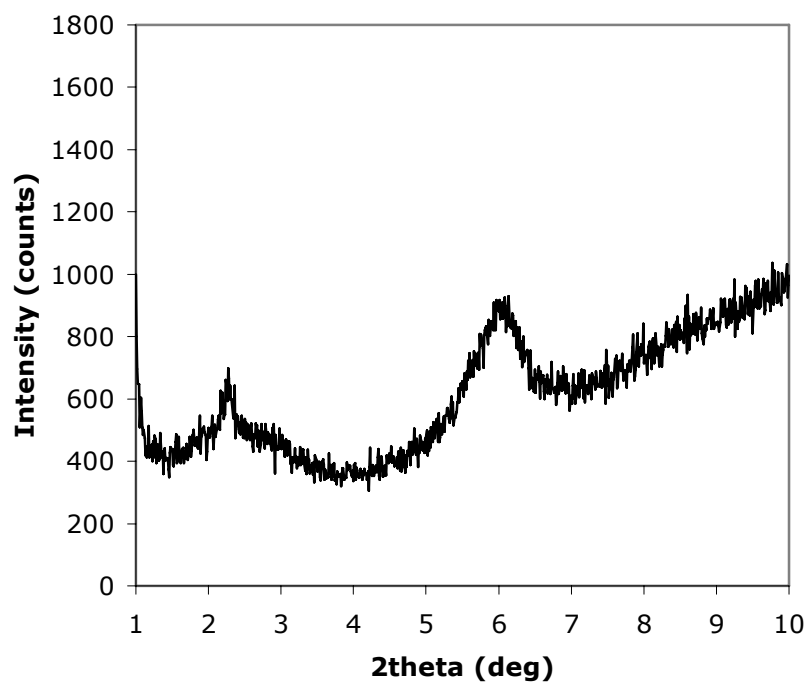


Figure A.13 X-ray diffraction pattern of nanocomposite synthesized by propylene glycol containing 1 wt. % Cloisite 25A

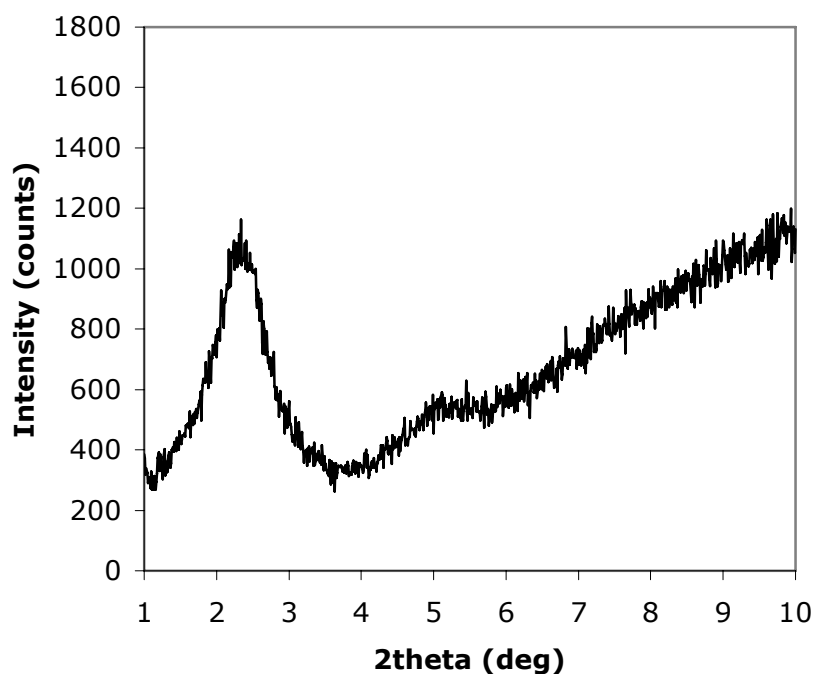


Figure A.14 X-ray diffraction pattern of nanocomposite synthesized by propylene glycol containing 1 wt. % Cloisite 15A

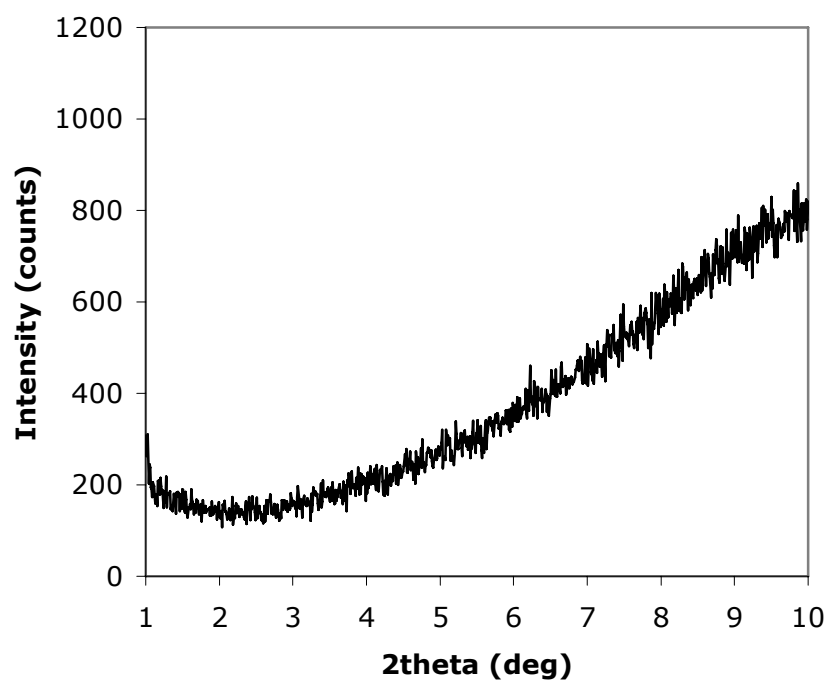


Figure A.15 X-ray diffraction pattern of pure unsaturated polyester synthesized by diethylene glycol

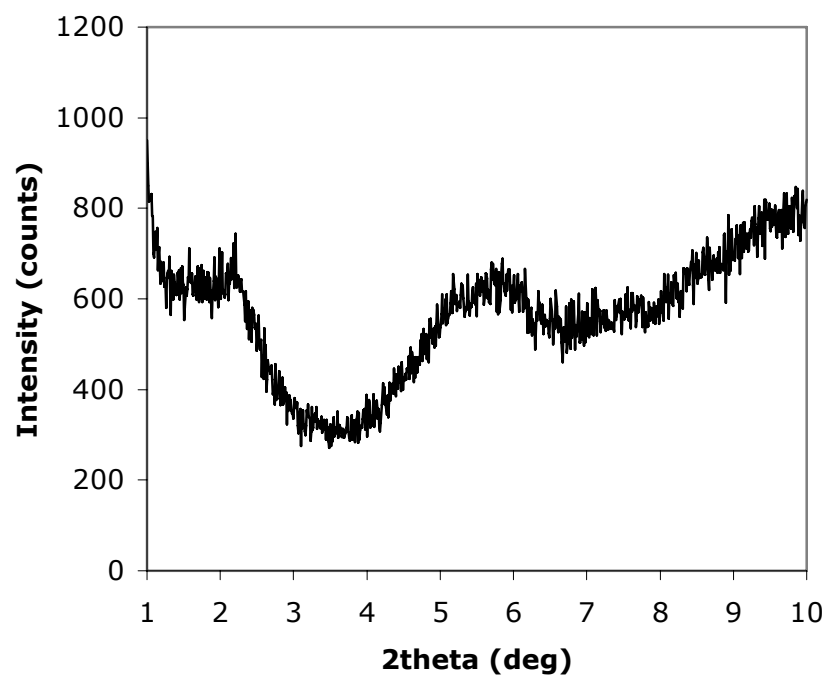


Figure A.16 X-ray diffraction pattern of nanocomposite synthesized by diethylene glycol containing 1 wt. % Cloisite 30B

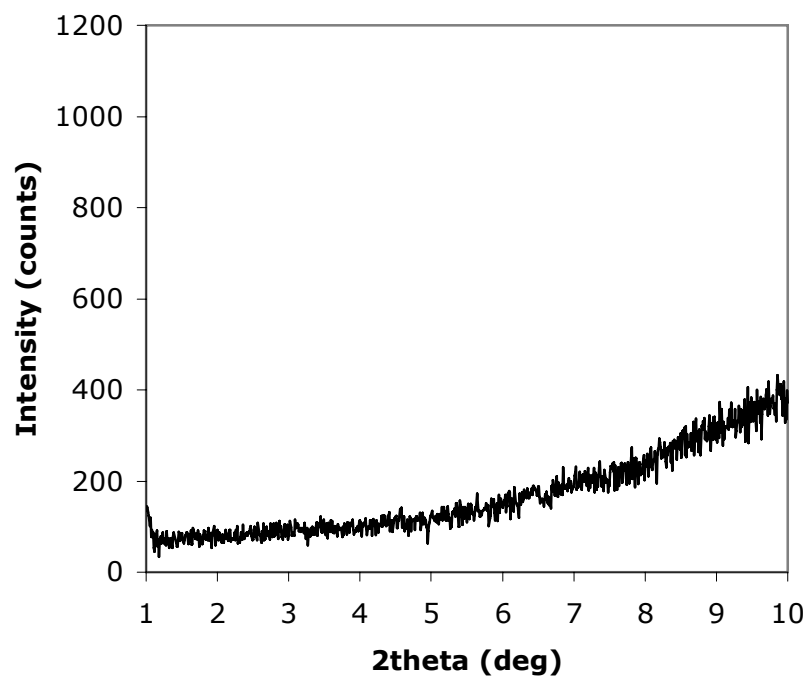


Figure A.17 X-ray diffraction pattern of nanocomposite synthesized by diethylene glycol containing 3 wt. % Cloisite 30B

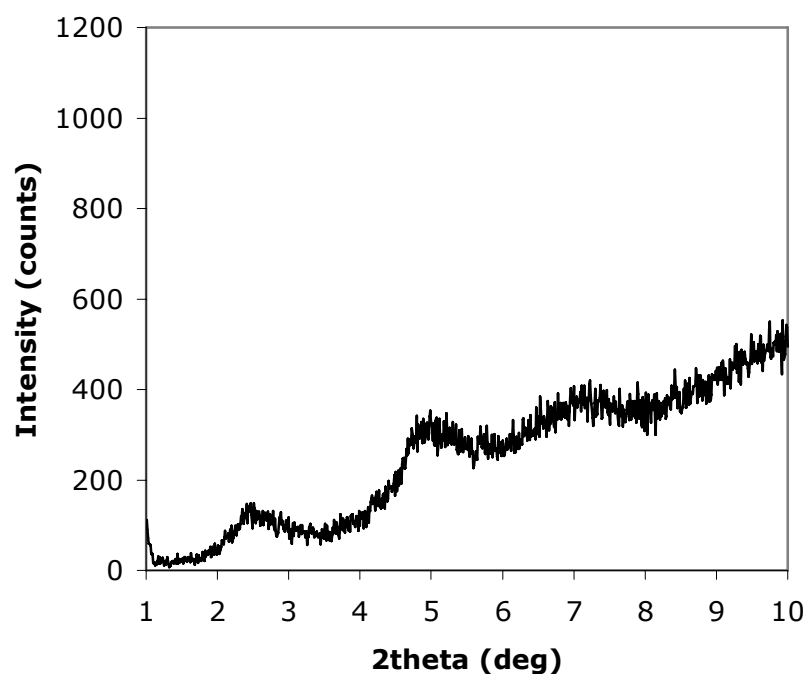


Figure A.18 X-ray diffraction pattern of nanocomposite synthesized by diethylene glycol containing 5 wt. % Cloisite 30B

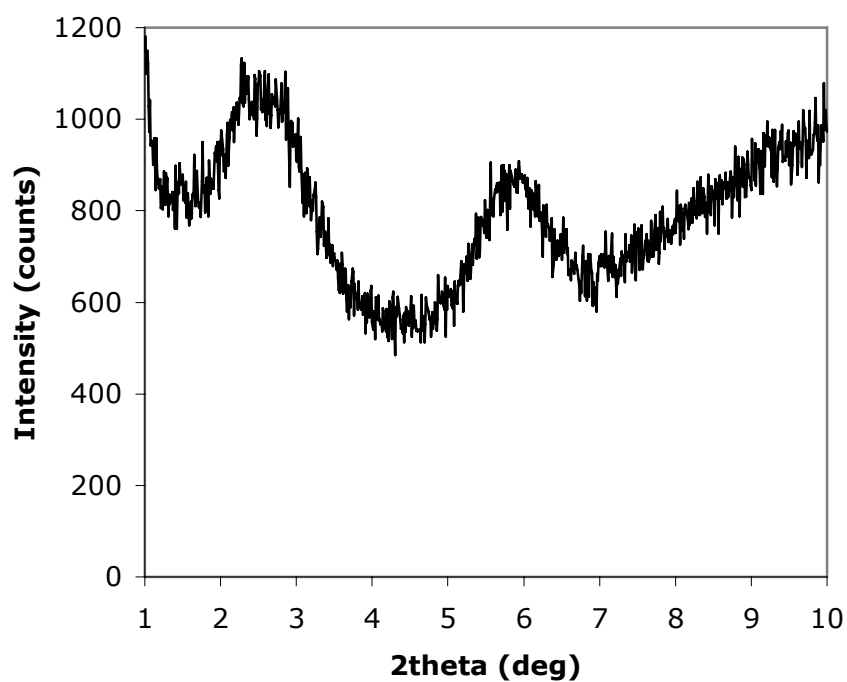


Figure A.19 X-ray diffraction pattern of nanocomposite synthesized by diethylene glycol containing 1 wt. % Cloisite 25A

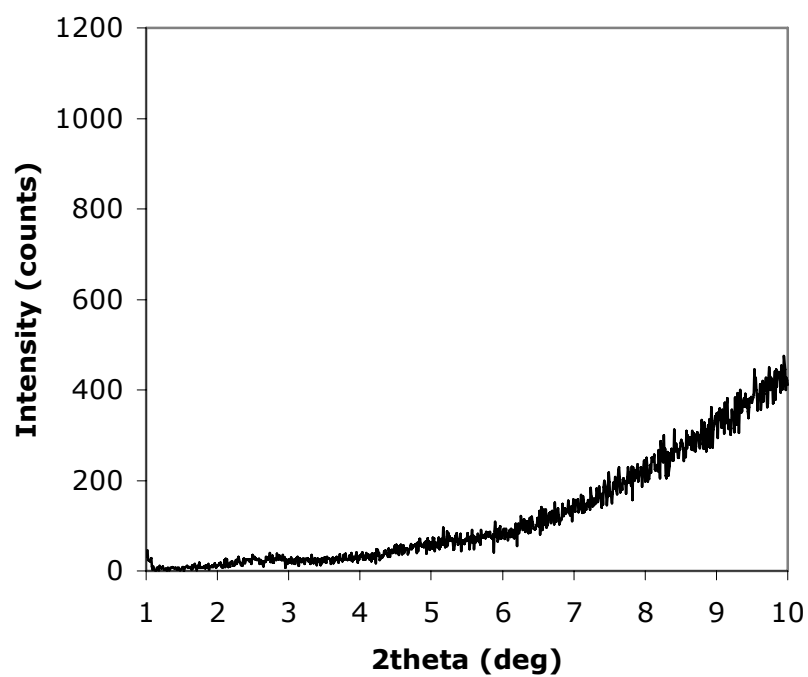


Figure A.20 X-ray diffraction pattern of nanocomposite synthesized by diethylene glycol containing 1 wt. % Cloisite 15A

APPENDIX B

Table B.1 Arithmetic means and standard deviations of tensile strength values of samples with respect to glycol type and organoclay (Cloisite 30B) content

Organoclay Weight %	EG		PG		DEG	
	Avg. Tensile Strength (MPa)	Stdev. (MPa)	Avg. Tensile Strength (MPa)	Stdev. (MPa)	Avg. Tensile Strength (MPa)	Stdev. (MPa)
0	46.1	7.9	25.1	3.1	23.9	0.8
1	49.3	4.7	22.5	0.6	35.5	0.9
3	26.9	3.3	33.3	2.5	22.4	0.9
5	-	-	29.3	1.8	5.6	0.4

Table B.2 Arithmetic means and standard deviations of tensile strength values of samples with respect to glycol type and organoclay type

Organoclay Type	EG		PG		DEG	
	Avg. Tensile Strength (MPa)	Stdev. (MPa)	Avg. Tensile Strength (MPa)	Stdev. (MPa)	Avg. Tensile Strength (MPa)	Stdev. (MPa)
Cloisite 30B	49.3	4.7	22.5	0.6	35.5	0.9
Cloisite 25A	40.8	3.9	27.8	5.9	14.0	0.7
Cloisite 15A	24.4	1.9	26.0	3.0	9.4	0.3

Table B.3 Arithmetic means and standard deviations of tensile modulus values of samples with respect to glycol type and organoclay (Cloisite 30B) content

Organoclay Weight %	EG		PG		DEG	
	Avg. Tensile Modulus (MPa)	Stdev. (MPa)	Avg. Tensile Modulus (MPa)	Stdev. (MPa)	Avg. Tensile Modulus (MPa)	Stdev. (MPa)
0	2330	81	3280	113	944	47
1	2894	63	3234	95	1457	55
3	2664	81	2904	166	936	50
5	-	-	2979	93	72	10

Table B.4 Arithmetic means and standard deviations of tensile modulus values of samples with respect to glycol type and organoclay type

Organoclay Type	EG		PG		DEG	
	Avg. Tensile Modulus (MPa)	Stdev. (MPa)	Avg. Tensile Modulus (MPa)	Stdev. (MPa)	Avg. Tensile Modulus (MPa)	Stdev. (MPa)
Cloisite 30B	2894	63	3234	95	1457	55
Cloisite 25A	2356	133	3009	130	676	24
Cloisite 15A	2386	126	2641	92	633	34

Table B.5 Arithmetic means and standard deviations of tensile strain at break (%) values of samples with respect to glycol type and organoclay (Cloisite 30B) content

Organoclay Weight %	EG		PG		DEG	
	Avg. Tensile Strain at Break (%)	Stdev. (%)	Avg. Tensile Strain at Break (%)	Stdev. (%)	Avg. Tensile Strain at Break (%)	Stdev. (%)
0	3.2	0.5	0.9	0.2	8.6	0.8
1	2.5	0.2	0.9	0.1	9.9	1.3
3	1.1	0.4	2.5	0.2	9.9	1.0
5	-	-	1.9	0.2	23.5	0.9

Table B.6 Arithmetic means and standard deviations of tensile strain at break (%) values of samples with respect to glycol type and organoclay type

Organoclay Type	EG		PG		DEG	
	Avg. Tensile Strain at Break (%)	Stdev. (%)	Avg. Tensile Strain at Break (%)	Stdev. (%)	Avg. Tensile Strain at Break (%)	Stdev. (%)
Cloisite 30B	2.5	0.2	0.9	0.1	9.9	1.3
Cloisite 25A	3.2	0.4	1.5	0.6	3.6	0.3
Cloisite 15A	1.7	0.3	1.7	0.4	1.9	0.2

Table B.7 Arithmetic means and standard deviations of flexural strength values of samples with respect to glycol type and organoclay (Cloisite 30B) content

Organoclay Weight %	EG		PG		DEG	
	Avg. Flexural Strength (MPa)	Stdev. (MPa)	Avg. Flexural Strength (MPa)	Stdev. (MPa)	Avg. Flexural Strength (MPa)	Stdev. (MPa)
0	92.5	14.1	50.0	9.8	26.0	1.9
1	78.8	10.0	48.5	5.8	35.5	1.3
3	61.0	4.3	45.6	6.0	10.0	0.8
5	-	-	52.3	2.6	2.6	0.1

Table B.8 Arithmetic means and standard deviations of flexural strength values of samples with respect to glycol type and organoclay type

Organoclay Type	EG		PG		DEG	
	Avg. Flexural Strength (MPa)	Stdev. (MPa)	Avg. Flexural Strength (MPa)	Stdev. (MPa)	Avg. Flexural Strength (MPa)	Stdev. (MPa)
Cloisite 30B	78.8	10.0	48.5	5.8	35.5	1.3
Cloisite 25A	93.8	5.3	62.3	10.4	14.0	0.4
Cloisite 15A	31.7	2.5	33.3	2.0	9.6	0.5

Table B.9 Arithmetic means and standard deviations of flexural modulus values of samples with respect to glycol type and organoclay (Cloisite 30B) content

Organoclay Weight %	EG		PG		DEG	
	Avg. Flexural Modulus (MPa)	Stdev. (MPa)	Avg. Flexural Modulus (MPa)	Stdev. (MPa)	Avg. Flexural Modulus (MPa)	Stdev. (MPa)
0	3075	73	3421	70	616	71
1	2969	75	3379	214	790	48
3	2897	138	3001	62	255	17
5	-	-	3103	65	37	2

Table B.10 Arithmetic means and standard deviations of flexural modulus values of samples with respect to glycol type and organoclay type

Organoclay Type	EG		PG		DEG	
	Avg. Flexural Modulus (MPa)	Stdev. (MPa)	Avg. Flexural Modulus (MPa)	Stdev. (MPa)	Avg. Flexural Modulus (MPa)	Stdev. (MPa)
Cloisite 30B	2969	75	3379	214	790	48
Cloisite 25A	3187	159	3172	160	497	17
Cloisite 15A	2821	157	2933	44	268	31

Table B.11 Arithmetic means and standard deviations of flexural strain at maximum stress values of samples with respect to glycol type and organoclay (Cloisite 30B) content

Organoclay Weight %	EG		PG		DEG	
	Avg. Flexural Strain at Max. (%)	Stdev. (%)	Avg. Flexural Strain at Max. (%)	Stdev. (%)	Avg. Flexural Strain at Max. (%)	Stdev. (%)
0	2.8	0.7	1.5	0.2	5.0	1.5
1	2.6	0.3	1.3	0.2	8.6	0.6
3	1.9	0.2	1.4	0.2	6.1	1.0
5	-	-	1.6	0.1	13.7	0.3

Table B.12 Arithmetic means and standard deviations of flexural strain at maximum stress values of samples with respect to glycol type and organoclay type

Organoclay Type	EG		PG		DEG	
	Avg. Flexural Strain at Max. (%)	Stdev. (%)	Avg. Flexural Strain at Max. (%)	Stdev. (%)	Avg. Flexural Strain at Max. (%)	Stdev. (%)
Cloisite 30B	2.6	0.3	1.3	0.2	8.6	0.6
Cloisite 25A	3.0	0.3	1.8	0.3	3.7	0.2
Cloisite 15A	1.0	0.1	1.1	0.1	4.6	0.9

Table B.13 Arithmetic means and standard deviations of impact strength values of samples with respect to glycol type and organoclay (Cloisite 30B) content

Organoclay Weight %	EG		PG		DEG	
	Avg. Impact Strength (kJ/m ²)	Stdev. (kJ/m ²)	Avg. Impact Strength (kJ/m ²)	Stdev. (kJ/m ²)	Avg. Impact Strength (kJ/m ²)	Stdev. (kJ/m ²)
0	3.38	1.01	1.41	0.17	4.69	1.02
1	2.39	0.78	1.21	0.20	3.72	0.64
3	1.78	0.38	1.09	0.21	2.64	0.44
5	-	-	1.32	0.21	2.55	0.68

Table B.14 Arithmetic means and standard deviations of impact strength values of samples with respect to glycol type and organoclay type

Organoclay Type	EG		PG		DEG	
	Avg. Impact Strength (kJ/m ²)	Stdev. (kJ/m ²)	Avg. Impact Strength (kJ/m ²)	Stdev. (kJ/m ²)	Avg. Impact Strength (kJ/m ²)	Stdev. (kJ/m ²)
Cloisite 30B	2.39	0.78	1.21	0.20	3.72	0.64
Cloisite 25A	3.22	0.61	1.38	0.15	2.34	0.38
Cloisite 15A	1.19	0.13	1.23	0.22	2.13	0.25